1-1-2006

Solvent enhanced block copolymer ordering in thin films.

Matthew J. Misner
University of Massachusetts Amherst

SOLVENT ENHANCED BLOCK COPOLYMER ORDERING IN THIN FILMS

A Dissertation Presented

by

MATTHEW J. MISNER

Submitted to the Graduate School of the
University of Massachusetts Amherst in partial fulfillment
of the requirements for the degree of

DOCTOR OF PHILOSOPHY

September 2006

Polymer Science and Engineering

SOLVENT ENHANCED BLOCK COPOLYMER ORDERING IN THIN FILMS

A Dissertation Presented

by

MATTHEW J. MISNER

Approved as to style and content by:

Thomas P. Russell, Chair

Samuel P. Gido, Member

Mark Tuominen, Member

Shaw Ling Hsu, Department Head
Polymer Science and Engineering

ACKNOWLEDGMENTS

To begin, I wish to thank my advisor, Professor Thomas P. Russell. When I came to campus to visit as a prospective student and met with Tom, I knew there was a great opportunity to do some very interesting and valuable work in his group. Tom later provided me with that opportunity and I am grateful. Tom has created an exceptional environment to foster students and research, continually providing opportunity as well as guidance which gives freedom as well as direction. During my time here, I have grown as a research and I am thankful to have him as my mentor. I would also like to extend my gratitude to my committee members, Samuel Gido and Mark Tuominen, for their discussions, support, and commitment to serve on my committee.

I would also like to thank Seung Hyun Kim, Masahiro Kimura, and Benjamin Ocko for their collaborations, guidance, and support, of which there is no limit of my appreciation.

I am thankful for all of my other collaborators: Habib Skaff, Ting Xu, Antonio Checco, Oleg Gang, Kevin Cavicchi, James Goldbach, James Sievert, Qingling Zhang, Ling Yang, David Butterfield, Du Yeol Ryu, Serkan Yurt, Joona Bang, Eric Drockenmuller, Vignesh Gowrishankar, Nathaniel Lynd, Scott Schmidt, Todd Emrick, Marc Hillmyer, Craig Hawker, Dhandapani Venkataraman, and Alain Gibaud. Also, I would like to thank Ted Atkins, Win de Jeu and Detlef Smilgies for valuable discussions.

I would like to thank the faculty in the department for teaching first year classes, discussions, and working to create an open research facility. Also, many

thanks to Linda Strzewgowski, Susan Ryan, Anne Gaddy, Eileeen Besse, Sophia Hsu, Ann Brainerd and Joann Chauvin for all of their help in administrative matters.

Further, I would like to thank all the group members I have had the pleasure to share time with here: Tobias, Hocheol, Dongha, Masahiro, Keisuke, Michael, Jason, Chris, Zhiqun, Amanda, Irene, Ting, Yao, Kris, James, Xiaodong, Kate, Julie, James, Suresh, Xiaochuan, Qingling, Nui, Siva, Dongseok, Jiun-Tai, Jinbo, Jiayu, Ravi, Kyusoon, Hongqi, Kevin, Mingfu, Martha, Kan Du, Priyanka, Xuan, Jiangshui, Ji, Wei, Yunxia, Bokyung, Malvika, Tejaswini, Liming, Joonwon, Qifang, Soojin, Tomomi, and Ling.

Finally, I want to thank my all my friends at UMass, in particular Amanda Leach, Kris Lavery, Donna Wrublewski, Bill Peters and Kevin Wier. They have been a family to me here and I have been very lucky to have found them. To that, I also wish to thank my family. It is though their hard work and life that I have arrived here. They have supported me tremendously and have always been there for any help or encouragement I needed.

ABSTRACT

SOLVENT ENHANCED BLOCK COPOLYMER ORDERING IN THIN FILMS

SEPTEMBER 2006

MATTHEW J. MISNER, B.S., COLORADO STATE UNIVERSITY

M.S., UNIVERSITY OF MASSACHUSETTS AMHESRT

Ph.D., UNIVERSITY OF MASSACHUSETTS AMHESRT

Directed by: Professor Thomas P. Russell

Diblock copolymer self-assembly of materials is emerging as a key element in the fabrication of functional nanostructured materials. By solvent casting or solvent annealing block copolymer thin films, we have demonstrated methods to produce diblock copolymer films with highly oriented, close-packed arrays of nanoscopic cylindrical domains with a high degree of long-range lateral order with few defects. The solvent imparts a high degree of mobility in the microphase-separated copolymer that enables a rapid removal of defects and a high degree of lateral order. Though the use of a selective cosolvent during solvent casting, it was found that the microdomain size and spacing could be increased, leading to a size-tunable system. Additionally, the presence of water also led to the ability to control the microdomain orientation during solvent annealing. Ionic complexation within cylinder-forming PS-*b*-EO block copolymer thin films was also investigated, where added salts bind PEO block as the minor component. Small amounts of added salts, on the order a few ions per chain, show large effects on the ordering of the copolymer films during solvent annealing. By using gold or cobalt salts, well-organized patterns of nanoparticles can be generated in the copolymer microdomains.

Topographically and chemically patterned surfaces were used as a route to sectorizing and controlling the lattice orientation of copolymer films. Topographically patterned surfaces allow well-defined boundaries to confine the copolymer microdomains on a surface and effectively direct the ordering and grain orientation of the copolymer microdomains. Chemically patterned surfaces provide a route to direct the block copolymer ordering on completely flat surface, which may have advantages in applications where adding additional topography may be undesirable.

To generate nanoporous templates from PS-b-PEO bases materials several routs were followed. The first route was through the addition and selective solvent removal of homopolymer PEO or PMMA. Second, we have incorporated a center block that is photodegradable by ultra violet radiation into PS-*b*-PMMA-*b*-PEO copolymers. Third, a tritylether junction was placed between the two blocks, which is cleavable by exposure to trifluoroacetic acid vapor.

Though the use of solvents in block copolymer thin films, were are able to markedly enhance the long range lateral ordering block copolymer films. Also, routes to sectorize surfaces to confine and direct the copolymer microdomains are shown. Also, three methods to generate nanoporous films from PS-b-PEO based copolymers are demonstrated. All of these results are important in the realization of addressable media from block copolymer nanolithography.

TABLE OF CONTENTS

LIST OF TABLES

LIST OF FIGURES

TABLE OF CONTENTS

LIS T OF TABLES

Table

Page

LIST OF FIGURES

CHAPTER 1

BACKGROUND

1.1 Block Copolymers

Polymers are molecules that are comprised of smaller monomers that are linked together through chemical bonds. Polymers have vast material applications due to a number of properties, which are dependent on the chemical and structural nature of the polymer, and can be augmented though blending with other polymers or diluents. Polymer blend phase behavior has been described by mean field arguments as in Equation 1.1.[1]

$$\frac{\Delta G}{RT} = \frac{f_A}{N_A}\ln\phi_A + \frac{(1-f_A)}{N_B}\ln(1-f_A) + f_A(1-f_A)\chi_{AB} \qquad \textbf{(1.1)}$$

Where A and B are two chemically distinct components with a volume fraction of A of N_A/N, where N is the sum of N_A and N_B, and B volume fraction of (1-f_A). The difference between the enthalpic interactions (ε_{ii}) between like and unlike segments is described by the Flory-Huggins interaction parameter, χ_{AB}, and is defined in Equation 1.2.

$$\chi_{AB} = z\left[\varepsilon_{AB} - \frac{\varepsilon_{AA}+\varepsilon_{BB}}{2}\right]/RT \qquad \textbf{(1.2)}$$

Only when the entropic contributions to the free energy of mixing (the first two terms in Equation 1.1) is overcome by the enthalpic gain of phase separation (last term in Equation 1.1), can the blend demix into two distinct phases.

Polymer phase behavior was extended to block copolymers,[2-5] where chemically distinct polymers covalently bound at a central junction point, as shown in Figure 1.1A. However, due to the connectivity of the chain, block copolymer generate microphases on

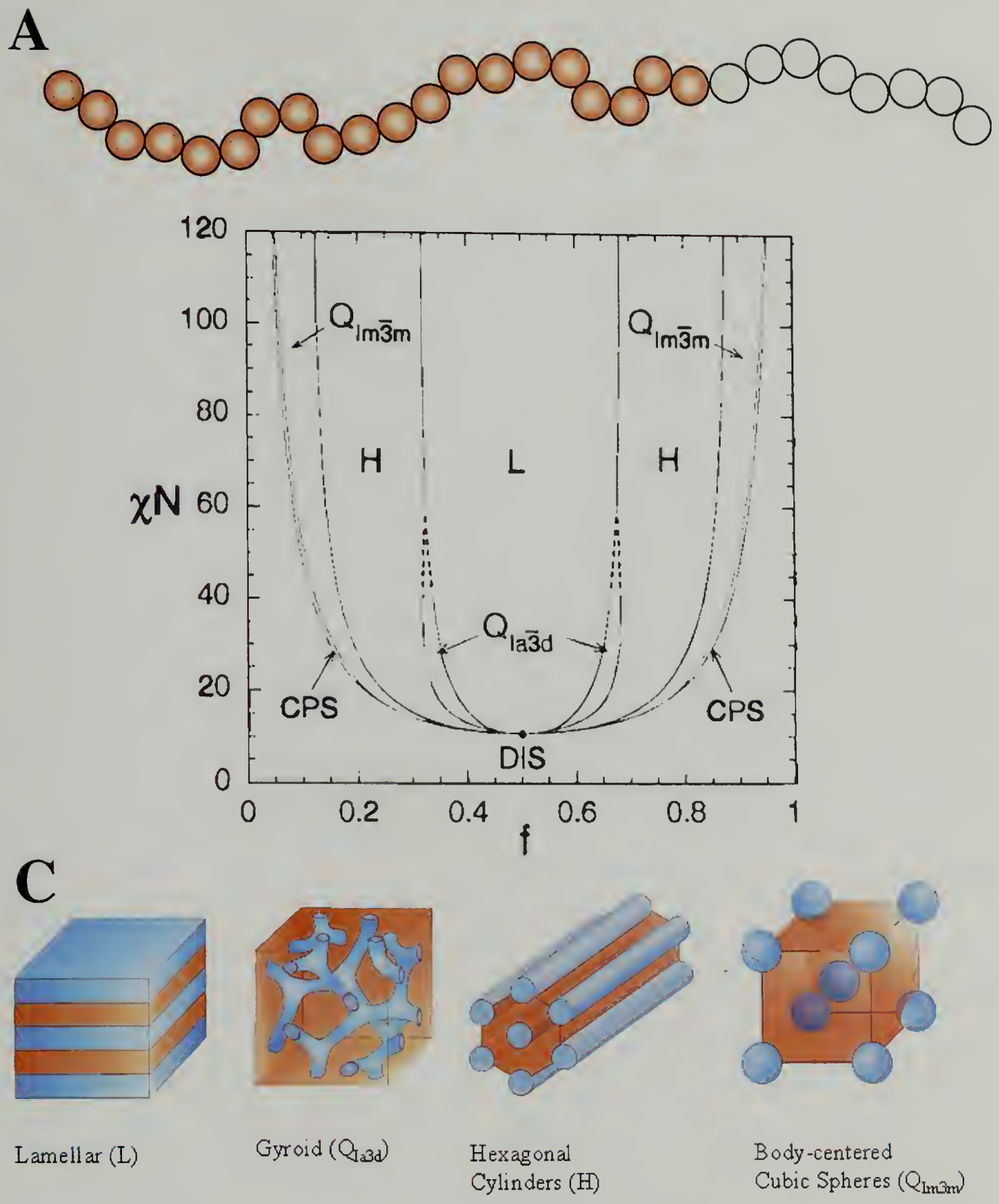

Figure 1.1: A) A diblock copolymer chain, B) a block copolymer phase diagram, and C) the morphologies resulting from diblock copolymer microphase separation.[2]

the order of the radius of gyration of the chain. An example of a block copolymer phase diagram is shown in Figure 1.1B. The degree of segregation, $\chi_{AB}N$, is on the ordinate and the volume fraction, f, of one block is on the abscissa. For any given composition, the block copolymer can be phase-mixed, or disordered, where there is no distinguishable morphology, or can exhibit well-defined microphase separated morphology. The boundary between the mixed and microphase separated structures is referred to as the order-disorder transition (ODT) and the boundary from one morphology to another is called the order-order transition. The observed morphology is dependent on the composition of the block copolymer, molecular weight, and the strength of the interactions. Generally, spherical, cylindrical, gyroid, and lamellar morphologies are observed in block copolymers, as diagrammed in Figure 1.1C.

Through the addition of a solvent, the block copolymer microphase separation can be significantly altered. In an favorable solvent is neutral for both blocks, an effective screening of the block segmental interactions can cause an ODT or ODT in the block copolymer. In the dilution approximation, the domain spacing, L_o, scales to the 1/3 power to the polymer concentration:[6]

$$L_o \approx \phi_p^{1/3} \tag{1.3}$$

As well as an effective segmental interaction parameter $\chi_{effective}$:

$$\chi_{effective} \approx \phi_p^{\beta} \chi \tag{1.4}$$

where β is unity for the dilution approximation. However, block copolymers in a preferential solvent deviate from this scaling due to preferential swelling and the overall solvent quality. For a good solvent, the domain spacing was found to scale:

$$L_o \approx \phi_p^{\alpha} \tag{1.5}$$

where $\alpha = 0.2$ at weak segregation and $\alpha = 0.5$ at strong segregation.[7] Lodge and coworkers found that the quality of the solvent also influences the scaling the domain spacing. For block copolymers in a highly selective solvent for one block and a poor solvent for the other, negative values for α are observed.[8]

Block copolymer self-assembly has been of considerable interest as a route to spontaneously generate nanostructured thin films for device applications. Most applications utilize the nanoporous structures to act as templates to deposit or grow materials in the domains, such as nanowires or nanoparticles.[9-11] Also, these materials can be used as etch masks, similar to what is used in conventional lithography, to transfer the pattern of the nanostructured film into another material.[12,13] Shown in Figure 1.2 is an example of block copolymer lithography from a nanoporous film from a PS-b-PB diblock copolymer film with spherical PB microdomains (A).[12] The sample is ozonated to degrade the PB spheres and subsequently etched by RIE transferring the nanostructure of the copolymer film into the silicon nitride substrate. SEM images of the copolymer film after ozonation and (B) paritailly RIE etched to expose the diblock copolymer and (C) full transfer of the nanostructure into the substrate.

Much work has been done on the spherical copolymer morphology, where monolayers of spheres on a surface can arrange in a hexatic array.[14,15] However, these types of structures are limited to an aspect ratio of unity, which can limit the range of applications that these materials can be used for. To surpass this limitation, one can use other morphologies, such as cylindrical nanostructures. Here, however, one as to pay

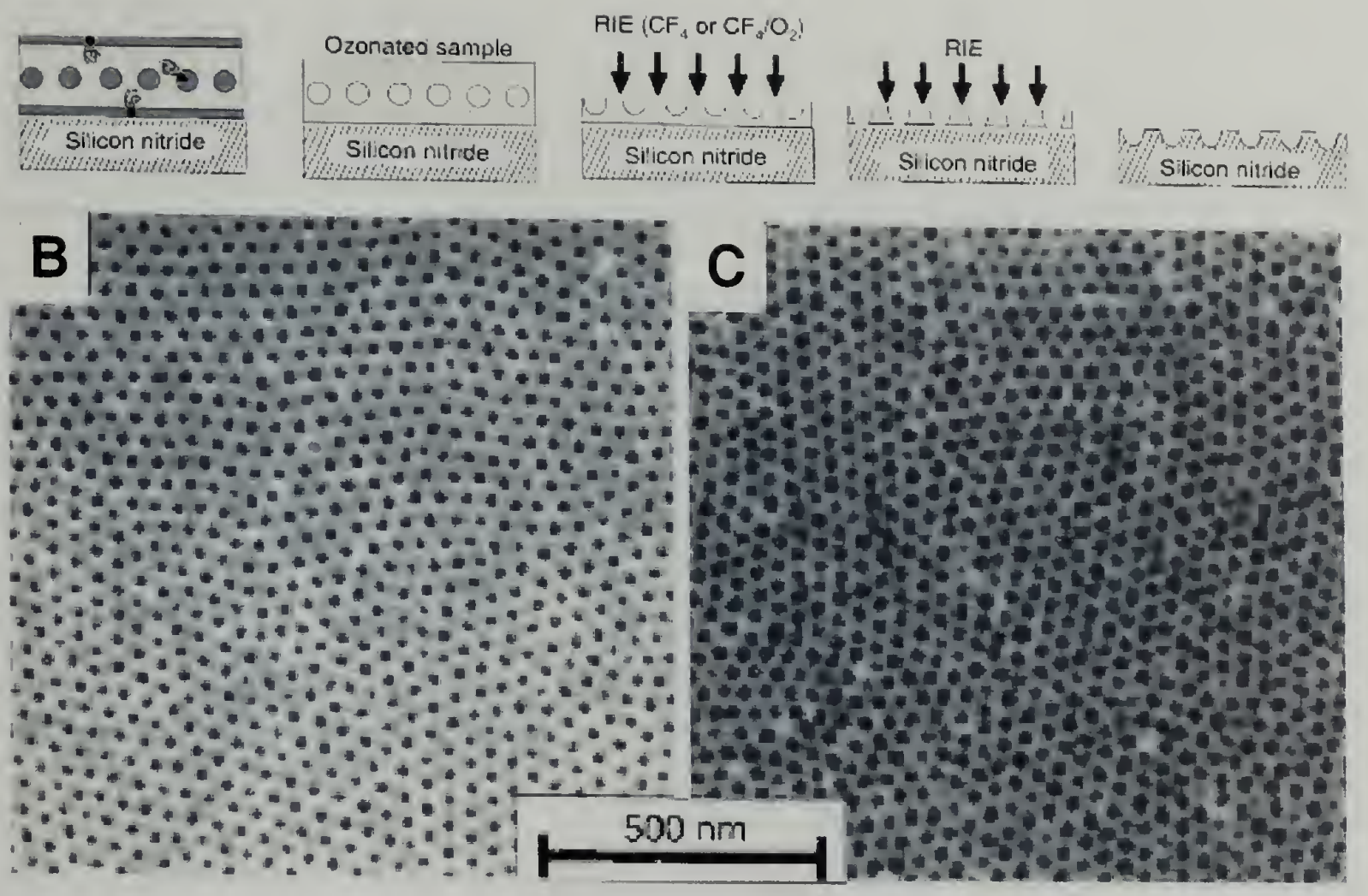

Figure 1.2 A) A Schematic of block copolymer lithography. SEM images of an ozonated diblock copolymer film after B) partially etching the nanoporous film and C) fully etching the nanoporous film and transferring the pattern into the substrate.[12]

close attention to the orientation of the copolymer microdomain in the thin film. Previous work has focused on orienting cylindrical microdomains through tailoring surfaces and interfaces, using commensurability, and external fields.[16]

Many of the applications that nanostructured films could be used for require that the copolymer microdomains have exceptional long-range lateral order. Data storage is one such application whereby, to fully utilize the available data density of the copolymer domains, one has to be able to address every domain. Previous work to improve on the lateral order of copolymer microdomains has employed epitaxy, graphioepitaxy, shear, and thermal fields.[15-20] In general, all of these techniques use

thermal annealing to remove defects from the copolymer arrays. This process, however, is subject to two competing factors. The first is the segmental interactions, χ, degree of polymerization, N, that drive the copolymer to phase separate and the subsequent removal defects from the copolymer structure.[3-5] The second is the kinetics of the removal of defects, which a large part of which is the diffusion of the copolymer, which also depends on χ and N.[5] In spherical copolymer thin films the rate of removal of defects scales as $t^{-1/4}$, which means that after a short amount of thermal annealing, subsequent annealing yields little gains in improving the long-range lateral order.

To overcome the limitations of thermal processes, we have chosen to investigate the use of solvents to reduce the glass transition temperature, and subsequently increase the mobility of the copolymer, screen segmental interactions, and align the copolymer microdomains.[21-27] The topics of research here will focus on the ordering of copolymer films in solvent casting and solvent annealing, the effects of a co-solvent on casting and annealing, the effects of complexation of ionic salts with the block copolymer during solvent annealing, confinement of the copolymer on topographically and chemically patterned surfaces, and routes to generate nanoporous films from the materials presented.

1.2 Characterization Techniques

1.2.1 Scanning Force Microscopy

Tapping mode Scanning Force Microscopy, SFM, is a non-destructive, high-resolution surface imaging technique that is directly applicable to block copolymer thin films.[28-30] A schematic of a SFM is shown in Figure 1.3. The surface being probed can have variation in height and composition. The SFM probe is oscillated at the resonance

frequency of the cantilever by a drive piezo. Simultaneously, a XYZ piezo scanner moved the tip across the surface with a fast and slow scan direction in the plane of the surface. The motion of the cantilever is measured by the deflection of the reflected beam of a laser off the surface of the cantilever. To measure the height image of the surface the amplitude of the tip oscillation is kept constant by a feedback controller controlling the Z position at a constant drive piezo voltage. Additionally, the phase difference between the drive oscillation and the measure oscillation of the tip can be used to determine information of the modulus of the surface. Areas of different modulus are illustrated by regions of different colors in the in the schematic.

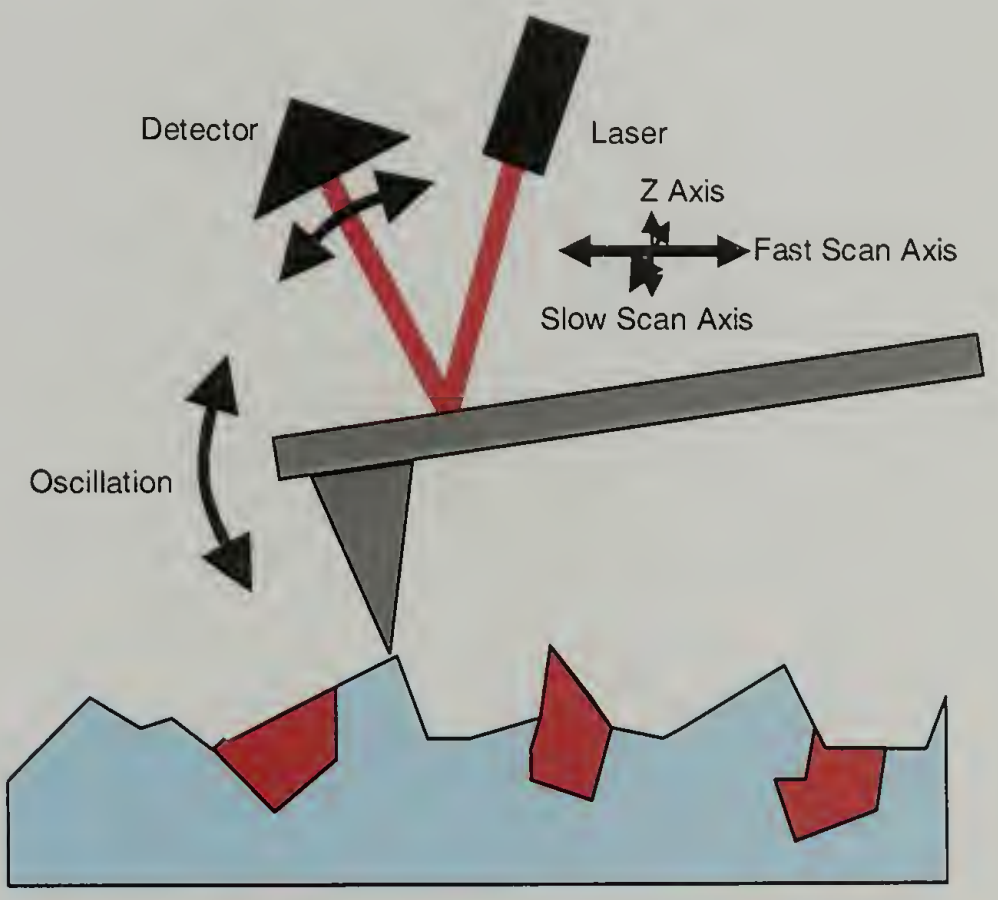

Figure 1.3 Schematic of a tapping mode SFM imaging a surface with variations in height and composition.

1.2.2 Interferometery

Reflectance interferometery is a method to measure film thickness optically.[31, 32] When a film is illuminated by a beam of light, the light is either transmitted or reflected at each interface of the film. When the reflected light from each surface is recombined, it

can interfere constructively or destructively. Along with the transmission and reflection coefficients of each interface, this nature of the interference will dictate the intensity of light observed coming from the surface. By measuring this intensity, the properties of the film can be determined. Shown in Figure 1.4A is schematic of a interferometer. As can be seen, light from the source and can be reflected or transmitted from the film surface. Light that is transmitted is then reflected from the bottom surface, shown here with a highly reflective substrate, and then interferes with light reflected from the film surface. This light is passed back through a fiber optic cable, which has a split to it, and received in the detector. For a interferometer that uses a monochromatic source, such as a laser, the measure reflectance is dependent on the film thickness, as shown in Figure 1.4B. The maxima in intensity occur when the reflected beams of light interfere constructively, or when the path difference though the film with a refractive index, n, and back is a multiple, m, of the wavelength, λ, of light, Equation 1.6.

$$d = \frac{m\lambda}{2n} \tag{1.6}$$

Interferometry using monochromatic light is useful technique in measuring changes in film thickness, such as growth of films in chemical vapor deposition or in the swelling of polymer films, by does is not effective for measuring discrete film thicknesses or in characterizing films that are structured. Instead, interferometers that have a white source are used to measure films in these applications. By using polychromatic light, the reflectance can be measured as a function of wavelength, as shown in Figure 1.4C. The analysis of these spectra is much more complicated than in

monochromatic interferometery. However, software is available to fit models of single and multilayer systems.

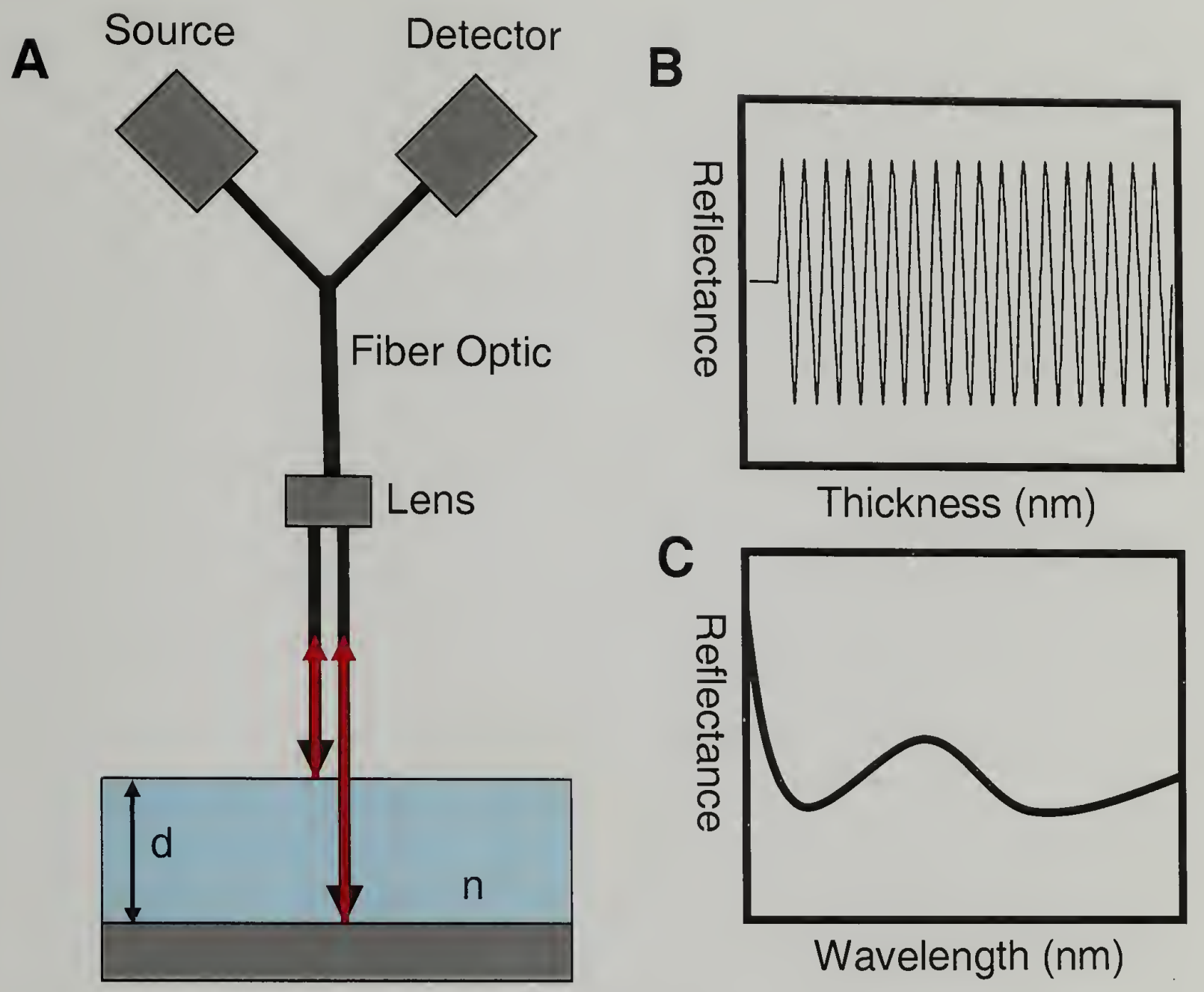

Figure 1.4 A) A schematic of a reflectance interferometer. Light is reflected off each interface of the film and interferes constructively or destructively. B) Monochromatic reflectance interferometery as a function of film thickness. The distance between maxima is given by $d = m\lambda/2n$. C) Spectroscopic reflectance interferometery, where reflectance is dependent on the wavelength of light, can be fit to model single and multilayer films.

1.2.3 X-Ray Scattering

Small angle x-ray scattering (SAXS) is a powerful tool in diblock copolymer characterization.[33,34] The wavelengths of x-rays used are on the order of one angstrom,

which is much smaller than the structures observed in block copolymer microphase separation; making x-rays apt method to resolve nanostructured materials. A general scattering diagram is shown in Figure 1.5, where the incident, $\vec{k}_i$ scattered, $\vec{k}_s$, and the scattering verctor, $\vec{q}$, are shown in by vector construction.

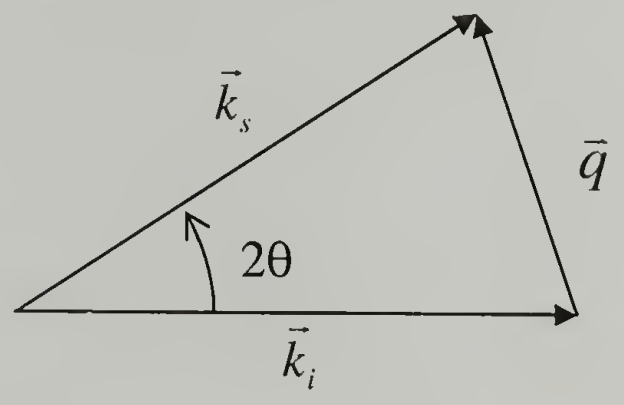

Figure 1.5 Vector construction of a general scattering geometry.

As can be seen $\vec{q} = \vec{k}_i - \vec{k}_s$, where the maginitude of the scattering vector, q, can be written as in Equation 1.7:

$$q = \frac{4\pi}{\lambda} \sin\theta \tag{1.7}$$

Where the λ is the wavelength and θ is half the scattering angle. Further, the relationship between the scattering angle and the distance between scattering objects, i.e. planes, is given by Bragg's Law in Equation 1.8:

$$m\lambda = 2d \sin\theta \tag{1.8}$$

The inverse relationship shown in Bragg's Law, where the larger the lattice, the smaller the scattering angle is the essence of reciprocal space and is further illuminated though the combination of Equations 1.7 and 1.8:

$$q = \frac{2\pi}{d} \tag{1.9}$$

There are two contributions to the scattering, one is the shape of the scattering particle, in block copolymers this would be the microdomain, and is referred to as the from factor, F(q). The form factor is the Fourier transform of the shape function of the scattering particle. The second contribution to the scattering is the structure factor, S(q). The structure factor contains information about the arrangement of the scattering particles, such as liquid-like ordering or hexagonally packed cylinders. The constructive and destructive interference of these scattering contributions give rise to the angular dependence of the small angle scattering and is described in Equation 1.10, where ρ_i is the electron density of the particles and the surrounding material.

$$I(q) = (\rho_1 - \rho_2)^2 S(q) F(q) \qquad \textbf{(1.10)}$$

Small angle x-ray scattering is useful in bulk samples of block copolymers to determine the microphase separated morphology, $\chi_{AB}(T)$, and, subsequently, the ODT. Also, SAXS can be used in thin films to determine in-plane correlation of the microdomains.

However, to measure in layer systems, such as lamellar block copolymers that are oriented parallel to the substrate, specular reflectivity, where the incident and exit angles of an x-ray beam reflecting from a surface are equal, is a preferable geometry, shown in Figure 1.6.[35]

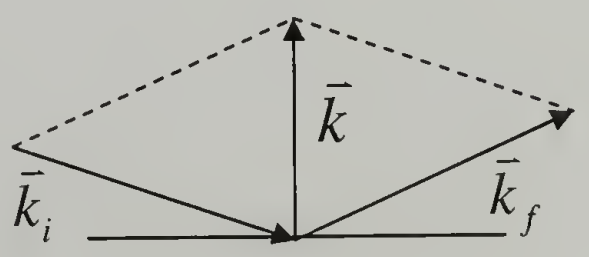

Figure 1.6 Vector construction of specular reflectivity from a flat surface.

When the x-ray beam impinges on the surface of a film, it can either totally reflect from the surface, if the angle of incidence is below the critical angle, or it can partially reflect and transmit into the film, as shown in Figure 1.7.

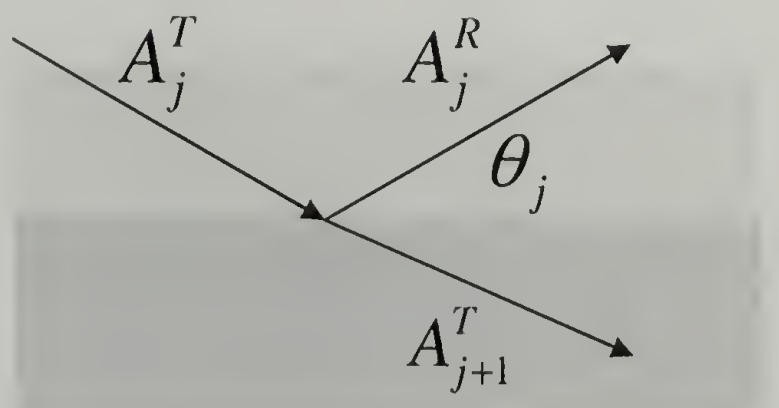

Figure 1.7 Reflection and Transmission from interface j in film.

The ratio of the reflected and incident beam is the called the reflectivity, which is the complex conjugate of the reflectivity coefficient, which is defined in Equation 1.11 for the reflection between the j and j+1 interface:

$$r_{j,j+1} = \frac{k_j - k_{j+1}}{k_j + k_{j+1}} \tag{1.11}$$

For a film and multilayered films, the relectivity coefficient depends in the underlaying layer, subsequently, the reflectivity coeffecients are calculated by starting at the substrate (considered to be a layer of infinite thickness) and working to the air/film surface, $r_{0,1}$, of which the complex conjugate is the reflectivity of the entire film. Further details on modeling layered systems and the incorporation of roughness can be found in the literature.[35] An example of a layered film is in Figure 1.8,[36] where the reflectivity is

normalized by the Fresnel reflectivity, R_F, which is the reflectivity from perfectly smooth interfaces and is proportional to θ^{-4}.

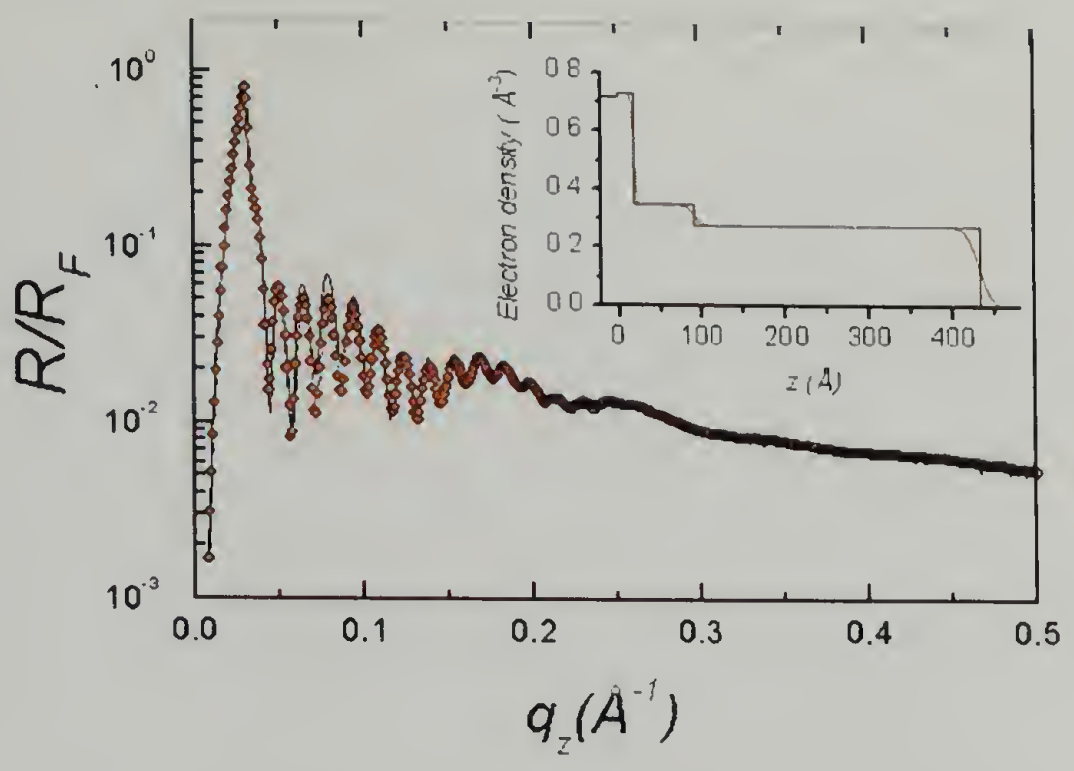

Figure 1.8 The reflectivity of a layered polymer film. The inset indicates the electron density profile of the film in the direction of the surface normal.[36]

The high frequency occilations, or Kiessig fringes, can be used to calculate the entire film thickness, $h = \pi/\Delta k_z$. The beating observed in the intensity of Kiessig fringes is given by the details of the electron density profile of the film, as seen in the inset in Figure 1.8. Because the specular reflectivity of layered film is sensitive to small changes in the electron density profile as well as the ability to resolve the structure of films on the sub-nanometer scale, makes this a very powerful tool to characterize block copolymer thin films.

Grazing incidence small angle scattering, GISAXS, is a method to characterize at nanostructured thin films.[37-39] Like SAXS, GISAXS has the ability to extract information about in the plane of the film, but, like reflectivity, GISAXS also gives information about the structure of the film in the direction of the surface normal. In GISAXS a monochromatic x-ray beam impinges onto a surface an angle near the critical

angle of the film. However, unlike specular reflectivity, additional information is extracted from angles in and out of the plane of incidence. The geometry for GISAXS is shown in Figure 1.9.

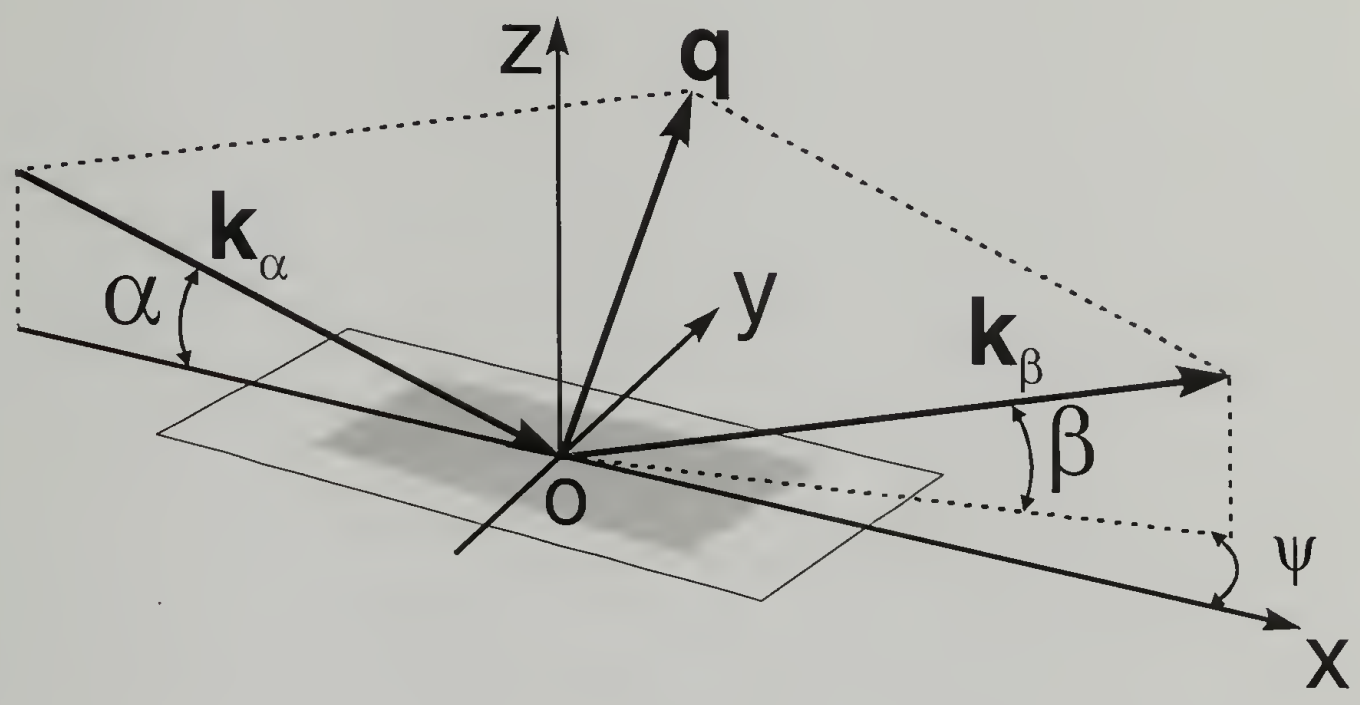

Figure 1.9 A schematic of the geometry for a GISAXS experiment.

Where α is the incident angle, β is the reflected angle in the z direction, ψ is the scattering angle off the plane of incidence, and q is the scattering vector. True GISAXS is taken at or below the critical angle, α_c, of the film, where there is total external reflection. The scattering observed here is from objects on the surface of the film as well as a small depth below the surface caused by the scattering from an evanescent wave that extends a few tens of nanometers into the film. The depth, Λ, of the wave is described in Equation 1.12, where δ is the absorption coefficient.

$$\Lambda = \frac{\lambda}{2\pi\sqrt{2}}\left[\sqrt{\left(\alpha^2 - \alpha_c^2 + 4\delta^2\right)} - \left(\alpha^2 - \alpha_c^2\right)\right]^{-1/2} \qquad \textbf{(1.12)}$$

At angles above the critical angle the depth of penetration of the x-ray beam into the film increases rapidly. This is sometimes referred to as glancing angle small angle x-ray scattering, GASAXS, however, GISAXS is often used for both cases in the literature. This ablility to probe different amounts of the film is an significant advantage in characterizing nanostructured films.

The distorted wave Born approximation, DWBA, is used to take in account for the reflections at the substrate before and after scattering. Typically four cases are included in the DWBA and are diagrammed in Figure 1.10. In black are the incident and reflected beams, while in red and blue are the scattered beams, which may or may not have a component out of the plane of incidence. It should be noted that the like colored beams have the same exit angle from the film. In fact, this causes an offset in two identical lattices, which to first approximation $\Delta\beta = 2(\alpha^2-\alpha_c^2)^{1/2}$. The scattering intensity

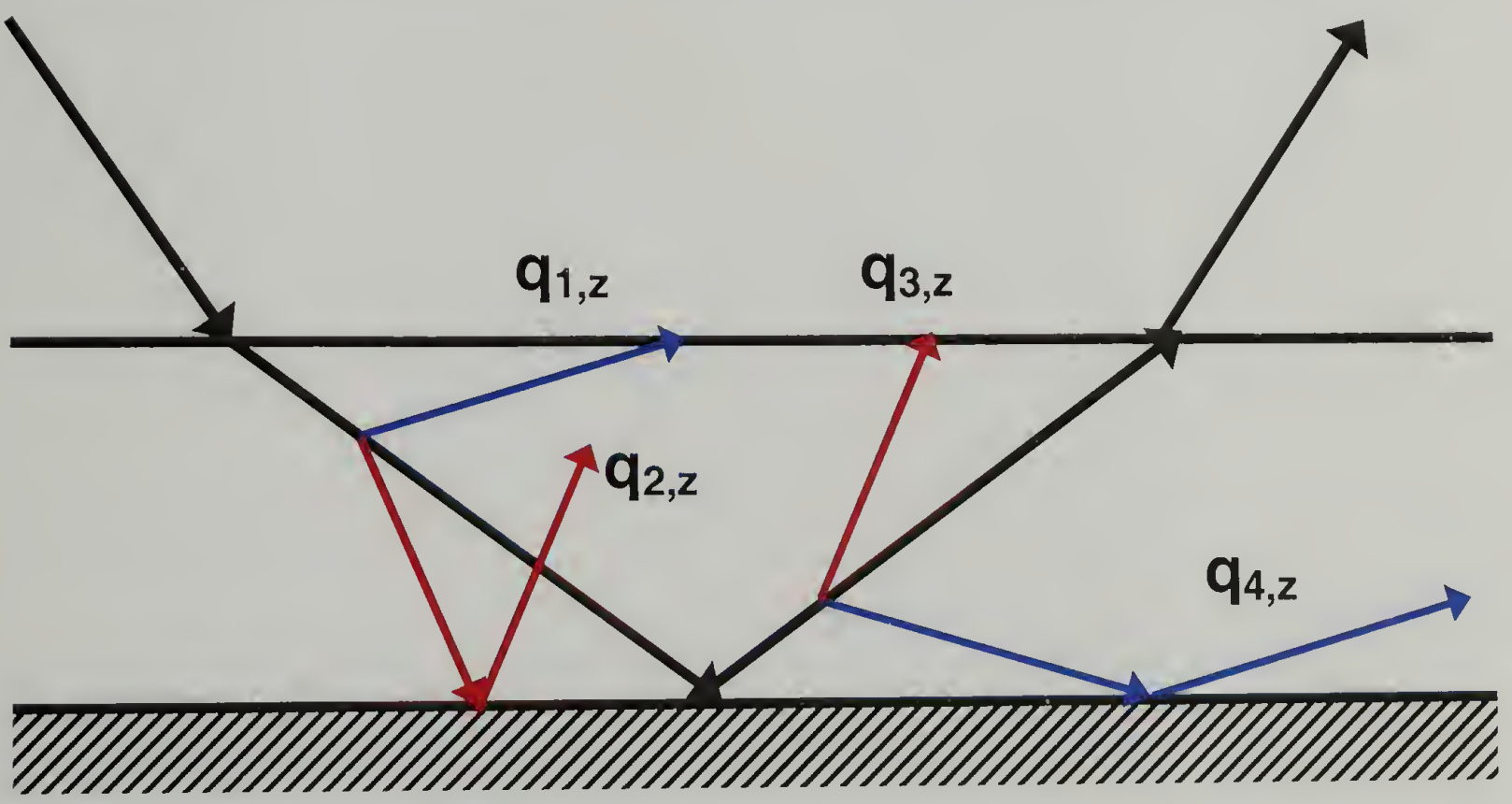

Figure 1.10 A schematic of the contributions to the DWBA.

from GISAXS, I_{GISAXS}, is a combination of scattering from the incident and reflected beams augmented by the transmission and reflectivity coefficients for each scattered beam. Complete derivations are available in the literature for 2-D films and 3-D films, shown here is an example for a film with a 3-D structure and form factor in Equation 1.13.[39]

$$I_{GISAXS} = \frac{1 - e^{-2\,\mathrm{Im}(q_z)d}}{32\pi^2\,\mathrm{Im}(q_z)} \left[\begin{array}{l} \left|T_i T_f\right|^2 I\left(q_{\parallel}, \mathrm{Re}\left(q_{1,z}\right)\right) + \left|T_i R_f\right|^2 I\left(q_{\parallel}, \mathrm{Re}\left(q_{2,z}\right)\right) + \\ \left|T_f R_i\right|^2 I\left(q_{\parallel}, \mathrm{Re}\left(q_{3,z}\right)\right) + \left|R_i R_f\right|^2 I\left(q_{\parallel}, \mathrm{Re}\left(q_{4,z}\right)\right) \end{array} \right] \qquad \textbf{(1.13)}$$

Where the subscripts i and f indicate the transmission and reflectivity coefficients before and after scattering, respectively. I is from Equation 1.10 and $q_{1,z} = k_{z,f} - k_{z,i}$, $q_{2,z} = -k_{z,f} - k_{z,i}$, $q_{3,z} = k_{z,f} + k_{z,i}$, and $q_{4,z} = -k_{z,f} + k_{z,i}$. Additional factors can be incorperated into these models, such diffuse scattering from surface roughness and additional effects from wave guiding inside the film.

While the calculations involved in simulating a 2D GISAXS pattern can be daunting, a great deal of information can be extracted from making selective line scans and a visual inspection of experimental data, making this GISAXS a very powerful tool to characterize block copolymer thin films.

1.3 References

1. Flory, P. J. *Principles of Polymer Chemistry,* Cornell University Press, Ithaca, NY, 1953.
2. Bates, F. S.; and Fredrickson, G. H. *Physics Today,* **1999,** 32.
3. Seul, M.; Andelman, D. *Science,* **1995**, *267*, 476.
4. Bates, F. S. *Science,* **1991**, *251*, 898.
5. Fredrickson, G. H.; Bates, F. S. *Annu. Rev. Mater. Sci.,* **1996**, *26*, 501.

6. Shibayama, M.; Hashimoto, T.; Hasegawa, H.; Kawai, H. *Macromolecules,* **1983**, *16(9)*, 1427-33.

7. Banaszak, M.; Whitmore, M. D. *Macromolecules,* **1992**, *25*, 3406.

8. Hanley, K. J.; Lodge, T. P.; Huang, C. I. *Macromolecules,* **2000**, *33(16)*, 5918-5931.

9. Thurn-Albrecht, T.; Schotter, J.; Kästle, G. A.; Emley, N.; Shibauchi, T.; Krusin-Elbaum, L.; Guarini, K.; Black, C. T.; Tuominen, M. T.; Russell, T. P. *Science,* **2000**, *290*, 2126-2129.

10. Li, R. R.; Dapkus, P. D.; Thompson, M. E.; Jeong, W. G.; Harrison, C.; Chaikin, P. M.; Register, R. A.; Adamson, D. H. *Appl. Phys. Lett.,* **2000**, *76*, 1689-1691.

11. Shin, K.; Leach, K. A.; Goldbach, J. T.; Kim, D. H.; Jho, J. Y.; Tuominen, M.; Hawker, C. J.; Russell, T. P. *Nano Letters,* **2002**, *2*, 933-936.

12. Park, M.; Harrison, C.; Chaikin, P. M.; Register, R. A.; Adamson, D. H. *Science,* **1997**, *276*, 1401-1404.

13. Thurn-Albrecht, T.; Steiner, R.; DeRouchey, J.; Stafford, C. M.; Huang, E.; Bal, M.; Tuominen, M.; Hawker, C. J.; Russell, T. P. *Advanced Materials* **2000**, *12*, 787-790.

14. Harrison, C.; Angelescu, D. E.; Trawick, M.; Cheng, Zhengdong, Huse, D. A.; Chaikin, P. M.; Vega, D. A.; Sebastian, J. M.; Register, R. A.; Adamson, D. H. *Europhysics Letters,* **2004**, *67*, 800-806.

15. Segalman, R. A.; Yokoyama, H.; Kramer, E. J. *Advanced Materials,* **2001**, *13*, 1152-1155.

16. Morkved, T. L.; Lu, M.; Urbas, A. M.; Ehrichs, E. E.; Jaeger, H. M.; Mansky, P.; Russell, T. P. *Science,* **1996**, *273*, 931-933.

17. Park, C.; De Rosa, C.; Thomas, E L. *Macromolecules,* **2001**, 34, 2602-2606.

18. Segalman, R. A.; Hexemer, A.; Hayward, R. C.; Kramer, E. J. *Macromolecules,* **2003**, *36*, 3272-3288.

19. Angelescu, D. Waller, J. H.; Register, R. A.; Chaikin, P. M. *Advanced* Materials, **2005**, *17*, 1878-1881.

20. Bodycomb, J.; Funaki, Y.; Kimishima, K.; Hashimoto, T. *Macromolecules,* **1999**, *32*, 2075-2077.

21. Dimarzio, E. A., Gibbs, J. H. *J. of Poly. Sci. Part A,* **1963**, *1*, 1417-1428.

22. Chow, T. S. *Macromolecules,* **1980**, *13*, 362-364.

23. Shibayama, M., Hashimoto, T., Hasegawa, H., Kawai, H. *Macromolecules,* **1983**, *16*, 1427-1433.

24. Fredrickson, G. H., Leibler, L. *Macromolecules,* **1989,** 22, 1238-1250.

25. Lodge, T. P., Pan, C., Jin, X., Liu, Z., Zhao, J., Maurer, W. W., Bates, F. S. *J. of Poly. Sci. Part B,* **1995**, *33*, 2289-2293.

26. Kim, G., Libera, M. *Macromolecules,* **1998**, 31, 2569-2577.

27. Lin, Z., Kim, D. H., Wu, X., Boosahda, L., Stone, D., LaRose, L., Russell, T. P. *Advanced Materials* **2002**, *14*, 1373-1376.

28. Wang, Y.; Song, R.; Li, Y.; Shen, J. *Surface Science,* **2003**, *530(3)*, 136-148.

29. *Dimension 3000 Instruction Manual*, Digital Instruments, Inc. Santa Barbara, CA, 1996.

30. Connell, S. D.; Collins, S.; Fundin, J.; Yang, Z.; Hamley, I. W. *Langmuir,* **2003**, *19(24)*, 10449-10453.

31. *Taking the Mystery Out of Thin-Film Measurement*, Filmetrics, Inc. San Diego, CA.

32. Tompkins, H. G. *A Users Guide to Ellipsometry*, Academic Press, Inc. San Diego, CA, 1993.

33. Alexander, L. E. X-Ray Diffraction Methods in Polymer Science, Wiley & Sons, Inc., New York, 1969.

34. Leibler, L. *Macromolecules*, **1980,** *13,* 1602-1617.

35. Russell, T. P. *Physica B*, **1996**, *221*, 267-283.

36. Xu, T.; Goldbach, J. T.; Misner, M. J.; Kim, S. H..; Gibaud, A.; Gang, O.; Ocko, B.; Guarini, K. W.; Black, C. T.; Hawker, C. J.; Russell, T. P. *Macromolecules,* **2004**, *37(8)*, 2972-2977.

37. Lazzari, R. *J. Appl. Cryst.*, **2002**, *35,* 406-421.

38. Lee, B.; Yoon, J.; Oh, W.; Hwang, Y.; Heo, K.; Jin, K. S.; Kim, J.; Kim, K W.; Ree, M. *Macromolecules,* **2005**, *38(8)*, 3395-3405.

39. Lee, B.; Park, I.; Yoon, J.; Park, S.; Kim, J.; Kim, K. W.; Chang, T.; Ree, M. *Macromolecules,* **2005**, *38(10)*, 4311-4323.

CHAPTER 2

LONG-RANGE ORDERING OF DIBLOCK COPOLYMERS INDUCED BY DROPLET PINNING

2.1 Introduction

Block copolymers self-assemble into well-defined morphologies having characteristic length scales of tens of nanometers[1]. Well-ordered, highly-aligned block copolymer films provide a simple route to nanoscopic templates that are finding uses in emerging applications[2-5], such as ultrahigh-density storage media[6] and quantum dot arrays[7]. By varying film thickness,[8,9] controlling interfacial interactions[10], or applying external fields, such as electrical fields[11], diblock copolymer microdomains can be readily oriented in thin films. In addition, directed self-assembly has been shown to be effective in controlling two-dimensional domain alignment[12-16]. However, attaining highly-oriented arrays with long-range lateral order requires coupling of more than one field in orthogonal directions.

Solvent evaporation presents a simple route in controlling the alignment of the microdomain morphology of block copolymers. Evaporation of solvent is highly directional, i.e. normal to the surface. In addition, the solvent imparts substantial mobility to the polymer and flow of the solution can be used to induce orientation. The solvent also mediates interactions between the segments of the copolymer and reduces differences in the surface energies of the components. With a material that can order, as in the case of a block copolymer, the morphology obtained upon evaporation of the solvent are, in general, trapped far from an equilibrium state. Multiple kinetic processes

are in play, including the ordering and orientation of the microdomains, and the vitrification or crystallization of one of the components. As such, when mobility is imparted to the system, as when the polymer is heating above it glass transition temperature, the morphology will change. Much previous work has focused on controlling the rate of solvent evaporation[17-20] and phase behavior[21-26]. Here, a method is described where long-range order in arrays of cylindrical microdomains of a diblock copolymer, oriented parallel to the surface, can be achieved. By pinning a solution droplet on a substrate, the evaporation of the solvent naturally produces two orthogonal fields: a strong flow of the solution within the droplet directed towards the pinned edge and an ordering front that initiates at the surface and propagates into the droplet. The coupling of these two fields produces highly-orineted, ordered arrays of cylindrical microdomains oriented parallel to the surface where the ordering persists over large lateral distances.

2.2 Experimental

PS-PBD (Polymer Source Inc.), having a styrene weight fraction of 0.68 and weight average molecular weight of 42 kg/mol and polydispersity of 1.03, was dissolved into MEK (1 wt%). One drop, about 20-50μL, of solution was placed on a silicon wafer that was tilted a few degrees and surrounded by an MEK reservoir in glass container, which was slightly open along the edge. After 15 hours, the samples were removed from the container.

SFM images were obtained in both height and phase contrast modes using a Digital Instruments Dimension TM 3000 scanning force microscope in tapping mode. TEM

images were obtained by staining the films with OsO_4. The films were embedded in resin, cured at 60°C, and then removed from the substrate by immersion in liquid nitrogen and fractured. The embedded films were then microtomed at room temperature and examined on a JEOL 2000KX transmission electron microscope at 100 kV. Sample thicknesses at different points in the film were measured by interference microscopy, TEM, and optical ellipsometry.

2.3 Results and Discussion

Maxwell first addressed contact line deposits in an evaporating drop in 1877.[27] As coffee dries on the countertop, it has recently been reported, both experimentally and theoretically, that contact line pinning and evaporation from the edge of a droplet cause the outward flow of solvent and the migration of solute to the edge.[28,29] In the case of a block copolymer solution, this flow, normal to the pinned contact line, leads to well-ordered, highly-aligned arrays of cylindrical microdomains over lateral length scales of several tens of micrometers. A drop of polystyrene-polybutadine (PS-PBD) diblock copolymer solution in methyl ethyl ketone (MEK) is placed on a silicon substrate in a chamber in the presence of a small reservoir of MEK to slow the evaporation. The substrate is slightly tilted so that the lower drop line spreads down the slide and the upper contact line remains pinned, as shown schematically in Figure 2.1A. Elevated evaporation rate at the pinned edge of the drop causes solution migration to the pinned edge as shown in Figure 2.1B. Thus, the thicknessof the pinned edge, as measured by interference colors and TEM, becomes much greater (a few microns) than that of the film interior (about 300 nm), as schematized in Figure 2.1C. The interior of the film has a

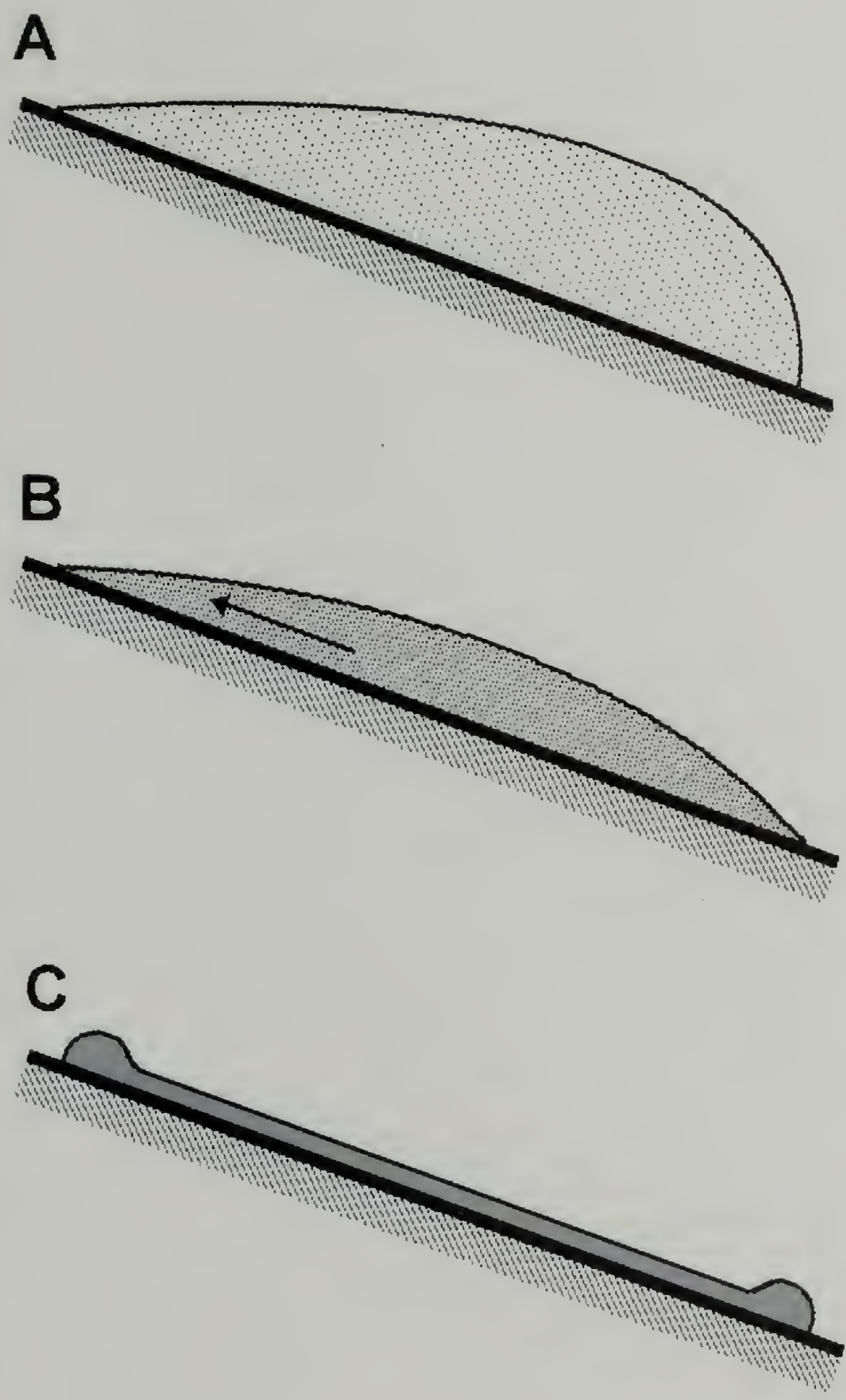

Figure 2.1 Schematic diagrams of: (A) a droplet of a block copolymer solution on a tilted substrate where the solution is pinned to the substrate; (B) a droplet as the solvent evaporates with the outwards flow of the solution indicated by the arrow ; and (C) the copolymer film after the solvent is fully evaporated.

uniform thickness and the droplet size is on the order of one to two centimeters.

The flow field in the direction of the pinned edge, generated by solvent evaporation, defines the orientation of the cylindrical microdomains and the degree of order. The tilting of the substrate is used to enhance the flow towards the pined edge. SFM images just inside the thick edge (Figure 2.2A) show that the cylinders are oriented parallel to the surface plane. Both components are present at the surface, due to the higher solubility of PS in MEK and the reduced difference in the surface energies of the components, since they are both swollen with MEK. The in-plane orientation of the cylindrical microdomains is normal to the pinned edge and, therefore, parallel to the flow direction within the drop. The series of SFM images in Figure 2.2A were taken just inside the thick, pinning edge, and shows that order and orientation are maintained over at least 20 μm. This is a remarkably large distance considering the simplicity and speed of the process. Due to the long-range over which the domains remain in register, it is difficult to see the individual domains in the large image. Consequently, several higher-magnification images taken across the film are shown to demonstrate the order and orientation.

As the strength of the flow field within the drop weakens with increasing distance from the pinning line, the degree of orientation and the grain size of the microdomain morphology decreases. An islands and hole topography is also seen, due to the commensurability between the film thickness and the natural period of the copolymer[30]. Figure 2.2B is a reflection optical interference micrograph of the film after complete

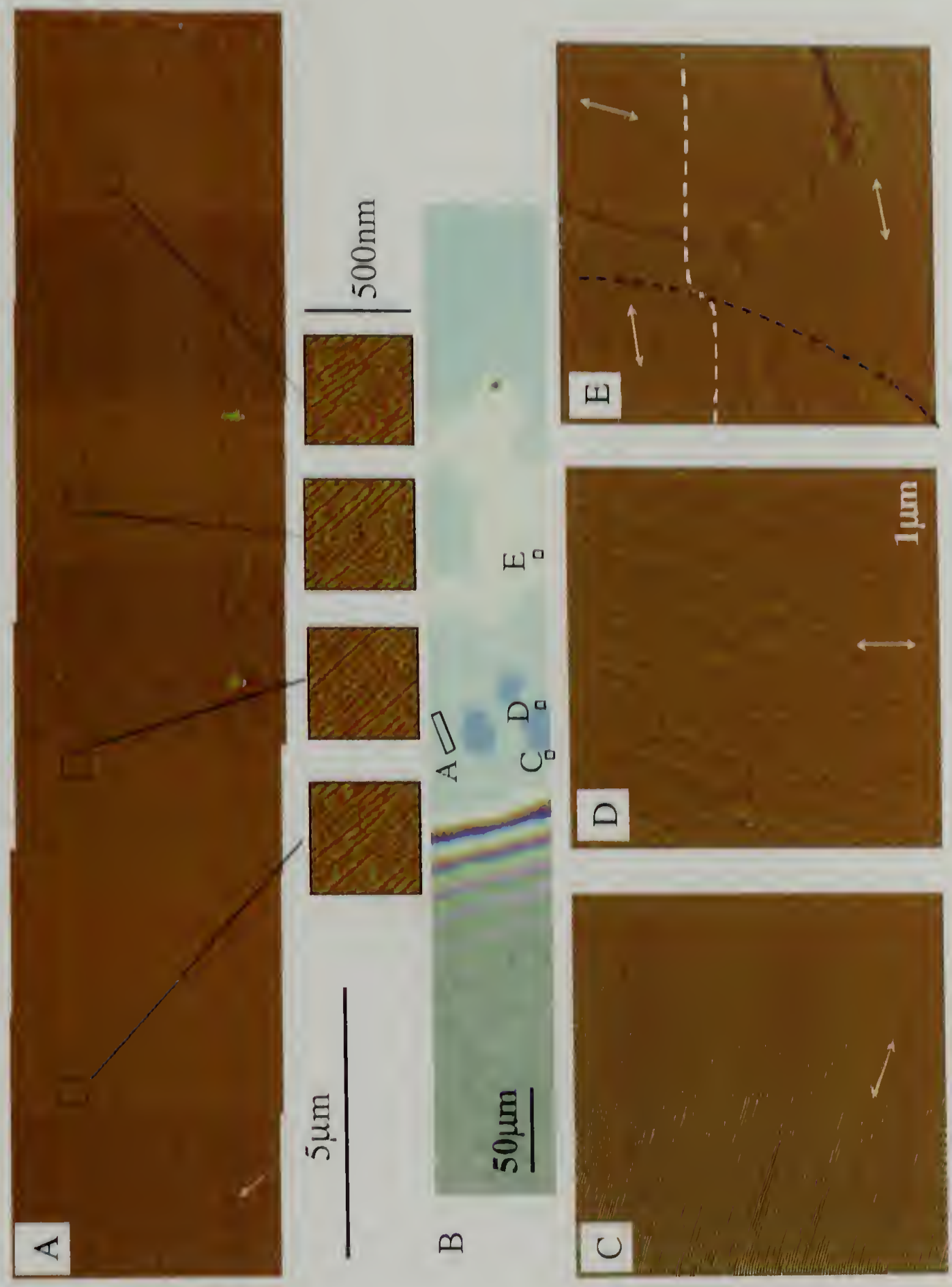

Figure 2.2 (A) SFM phase images of a PS-PBD block copolymer film obtained from droplet pinning. The series of joined micrographs were obtained where noted in the optical micrograph. Magnifications of selected areas of the images are shown to illustrate the ordering and orientation of the cylindrical microdomains. (B) Optical interference micrograph of the block copolymer film. Colors correspond to film thickness. (C, D) SFM phase images from the areas indicated on the optical micrograph. (E) SFM phase image obtained from the area indicated in the optical micrograph. The black dotted line shows the edge of an island, as noted by the dashed white line, a profile obtained by SFM.

evaporation of the MEK. The interference colors correspond to different film thickness and the discrete color changes of the islands and holes correspond to a thickness change of one period of the copolymer morphology. A series of SFM images, taken at different positions on the film, is shown in Figures 2C-E. Figure 2.2C was obtained from just within the pinning edge, where a defect-free ordering is seen parallel to the flow field. Further into the film (Figure 2.2D), the grains of the cylindrical domains, while highly ordered, lose the orientation with respect to the flow field. The SFM height profile (denoted by the white line in the image) in Figure 2.2E shows that the grain boundaries and the orientation of the microdomains are not correlated with the topography. As shown, the orientation of the microdomains can be preserved across step-height changes in the topography. Conversely, changes in the grain orientation are seen with no change in the topography. Taken together, these data show that the strength of the flow field within the drop as the solvent evaporates plays a key role in the orientation of the copolymer microdomains. Since the center-to-center domain spacing of the copolymer microdomains in these films (~36 nm as measured by SFM) is greater than that obtained by small angle x-ray scattering (SAXS) from a bulk sample (L_o = 31 nm), the morphology of the cast films are clearly in a non-equilibrium state.

The direction of the evaporative flow is also important. THF, like MEK, is a selective solvent for PS, but has a higher vapor pressure and, consequently, the evaporation rate is much faster. This leads to a more rapid migration of an ordering from the free-surface that results in orientations of the cylindrical microdomains both normal to and parallel to the film surface (not shown). This is consistent with the results reported by Kim and

Libera[19] where rapid solvent evaporation was shown to produce a vertical orientation of the copolymer microdomains, whereas a slow evaporation yielded a parallel orientation.

Figure 2.3 shows transmission electron microscope (TEM) images of microtomed cross-sections of the copolymer films after staining with OsO_4. In the TEM image, the brighter and darker areas correspond to the PS matrix and OsO_4 selectively stained PBD cylinders, respectively. In Figure 2.3A and Figure 2.3B cross-sections of the film are shown where the cutting directions were parallel to and perpendicular to the edge, respectively. As seen, the PBD cylinders are hexagonally packed, oriented parallel to the film surface and perpendicular to the pinning line (the edge of the film). The ordering of the cylindrical microdomains spans the entire film thickness. Both PS and PBD are located at the free surface, even though the surface energy of PBD is less than that of PS. This results from the preferential solubility of the PS block in MEK and a reduction in the difference in the surface energies due to the presence of the MEK. The morphology in Figure 2.3C is consistent with the in-plane order demonstrated in the SFM images in Figure 2.2. It should be noted that there is some elongation of the cylindrical domains in the cutting direction of the section. The rough edge at the bottom of the micrographs, corresponding to the film-substrate interface, arises from the removal of the film from the substrate by freeze fracturing after embedding in an epoxy resin.

From the micrographs in Figure 2.3 it appears that the microphase separation of the copolymer is better defined at the free surface than at the substrate. This, however, results from the sample preparation. The micrograph in Figure 2.4, taken from a different sample, shows the defect-free ordering and orientation of the copolymer microdomains throughout the sample. Half-cylinders of PBD at the free surface are, also, clearly seen

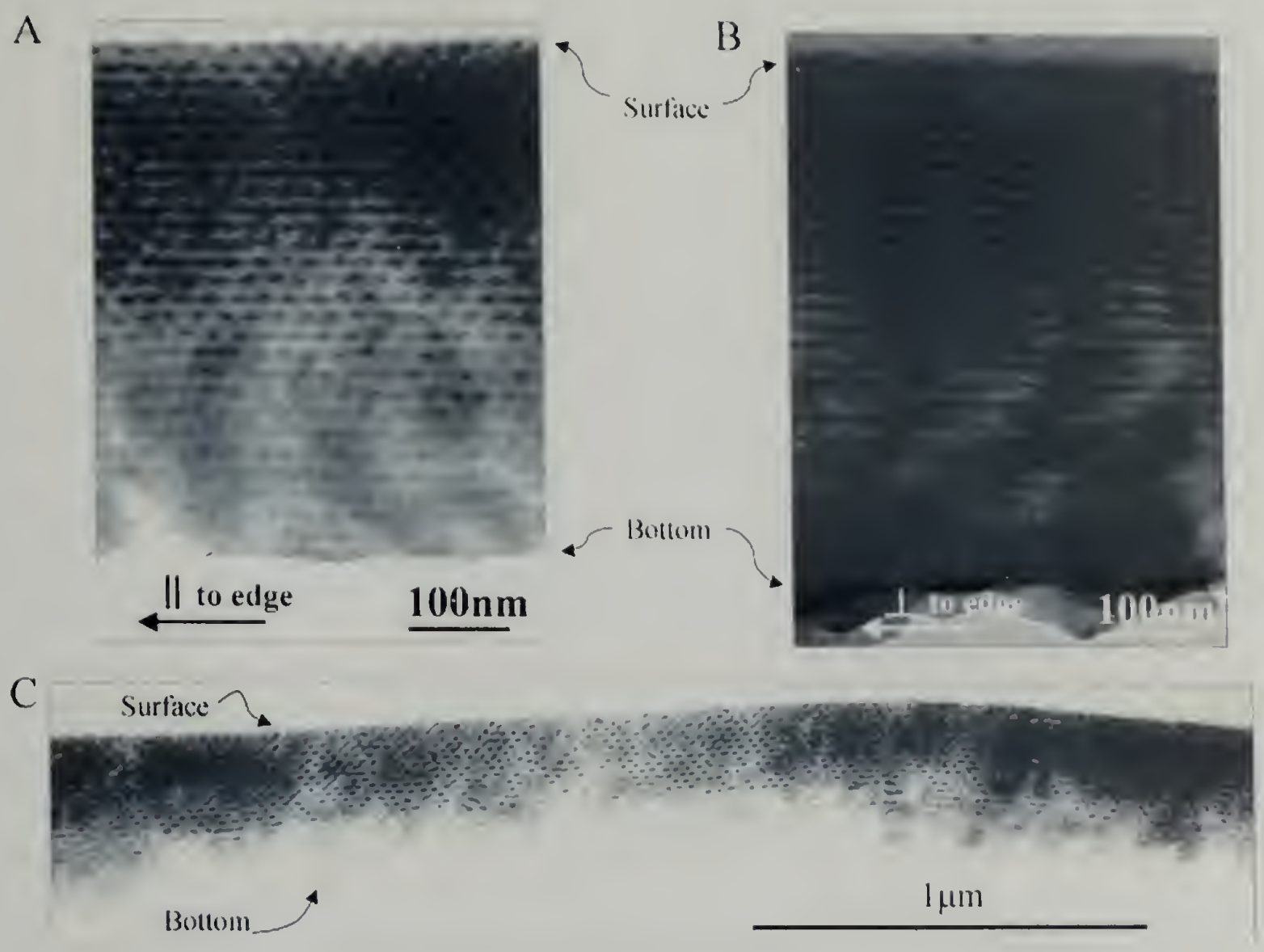

Figure 2.3 TEM of a thin cross-sections of the copolymer film where the cutting direction was (A, C) parallel and (B) normal to the film edge, i.e. normal to the flow direction of the copolymer solution in the droplet during evaporation. The film was stained with OsO_4 to enhance the contrast. In each the magnifications are indicated and the darker regions correspond to the PBD block.

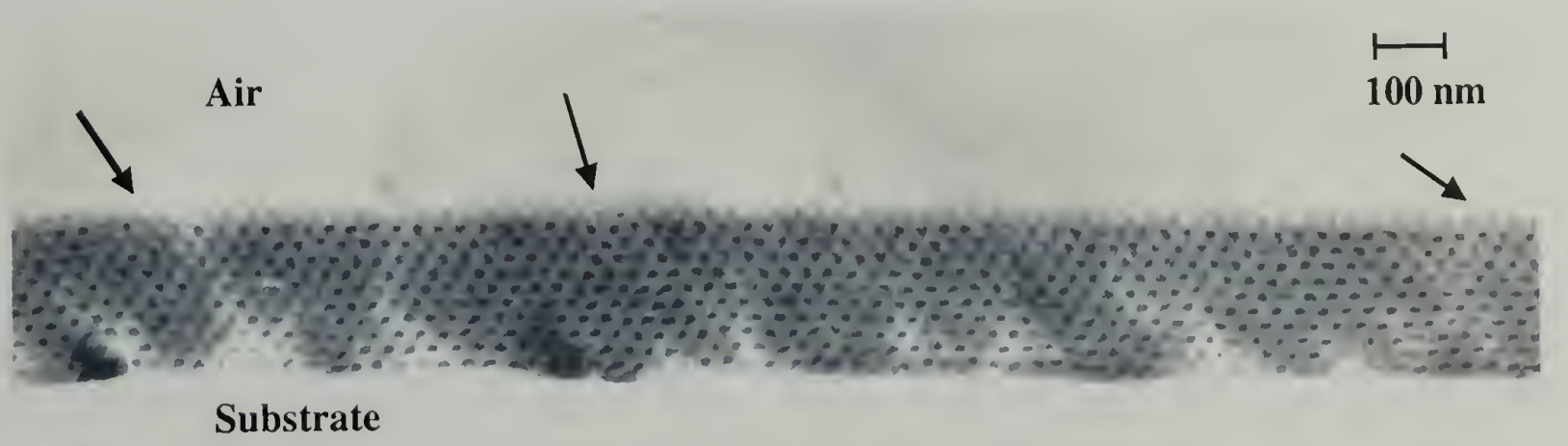

Figure 2.4 TEM of a thin cross-section of the copolymer film where the cutting direction is parallel to the pinning edge. The film was stained with OsO_4 and the darker regions correspond to the PBD block. Indicated in the image are locations of the substrate and air and examples of half-cylinders at the air surface (arrows).

(indicated by arrows). Consequently, both components are located at the surface during evaporation, due to the influence of the MEK on the surface energy.

2.4 Conclusions

In summary, the pinning of a droplet on a surface coupled with solvent evaporation affords a simple route to produce well-ordered, highly-aligned, cylindrical microdomains in thin block copolymer films that are oriented parallel to the substrate. The pinning of the drop causes a highly directional flow within the droplet, normal to the pinned edge. The microphase separation of the copolymer, initiated at the air surface, propagates into the interior of the drop and is oriented by the flow field. The structures realized by coupling two orthogonal fields exhibit ordering over very large distances making this a promising route toward addressable arrays. The concepts outlined here are applicable to blade- and dip-coating processes where the flow rate and evaporation rate can be controlled in a continuous manner.

2.5 References

1. Fredrickson, G. H.; Bates, F. S. *Ann. Rev. Mat Sci* **1990** 1-70.

2. Mansky, P.; Harrison, C. K.; Chaikin, P. M.; Register, R. A.; Yao, N. *Appl. Phys. Lett.* **1996**, *68*, 2586-2588.

3. Park, P.; Harrison, C. K.; Chaikin, P. M.; Register, R. A.; Adamson, D. H. *Science* **1997**, *276*, 1401-1404.

4. Heier, J. Genzer, J.; Kramer, E. J.; Bates, F. S.; Walheim, S.; Krausch, G. *J. Chem. Phys.* **1999**, *111*, 11101-11110.

5. Jeong, U.; Kim, H. C.; Rodriguez, R. L.; Tsai, I. Y.; Stafford, C. M.; Kim, J. K.; Hawker, C. J.; Russell, T. P. *Adv. Mater.* **2002**, *14*, 274-276.

6. Thurn-Albrecht, T.; Schotter, J.; Kästle, G. A.; Emley, N.; Shibauchi, T.; Krusin-Elbaum, L.; Guarini, K.; Black, C. T.; Tuominen, M. T.; Russell, T. P. *Science* **2000**, *290*, 2126-2129.

7. Li, R. R.; Dapkus, P. D.; Thompson, M. E.; Jeong, W. G.; Harrison, C.; Chaikin, P. M.; Register, R. A.; Adamson, D. H. *Appl. Phys. Lett.* **2000**, *76*, 1689-1691.

8. M. S. Turner, *Phys Rev. Lett.* **1992**, *69*, 1788-1791.

9. Lambooy, P.; Russell, T. P.; Kellogg, G. J.; Mayers, A. M.; Gallagher, P. D.; Satija, S. K. *Phy. Rev. Lett.* **1995**, *72*, 2899-2902.

10. Mansky, P.; Liu, Y.; Huang, E.; Russell, T. P.; Hawker, C. *Science* **1997**, *275*, 1458-1460.

11. Morkved, T. L.; Lu, M.; Urbas, A. M.; Ehrichs, E. E.; Jaeger, H. M.; Mansky, P.; Russell, T. P. *Science* **1996**, *273*, 931.

12. Fasolka, M. J.; Harris, D. J.; Mayes, A. M.; Yoon, M.; Mochrie, S. G. *J. Phys. Rev. Lett.* **1997**, *79*, 3018-3021.

13. Rockford, L.; Liu, Y.; Mansky, P.; Russell, T. P.; Yoon, M.; Mochrie, S.G. *J. Phys. Rev. Lett.* **1999**, *82*, 2602-2605.

14. Rosa, C. D.; Park, C.; Thomas, E. L.; Lotz, B. *Nature* **2000**, *405*, 433-437.

15. Segalman, R. A.; Yokoyama, H.; Kramer, E. J. *Adv. Mater.* **2001**, *13*, 1152-1155.

16. Yang, X. M.; Peters, R. D.; Nealey, P. F.; Solak, H. H.; Cerrina, F. *Macromolecules* **2000**, *33*, 9575-9582.

17. Shibayama, M.; Hashimoto, T.; Kawai, H. *Macromolecules* **1983**, *16*, 1434-1443.

18. Kim, G.; Libera, M. *Macromolecules* **1998**, *31*, 2569-2577.

19. Fukunaga, K.; Elbs, H.; Magerle, R.; Krausch, G. *Macromolecules* **2000**, *33*, 947-953.

20. Lin, Z.; Kim, D. H.; Wu, X.; Boosahda, L.; Stone, D.; LaRose, L.; Russell, T. P. *Adv. Mater.* **2002**, *14*, 1373-1376.

21. Hahn, J.; Sibener, S. J. *Langmuir* **2000**, *16*, 47766-4769.

22. Sundrani, D. Sibener, S. J. *Macromolecules* **2002**, *35*, 8531-8539.

23. Reiter, G.; Castelein, G.; Hoerner, P.; Riess, G.; Blumen, A.; Sommer, J. U. *Phys. Rev. Lett.*, **1999**, *83*, 3844-3847.

24. Zhang, Q.; Tsui, O. K. C.; Du, B.; Zhang, F.; Tang, T.; He, T. *Macromolecules* **2000**, *33*, 9561-9567.

25. Knoll, A.; Horvat, A.; Lyakhova, K. S.; Krausch, G.; Sevink, G. J. A.; Zvelindovsky, A. V.; Magerle, R. *Phys. Rev. Lett.* **2002**, *89*, 035501-1-4.

26. Meiners, J. C.; Quintel-Ritzi, A.; Mlynek, J.; Elbs, H.; Krausch, G. *Macromolecules* **1997**, *30*, 4945-4951.

27. Fuchs, N. *Evaporations and Droplet Growth in Gaseous Media,* Pergamon, Oxford, 1951.

28. Deegan, R. D.; Bakajin, O.; Dupont, T. F.; Huber, G.; Nagel, S. R.; Witten, T. A. *Nature* **1997**, *389*, 827-829.

29. Deegan, R. D.; Bakajin, O.; Dupont, T. F.; Huber, G.; Nagel, S. R.; Witten, T. A. *Phys. Rev E* **2000**, *62*, 756-765.

30. Coulon, G.; Daillant, J.; Collin, B.; Benattar, J. J.; Gallot, Y. *Macromolecules* **1993**, *26*, 1582-1589.

CHAPTER 3

HIGHLY ORIENTED AND ORDERED ARRAYS FROM BLOCK COPOLYMERS VIA SOLVENT EVAPORATION

3.1 Introduction

The use of self-assembly to obtain well-ordered structures has attracted increasing interest due to the ease of accessing complex structures with small feature sizes[1–4]. Block copolymers comprised of chemically distinct polymers covalently joined at one end, self-assemble into well-defined, ordered arrays of nanoscopic domains ranging from spheres to cylinders to lamellae, depending on the volume fraction of the components.[5,6] The absolute size of the domains is defined by the molecular weight of the copolymer and the strength of the segmental interactions between the blocks. Functionality can also be introduced in the copolymer chains which opens pathways to multi-length scale ordering and, consequently, hierarchical ordering.[7, 8] Thus, block copolymers represent an extremely versatile class of materials for generating functional nanoscopic structures. However, it is essential that both the orientation and lateral ordering of the nanoscopic domains be controlled to fully realize the potential of these materials. This requires the use of external fields, such as electric fields,[9,10] shear,[11, 12] temperature gradients,[13] graphoepitaxy,[14, 15] crystallization,[16,17] chemically patterned substrate,[18-21] or controlled interfacial interactions.[22,23] Solvent evaporation is also a strong, highly directional. Libera and Kim demonstrated that the rate of solvent evaporation from thin, solution-cast films of block copolymers could be used to manipulate the growth and orientation of copolymer assemblies[24,25]. Ham and Sibener and coworkers[26] and

Kimura *et al.*[27] have also shown that evaporation-induced flow in solvent-cast block copolymer films can produce arrays of nanoscopic cylindrical domains having a high degree of in-plane orientation and lateral order. Krausch and coworkers recently showed that solvent annealing could markedly enhance the ordering of copolymer morphologies in very thin films.[28,29] Here it is shown that, by controlling the rate of solvent evaporation or solvent annealing, an ordering of the copolymer is induced at the surface, which propagates through the entire film. The solvent imparts mobility to the copolymer enabling a rapid removal of defects. Thus, highly oriented, nearly defect-free arrays of nanoscopic, cylindrical domains are produced that span the entire film thickness and have a high degree of long-range lateral order. Similar results are found on patterned surfaces, opening routes towards large-area, addressable ultrahigh-density arrays of nanoscopic elements.

3.2 Experimental

Polystyrene-*block*-poly(ethylene oxide) copolymer, PS-*b*-PEO, with a molecular weight of 25.3 kg/mol and a dispersity of 1.04 was purchased from Polymer Source, Inc. The weight fraction of PS was 0.75 and, in the bulk, the copolymer self-assembles into hexagonally packed arrays of 20.7 nm diameter cylindrical PEO domains in a PS matrix with a lattice period of 31.9 nm. Thin PS-*b*-PEO films were prepared either by spin-coating or solvent-casting benzene solutions of the copolymer onto silicon wafers in a benzene vapor atmosphere. In one case the substrate contained 0.875 □m wide and 0.325 □m deep channels prepared by standard photolithographic procedures. Benzene is a good solvent for both the PS and PEO blocks. To investigate the influence of solvent on

the copolymer ordering, dried spin-coated and solution-cast films were placed in a benzene-saturated chamber at room temperature. Since the PEO block is water-soluble, studies were also performed in a water/benzene vapor environment. The thicknesses of the films were varied from tens of nanometers to microns by controlling the concentration and/or spinning speed.

GASAXS (Grazing Angle Small Angle X-ray Scattering) measurements were performed on beamline X22B at the National Synchrotron Light Source at the Brookhaven National Laboratory.

3.3 Results and Discussion

Shown in Figure 3.1A is a scanning force microscopy (SFM) phase image of a 255 nm thick, spin-coated PS-*b*-PEO film. An array of nanoscopic cylindrical domains is seen at the surface of the film, where the minor component, PEO, comprises the cylindrical domains (darker in the image) and PS, the major component, constitutes the matrix (lighter in the image). The average center-to-center distance between the cylindrical domains is 42.5 nm, which is greater than that observed in the bulk at equilibrium. As discussed previously (*29*), the cylindrical PEO domains are oriented normal to the surface of the film and span the entire film thickness. The morphology obtained by spin coating is far from equilibrium and the degree of lateral order is low. By placing the film in benzene vapor at room temperature, the films swells (~45% by volume), and upon removal from the benzene atmosphere, the solvent evaporates and the ordering of the PEO domains is seen to improve dramatically (Figure 3.1B). The phase

A

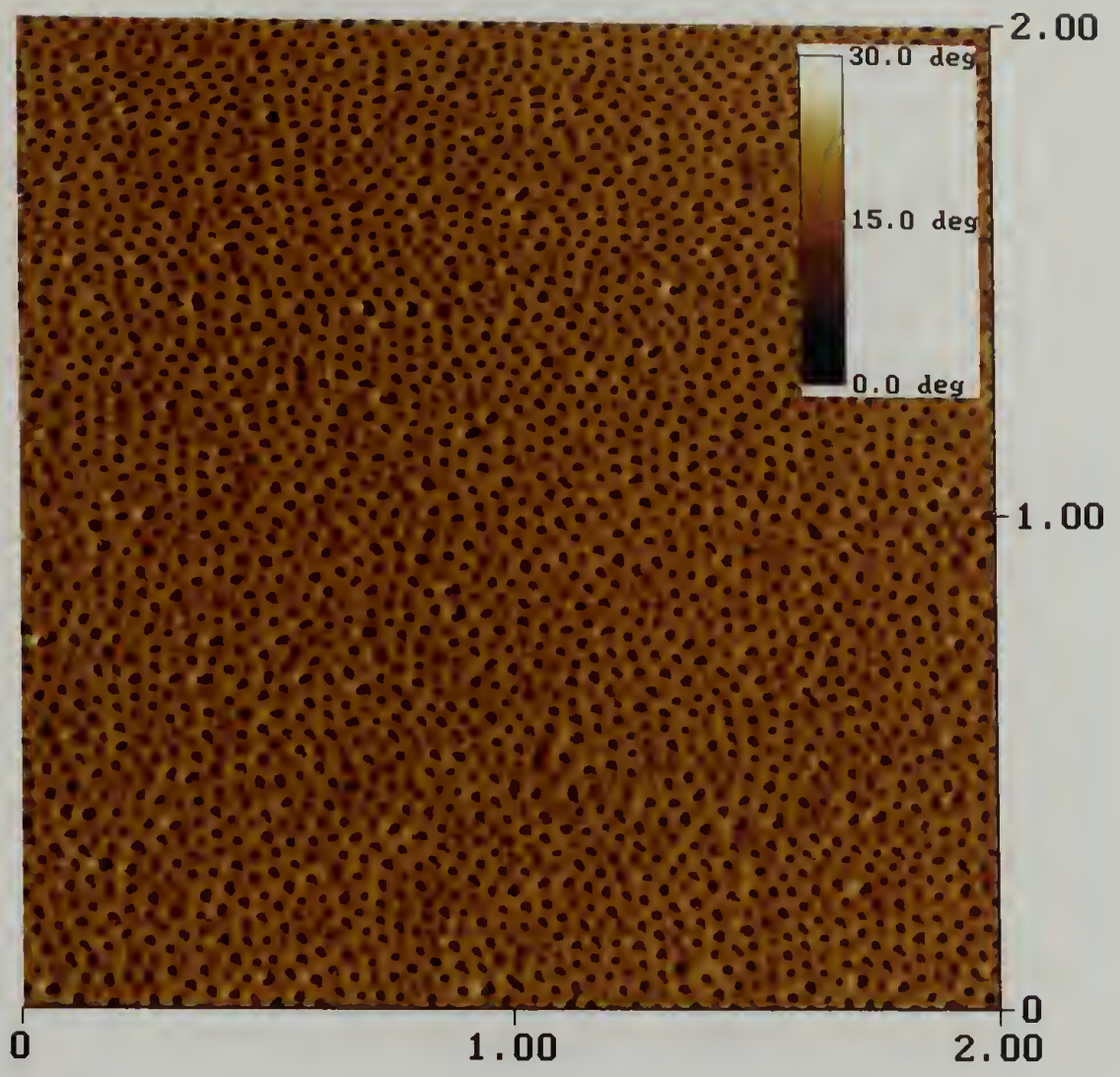

B

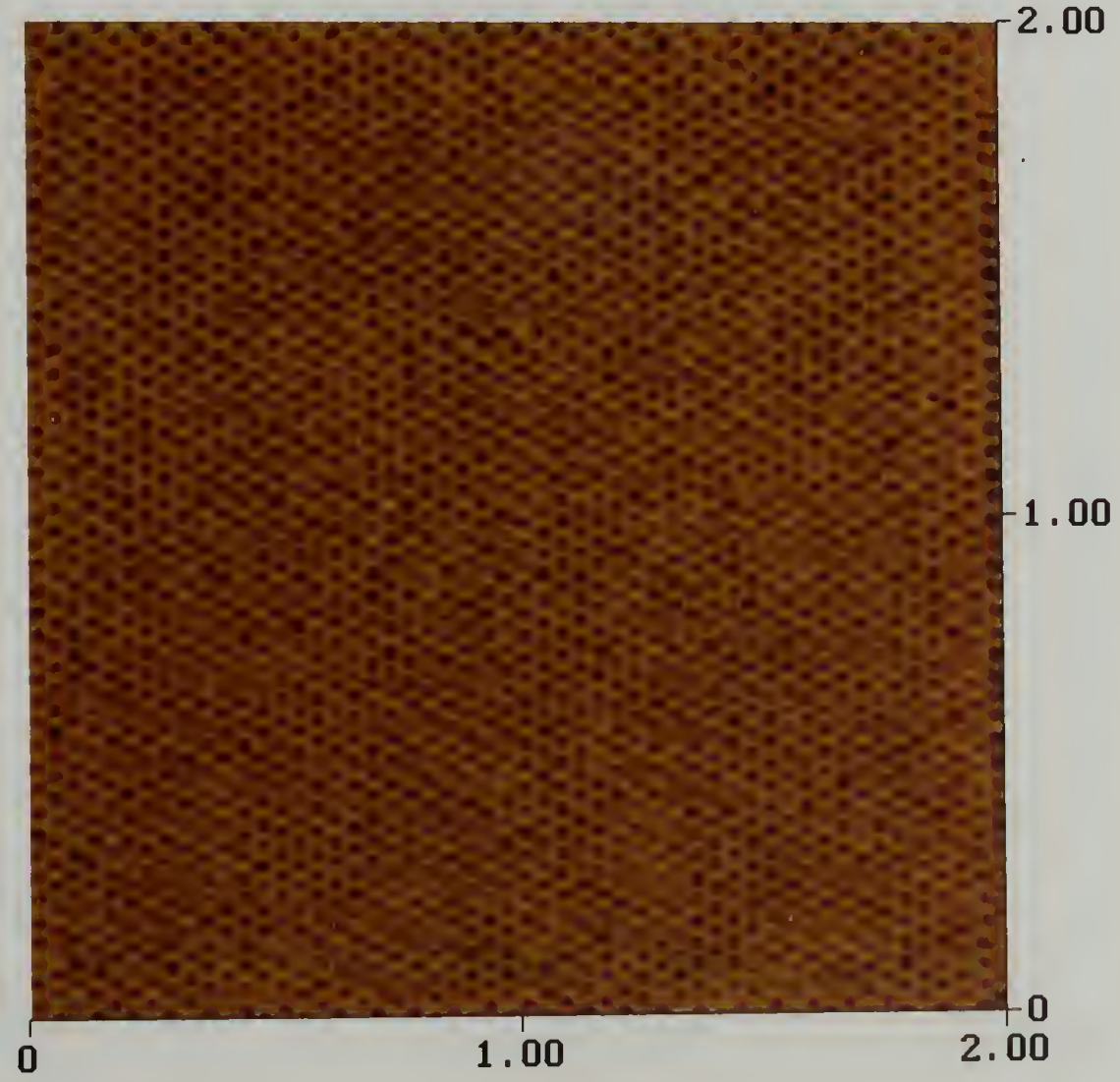

C

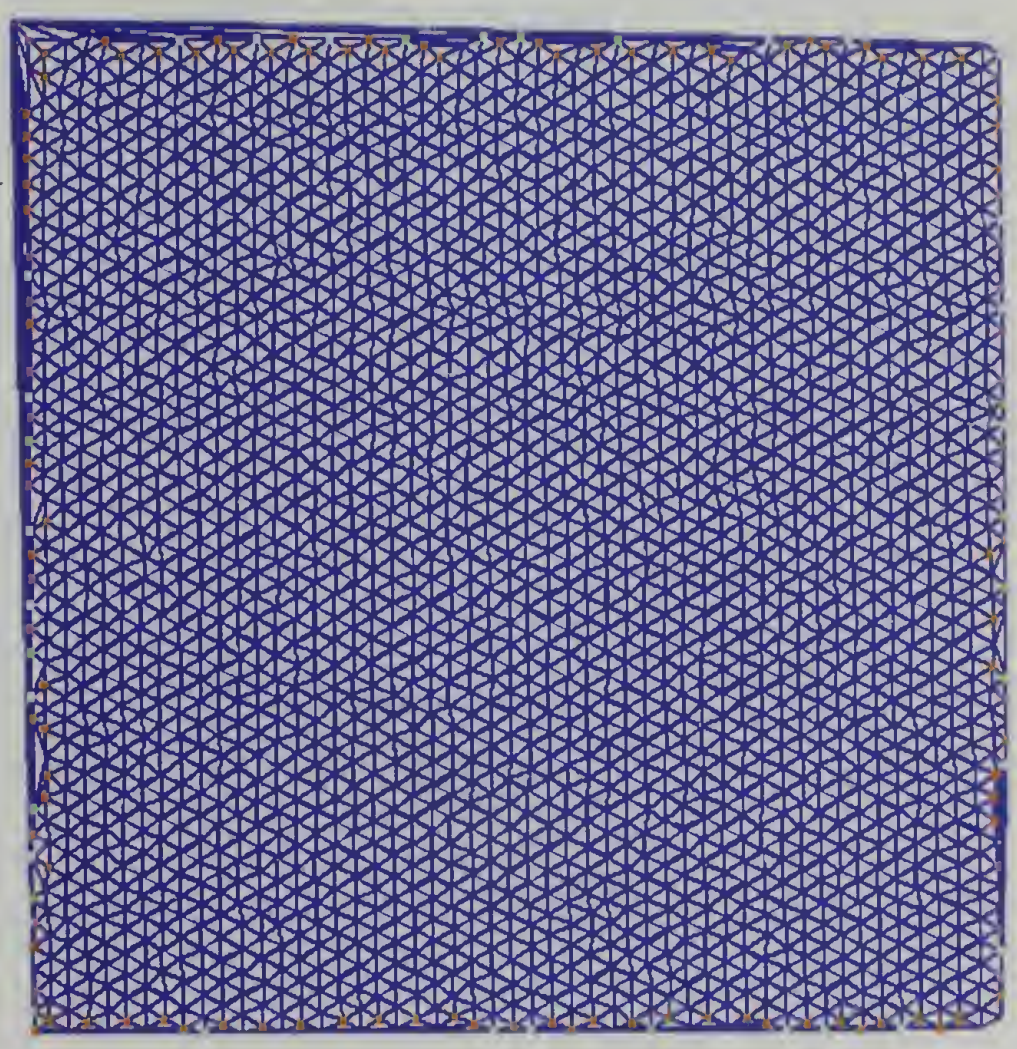

Figure 3.1. (A) A PS-*b*-EO thin film (255 nm in thickness) obtained by spin-coating: SFM phase image of a spin-coated sample, (B) SFM phase image after annealing for 48 hrs in a benzene vapor, (C) triangulation image of the SFM image shown in (B).

image shows a highly-ordered array of hexagonally-packed, cylindrical PEO domains in a glassy PS matrix with an average diameter of 23.5 nm and a lattice spacing of 43.8 nm. The perfection in the ordering of the cylindrical array is shown graphically in Figure 3.1C. Here, using software developed at Princeton University *(31)*, a triangulation routine is used where a line connects the center of adjacent cylindrical domains. Each domain with six-nearest neighbors is colored blue. Defects, where there are five or seven nearest neighbors, are colored red and yellow, respectively. As can be seen, every domain has six nearest neighbors. In addition, the high degree of translational and orientational order is evident. Consequently, this image shows a $2 \times 2\ \mu m^2$ grain of hexagonally-packed cylindrical domains. This ordering behavior exhibits strong time-dependence, as shown in Figure-2. Triangulation maps of SFM images taken after solvent annealing for 0, 6, 24, and 48 hours (A, B, C, and D respectively) demonstrate the removal of defects and growth of the grain size in the copolymer film. In Figure-2E, the number of five-neighbor defects is shown as a function of time. The density of seven-neighbor defects shows almost identical behavior. The average of number of defects was taken from five AFM images on different samples over a $2\ \mu m \times 2\ \mu m$ area. As seen, the annihilation of defects occurs very rapidly initially where, within 1 h, half of the defects have been removed. Within 6 h, the average grain size has increased to the micrometer size scale and the number of defects is over an order of magnitude smaller than initially. With increasing time, the reduction in the number of defects slows and, after 48 h, all defects have been removed from the $2\ \mu m \times \mu m$ area. The solvent imparts such mobility that, even at room temperature, after long annealing times the film will begin to

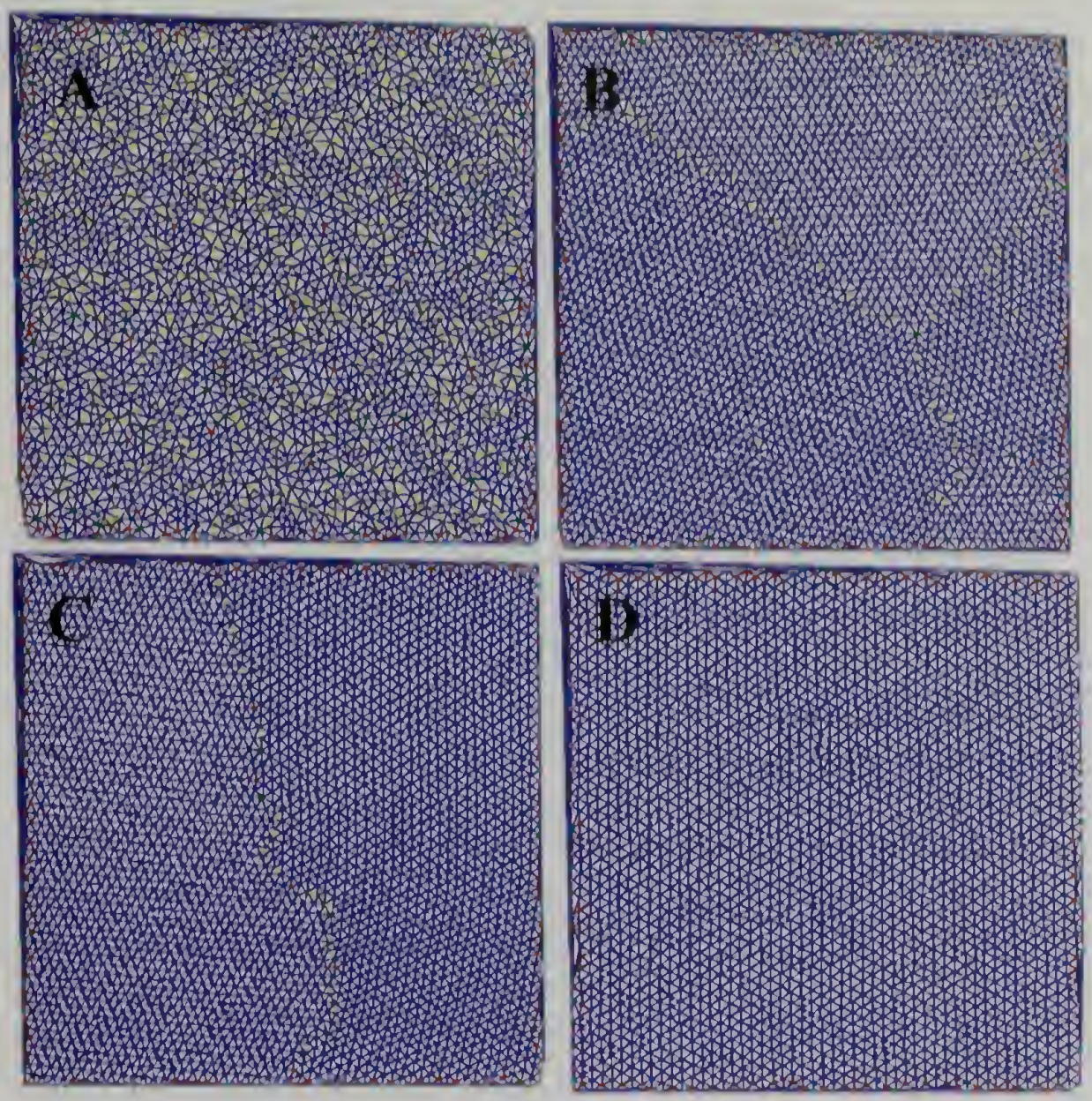

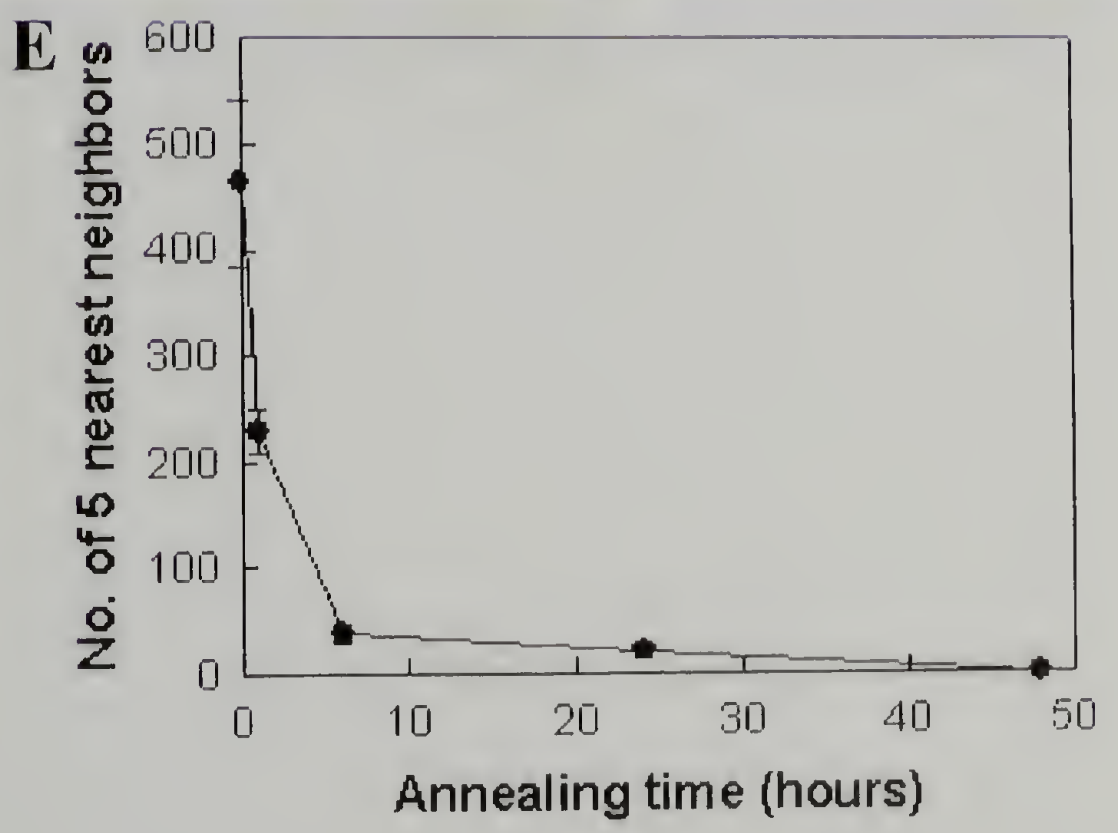

Figure 3.2. Triangulation maps of 2 μm × 2 μm SFM images after solvent annealing for A) 0 h, B) 6 h, C) 24 h, and D) 48 h. E) The number of five-neighbor defects in a 2 μm × 2 μm area as a function of annealing time in solvent vapor.

heterogeneously dewet. However, even in those regions, the film still exhibits excellent lateral order over several micrometers.

Considering the simplicity of the preparation, the degree of long-range order achieved in PS-*b*-PEO thin films is remarkable. The exposure of the film to benzene vapor causes a rapid swelling of the film by ~45%, corresponding to a copolymer volume fraction of ~0.69. Small angle x-ray scattering shows that the ordering of the copolymer is lost when the copolymer volume fraction is less than ~0.9. Thus, the initial film is disordered, and as solvent evaporates, the copolymer microphase separates into a highly ordered array of cylindrical microdomains oriented normal to the surface.

The evolution of order during the evaporation of the solvent was investigated by grazing angle small angle x-ray scattering. A schematic diagram of the scattering geometry is shown in Figure 3.3A. Here, a highly collimated, monochromatic x-ray beam impinges at an angle α_i onto the surface of the copolymer solution spread on a silicon substrate. The x-rays are specularly reflected at an angle α_f and structure within the film is seen by x-rays scattered out of the plane of incidence. Shown in Figure 3.3B is the 3-C scattering profile from a PS-b-PEO sample in the latter stages of solvent evaporation where $\alpha = 0.23^{\circ}$. A beamstop blocks all the radiation (reflected and scattered) in the plane of incidence, so that the much weaker off-specular scattering can be seen. The off-specular scattering consists of two spots parallel to the surface of the film, which is characteristic of the cylindrical microdomains oriented normal to the surface. It should be noted that no other reflections are evident, indicating that the microdomains are oriented only normal to the surface. In addition, from the two spots there are weak vertical streaks of scattering that are characteristic of cylinders of finite

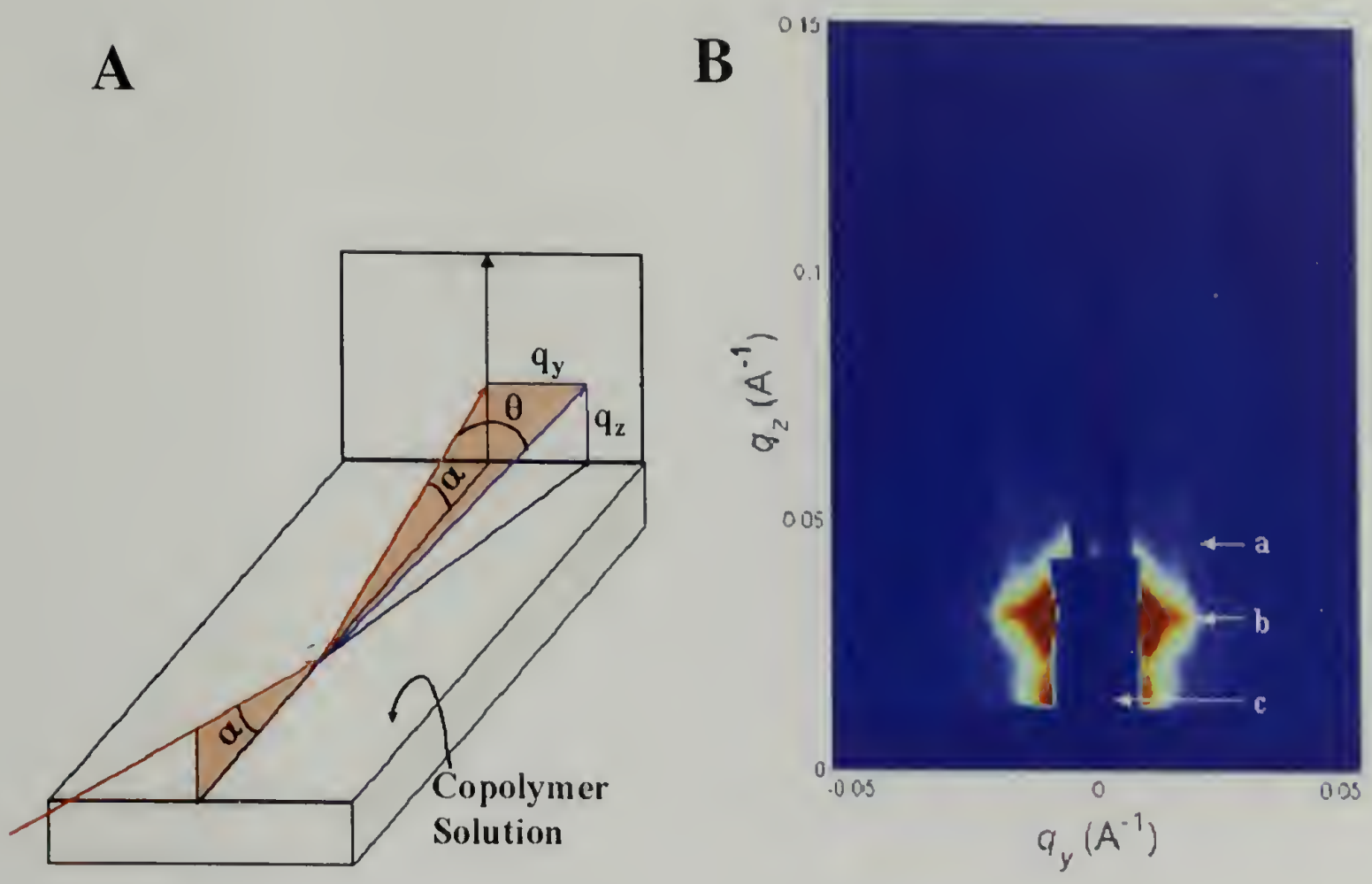

Figure 3.3. (A) Schematic diagram of the grazing angle x-ray scattering experiments where the x-rays are incident on the surface at an angle α, the specular reflection occurs at an angle α. An area detector collects all the reflected and scattered x-rays. (B) 2D x-ray scattering profile from a PS-b-PEO film during the latter stages of solvent evaporation. Indicated in the profile is (a) the scattering from the truncation of the cylinders at the film surface, (b) the scattering from the cylindrical microdomains oriented normal to the surface, and (c) the beamstop. (C) The in-plane scattering measured at an angle α as a function of time or solvent concentration.

length truncated at the surface. The time dependence of the in-plane x-ray scattering as the solvent evaporates is shown in Figure 3.3C. Initially, when the solvent concentration is high, no substantial scattering is seen. As the solvent evaporates, a diffuse reflection, typical of a phase mixed copolymer, is seen at $q=0.173\ nm^{-1}$, corresponding to a spacing d~ 41 nm. Here, $q = (4\pi/\lambda)\sin\theta$, where λ is the wavelength and θ is the scattering angle. As solvent evaporation continues, the refection intensifies. It should be noted that the peak position does not change as the copolymer microphase separates. An increase in the spacing is typically seen as ordering occurs, however, this is offset by a reduction in volume due to solvent loss. Further removal of the solvent, causes the peak to intensity further.

The lateral order achieved in thin films of PS-*b*-PEO block copolymers upon solvent casting or annealing in a solvent vapor is exceptional. The ordering is independent of the substrate, and, thereby, it must begin at the surface. In copolymers containing two highly immiscible blocks, the solvent mediates non-favorable interactions between the segments forcing the copolymer to disorder. In addition, the glass transition temperature of the solvent-swollen film is well below room temperature. As the solvent evaporates (schematically shown in Figure 3.4), the concentration of solvent at the surface is lowest and a gradient in solvent concentration develops normal to the surface. With time, the concentration of solvent at the surface decreases and a microphase separation of the PS-*b*-PEO occurs only at the surface. Since the ordered copolymer at the surface is well above Tg and there are strong nonfavorable interactions between the blocks, defects in the hexagonal packing of the cylindrical microdomains are rapidly removed. Consequently, long-range lateral order of the copolymer morphology is

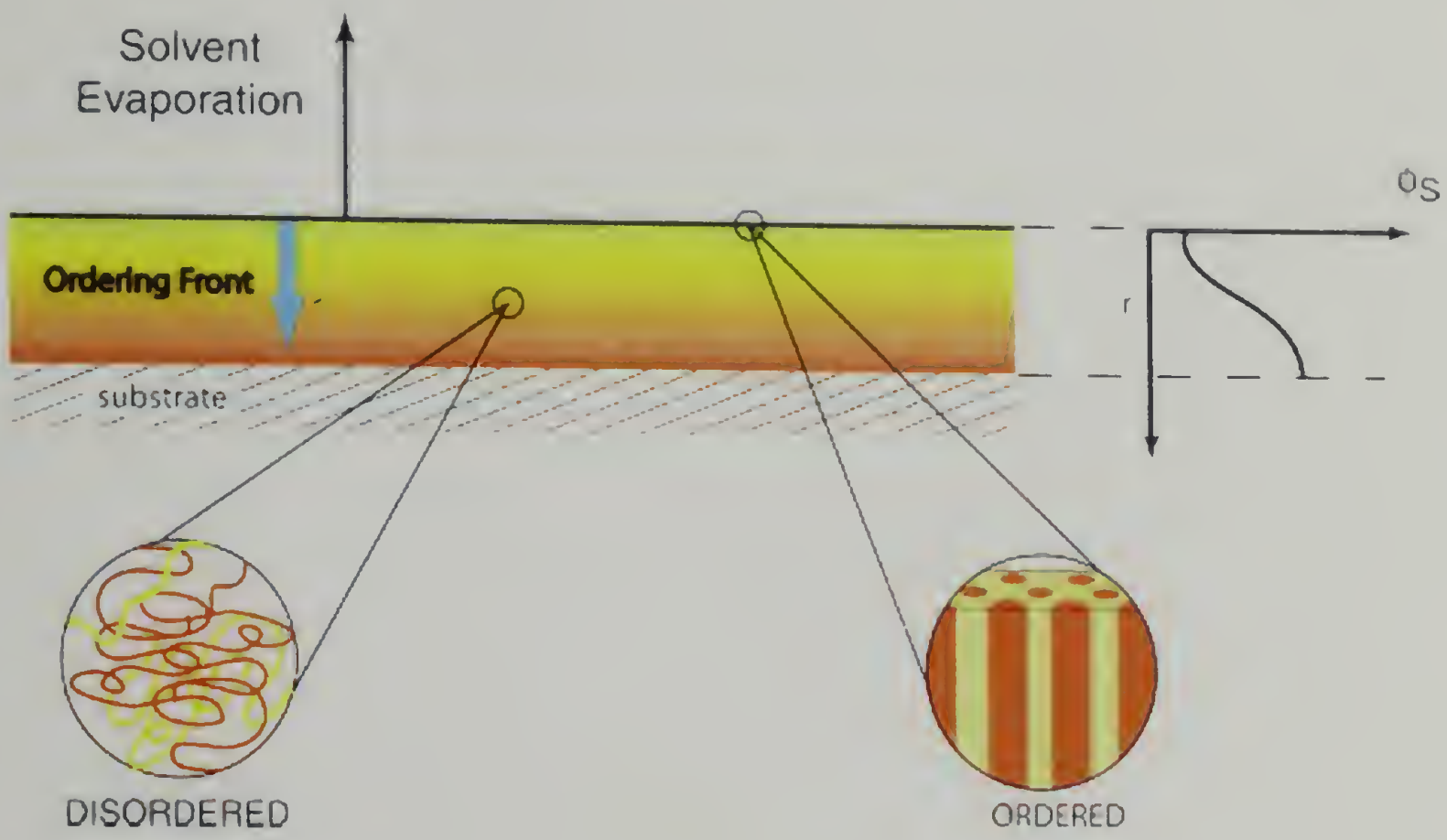

Figure 3.4. Schematic diagram of the solvent evaporation in a thin block copolymer film. At the surface, the concentration of solvent is lowest and the copolymer undergoes an ordering or microphase separation. A gradient in the concentration of the solvent, as a function of depth *r*, is established normal to the film surface with the solvent concentration increasing with depth. This increase in solvent concentration leaves the copolymer disordered in the interior of the film. As the solvent evaporates, an ordering front propagates through the film, akin to zone refinement, producing a highly ordered and oriented array of cylindrical microdomains in the film.

achieved. The copolymer within the film, however, is still disordered, due to the higher concentration of solvent. Further solvent evaporation causes an ordering front to propagate through the film, and similar to that which is seen in a classic zone refinement. Subsequently, ordered domains grow on the existing microphase separated morphology, extending through the film. The solvent gradient is, of course, highly directional and, therefore, the domains are highly oriented normal to the surface. Thus, highly ordered arrays of nanoscopic cylindrical domains with high aspect ratios (dictated by the film thickness) can be obtained with long-range lateral order. Such order is necessary for the fabrication of addressable media where the spatial positioning of each element must be defined to within a fraction of a repeat period. The process described here for PS-*b*-PEO can easily be transferred to other block copolymers containing highly immiscible blocks where there is a strong dependence of the ordering transition on solvent concentration.

The difference in the solubility of the PEO and PS blocks opens unique opportunities to further manipulate the domain size and separation distances in thin films. The PEO block is water soluble, whereas the PS block is not. A 260 nm thick film of PS-*b*-PEO was solution-cast from benzene, over a 48 hr period, in a chamber containing reservoirs of benzene and water. Phase contrast SFM images of $2 \times 2\ \mu m^2$ and $5 \times 5\ \mu m^2$ areas of the films are shown in Figures 5A and 5B, respectively. Shown, also, are the triangulation maps of the corresponding SFM images. As can be seen, the diameter of the nanoscopic cylindrical domains and the repeat period of the lattice have increased to 32.7 and 85.8 nm, respectively, due to the retention of water in the PEO domains during the casting process. Transmission electron microscopy and GASAXS studies show that the cylindrical domains penetrate through the entire film. It should be noted that the areal

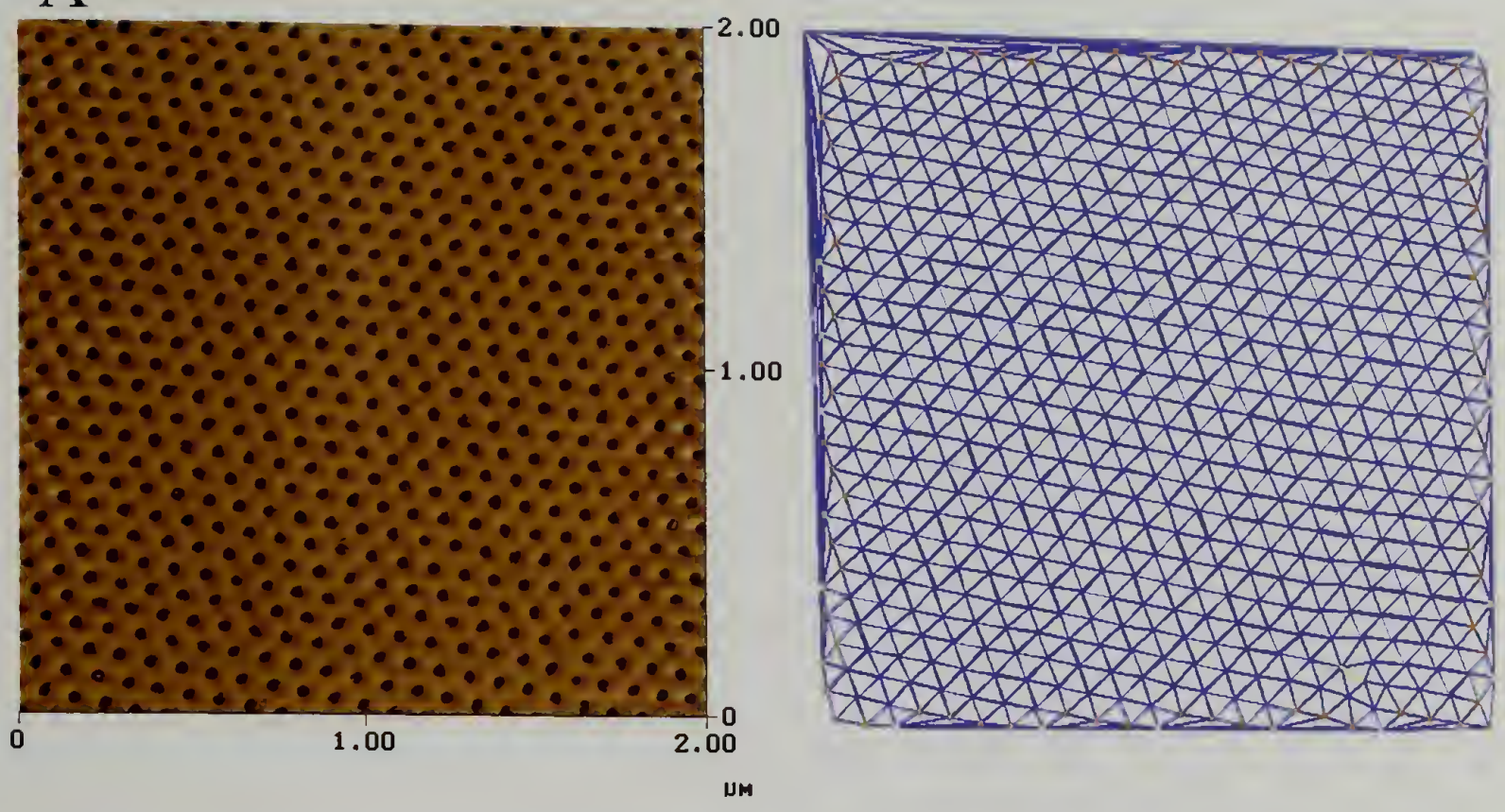

Figure 3.5. An SFM phase images of PS-*b*-PEO films 260 nm in thickness, solution cast from benzene in a benzene/water atmosphere for 48 hrs. The upper series (A) is for a 2×2 μm^2 area, whereas the lower series (B) is for a 5×5 μm^2 area. The SFM phase images and the corresponding triangulation maps are shown. Only one defect is seen in these images.

density of the cylinders, i.e. the total number of cylindrical domains on the surface, has decreased in comparison to the copolymer cast from benzene. As with films prepared under dry conditions, long-range order of the array is evident with only one dislocation seen over the $2 \times 2\ \mu m^2$ and $5 \times 5\ \mu m^2$ areas as shown. Thus, by using a second solvent that dissolves only the minor component, further control over the size and separation distance of the nanoscopic domains can be achieved.

To further underscore the ability in fabricating such arrays over large areas, a solution of the PS-*b*-PEO was spin-coated onto a silicon oxide surface containing 0.875 μm-wide, 0.325 μm-deep channels. The spin-coated film dewets the oxide surface during exposure to solvent, however capillary forces cause the film to be trapped within the channels. As the solvent evaporates the ordering process described above occurs within the channels and the SFM phase image shown in Figure 3.6 is obtained. As can be seen, essentially a defect-free array of cylindrical domains oriented normal to the surface is obtained within each of the channels. This order propagates along the length of the channels over hundreds of microns. A Fourier transform of the SFM image is shown in the inset where a six-point pattern, with multiple higher order reflections is obtained, characteristic of the long-range order. It should be noted that the lattice is highly aligned with respect to the channel walls. Consequently, by topographically sectoring a surface with standard lithographic processes, addressable arrays can be readily produced with a high degree of lateral order and a well-defined lattice orientation.

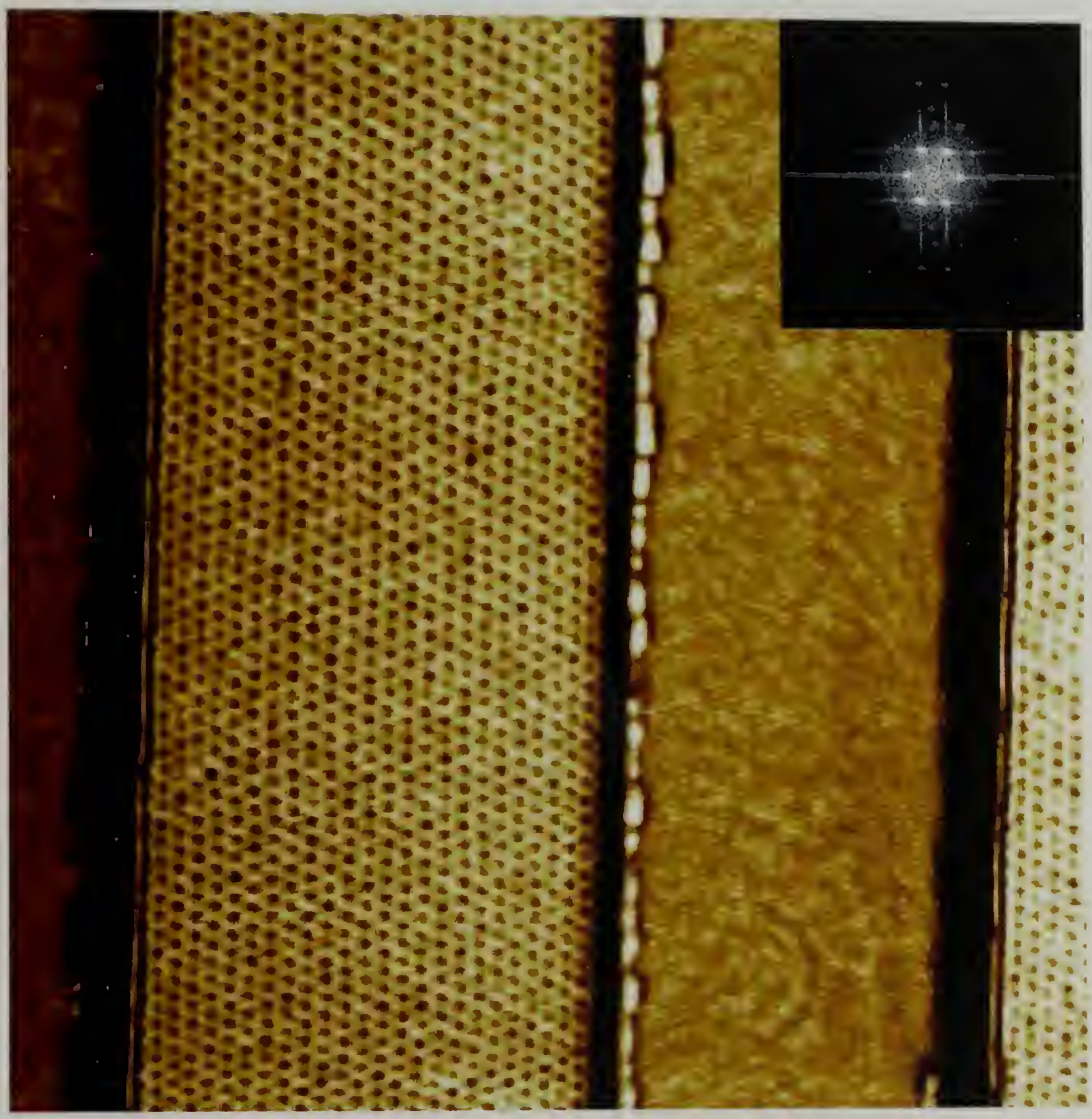

Figure 3.6. An SFM phase image of PS-*b*-PEO spin-coated onto a surface containing lithographically etched 0.875 μm-wide, 0.325 μm deep channels. Upon solvent annealing the film dewets and is trapped within the channels and solvent evaporates producing the highly aligned arrays of cylinders oriented normal to the surface within the channels. In the inset a Fourier transform of the SFM image shows a pattern with multiple reflections characteristic of a highly–ordered hexagonal array.

3.4 Conclusions

The simple process of solvent evaporation has been shown to produce highly order arrays of cylindrical microdomains in block copolymers with long-range lateral order. Solvent evaporation in thin films is unidirectional, which produces a self-assembly directed normal to the film surface, akin to a zone refinement. Further control over the size and separation distance of the domains can be achieved with cosolvents, which markedly extends the flexibility of the process. Sectored surfaces can also be used, which open routes to the fabrication of addressable media.

3.5 References

1. Seul, M.; Andelman, D. *Science* **1995**, *267*, 476.

2. Stupp, S. I.; LeBonheur, V.; Walker, K.; Li, L. S.; Huggins, K. E.; Keser, M.; Amstutz, A. *Science* **1997**, *276*, 384.

3. Cha, J. N.; Stucky, G. D.; Morse, D. E.; Deming, T. J. *Nature* **2000**, *403*, 289.

4. Whitesides, G. M.; Grzybowski, B. *Science* **2002**, *295*, 2418.

5. Bates, F. S. *Science* **1991**, *251*, 898.

6. Fredrickson, G. H.; Bates, F. S. *Ann. Rev. Mat. Sci.* **1996**, *26*, 501.

7. Muthukumar, M.; Ober, C. K.; Thomas, E. L. *Science* **1997**, *277*, 1225.

8. Ruokolainen, J.; Makinen, R.; Torkkeli, M.; Makela, T.; Serimaa, R.; Ten Brinke, G.; Ikkala, O. *Science* **1998**, *280*, 557.

9. Morkved, T. L.; Lu, M.; Urbas, A. M.; Ehrichs, E. E.; Jaeger, H. M.; Mansky, P.; Russell, T. P. *Science* **1996**, *273*, 931.

10. Thurn-Albrecht T.; Schotter J.; Kastle G. A.; Emley N.; Shibauchi T.; Krusin-Elbaum L.; Guarini K.; Black C. T.; Tuominen M. T.; Russell T. P. *Science* **2000**, *290*, 2126.

11. Albalak, R. J.; Thomas, E. L.; Capel, M. S. *Polymer* **1998**, *38*, 3819.

12. Villar, M. A.; Rueda, D. R.; Ania, F.; Thomas, E. L. *Polymer* **2002**, *43*, 5139.

13. Bodycomb, J.; Funaki, Y.; Kimishima, K.; Hashimoto, T. *Macromolecules* **1999**, *32*, 2075.

14. Segalman, R. A.; Yokoyama, H.; Kramer, E. J. *Adv. Mater.* **2001**, *15*, 1152.

15. Cheng, J. Y.; Ross, C. A.; Thomas, E. L.; Smith, H. I.; Vancso, G. J. *Appl. Phys. Lett.* **2002**, *81*, 3657.

16. Reiter, G.; Castelein, G.; Hoerner, P.; Riess, G.; Blumen, A.; Sommer, J. U. *Phys. Rev. Lett.* **1999**, *83*, 3844.

17. De Rosa, C.; Park, C.; Thomas, E. L.; Lotz, B. *Nature* **2000**, *405*, 433.

18. Fasolka, M. J.; Harris, D. J.; Mayes, A. M.; Yoon, M.; Mochrie, S. G. J. *Phys. Rev. Lett.* **1997**, *79*, 3018.

19. Rockford, L.; Liu, Y.; Mansky, P.; Russell, T. P.; Yoon, M.; Mochrie, S. G. J. *Phys. Rev. Lett.* **1999**, *82*, 2602.

20. Rockford, L.; Russell, T. P.; Yoon, M.; Mochrie, S. G. J. *Macromolecules* **2001**, *34*, 1487.

21. Kim, S.O.; Solak, H.H.; Stoykovich, M.P.; Ferrier, N.J.; dePablo, J.J.; Nealey, P.F. *Nature* **2003**, ***424***, 411.

22. Mansky, P.; Liu, Y.; Huang, E.; Russell, T. P.; Hawker, C. *Science* **1997**, 275, 1458.

23. Huang, E.; Rockford, L.; Russell, T. P.; Hawker, C. *Nature* **1998**, *395*, 757.

24. Kim, G.; Libera, M. *Macromolecules* **1998**, *31*, 2569.

25. Kim, G.; Libera, M. *Macromolecules* **1998**, *31*, 2670.

26. Ham, J.; Sibener, S. *Langmuir* **2000**, *16*, 4766.

27. Kimura, M.; Misner, M. J.; Xu, T.; Kim, S. H.; Russell, T. P. *Langmuir* **2003**, *19(23)*, 9910-9913.

28. Fukunaga, K.; Elbs, H.; Magerle, R.; Krausch, G. *Macromolecules* **2000**, *33*, 947.

29. Fukunaga, K.; Hashimoto, T.; Elbs, H.; Krausch, G. *Macromolecules* **2002**, *35*, 4406.

30. Lin, Z.; Kim, D. H.; Wu, X.; Boosahda, L.; Stone, D.; LaRose, L.; Russell, T. P. *Adv. Mater.* **2002**, *14*, 1373.

31. Angelescu, D. Ph.D. Thesis, Princeton University (2003).

32. Muller-Buschbaum, P.; Cubitt, R.; Petry, W. Langmuir **2003**, *19*, 7778.

CHAPTER 4

SALT COMPLEXATION IN BLOCK COPOLYMER THIN FILMS

4.1 Introduction

The self-assembly of block copolymers provides a versatile platform for the fabrication of nanostructured materials. Scaffolds and templates produced from oriented morphologies of block copolymers have been used in applications ranging from filters with well-defined pore sizes for the separation of viruses to floating gates in flash memory storage devices.[1-16] Yet, to utilize fully the areal density of elements afforded by block copolymers and to realize the potential of generating addressable media, control over the orientation and long-range lateral ordering of the copolymer microdomains is necessary. While external fields, such as applied electrical fields or controlled interfacial interactions, provide control over the orientation of the microdomain morphology, [6,9,24,25] producing morphologies with long-range lateral order requires fields in two orthogonal directions. These fields may be either applied, as in the case of an electric field, or there may exist an internal driving force, such as a defect energy in packing, that promotes lateral order.[16-27] In the case of defects, the higher the energetic penalty associated with the presence of the defect, the greater will be the driving force to remove defects and produce long-range lateral order.

Polymer/salt complexes have received considerable attention, since they exhibit high ionic conductivity, stable electrochemical characteristics and excellent mechanical properties.[28-35] In polymer-based electrochemical technologies these complexes are used in solid-state lithium batteries, fuel cells, chemical sensors, and flexible displays. In addition, metal-precursor salts can be confined within the nanoscopic microdomains of

the block copolymers and, through subsequent reduction reactions, the precursor salts can be converted to the corresponding metal, providing a simple route for the generation of metallic nanoparticles within the minor component phase of the block copolymer.[36-38] Here, we show that the complexation of alkali-halide or metal salts with the poly(ethylene oxide) (PEO) block of a polystyrene (PS)-*block*-PEO copolymer, having cylindrical microdomains of PEO, produces a dramatic, unexpected result during solvent annealing, wherein the microdomains of the block copolymer are found to orient normal to the surface of the film with markedly enhanced lateral order, in comparison to the same films prepared in the absence of salt.

4.2 Experimental

Commercially available polystyrene-*block*-poly(ethylene oxide) diblock copolymer, PS-*b*-PEO, with a molecular weight of 25.3 kg/mol a PS weight fraction of 0.75 (corresponding to a volume fraction of 0.76) was used in this study. In the bulk, this asymmetric diblock copolymer self-assembles into hexagonally packed arrays of cylindrical microdomains with diameters of 21 nm with a mean separation of ~32 nm. Solutions of the block copolymer with and without added salts were spin-coated onto cleaned silicon substrates where the film thickness was controlled by the spinning rate and/or the solution concentration. In cases where salt was added to the copolymer, the copolymer was dissolved in tertrahydrofuran and the salt in methanol. Equal volumes of these two solutions were then mixed. After 8-12 hours the copolymer was precipitated by the addition of hexane. The precipitate was then dried, and re-dissolved into benzene. Spin-coated films were placed in a benzene-saturated chamber at room temperature,

allowing the benzene vapors to swell the film and solvent-anneal the morphology, as described previously.[27] For copolymer films with added salts, the solvent-annealing experiments were performed in a chamber where the relative humidity was controlled between 40 to 60 %. SFM images were obtained in both the height and phase contrast modes using a Digital Instruments Dimension 3000 scanning force microscope in tapping mode. Transmission electron microscopy (TEM) studies were performed on a JEOL 100CX electron microscope operated at 100 kV. For TEM, the samples were prepared on silicon substrates with a thick layer of silicon oxide. The polymer film was then floated onto the surface of an aqueous solution containing 5 wt% HF, transferred to a water bath, and then retrieved with a Cu grid for measurement. Grazing incident angle small angle x-ray scattering (GISAXS) measurements were performed at the X22B beamline at the National Synchrotron Light Source (Brookhaven National Laboratory) and at the G1 beamline at CHESS (Cornell University).

4.3 Results and Discussion

Previously, we demonstrated that solvent annealing produced a high degree of long-range lateral order of cylindrical microdomains, oriented normal to the surface, in thin films of PS-*b*-PEO.[27] More recently, we have observed large variations on microdomain orientation between two samples purchased from Polymer Source. The original sample consistently demonstrated copolymer microdomain orientation that was normal to the surface. However, with the new material, both normal and parallel microdomain orientations were observed. The SFM images in Figure 4.1A and Figure 4.1B are thin films of the original copolymer material after spin coating and solvent

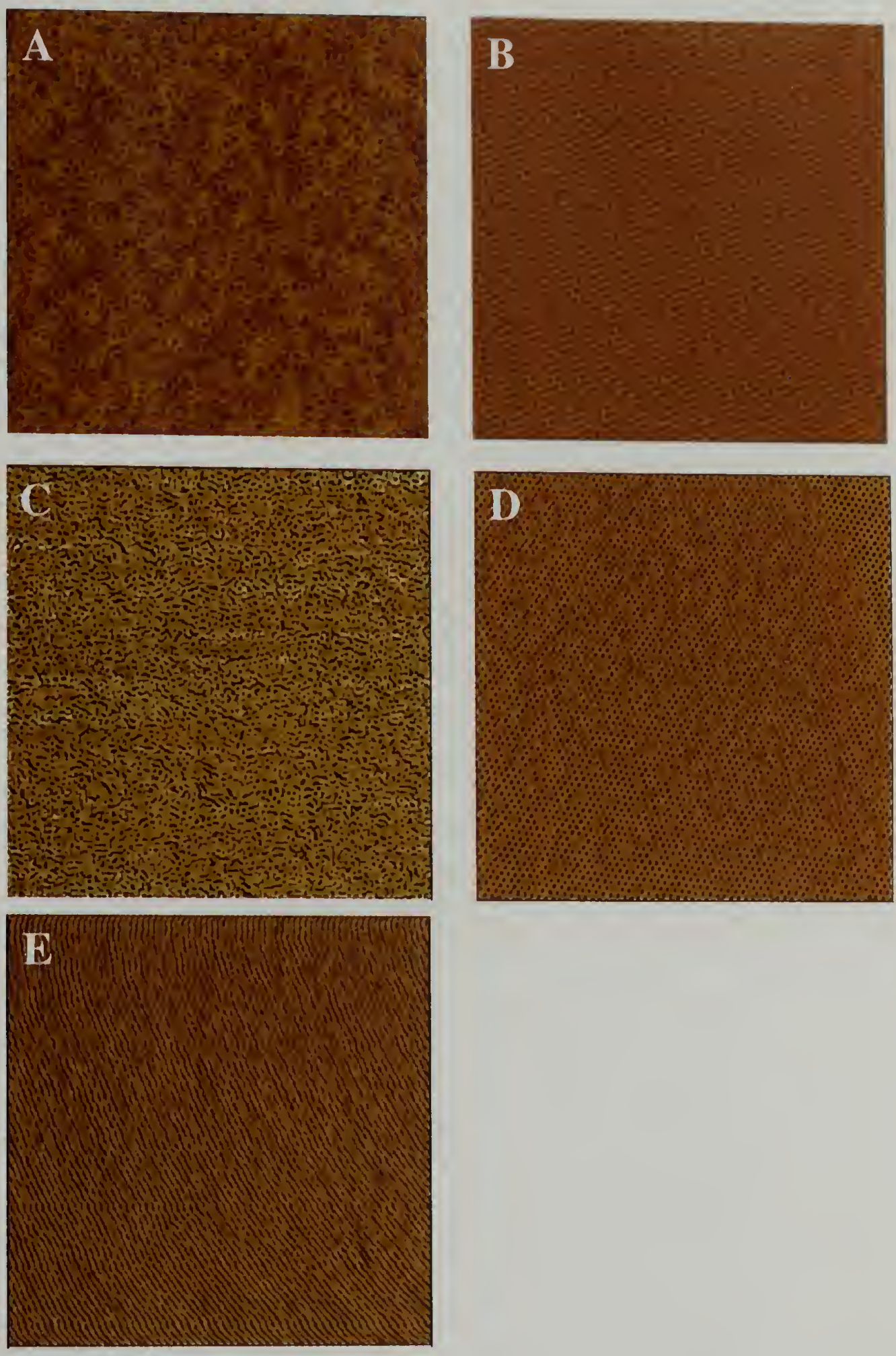

Figure 4.1 SFM images of the original batch of PS-*b*-PEO A) as spun and B) solvent annealed in benzene. The second batch of PS-*b*-PEO C) as spun, D) solvent annealed in benzene/water atmosphere, and E) solvent annealed in benzene. All images are 2×2 μm.

annealing for 48 hours in a benzene atmosphere, respectively. Such results could be obtained consistently, regardless of humidity. However, after a second batch of newly synthesized material was obtained, a large dependence on humidity was observed. In Figure 4.1C, the as spun film showed significantly less microdomains oriented normal to the surface. Furthermore, after solvent annealing, the microdomains were oriented normal and parallel to the substrate, Figure 4.1D and Figure 4.1E, respectively. The SFM image in Figure 4.1D was obtained by annealing the copolymer thin film in an atmosphere of benzene and water, while the image in Figure 4.1E was obtained by annealing in an atmosphere of benzene only.

The series of images in Figure 4.2 demonstrate the transition of the microdomain orientation from parallel to perpendicular as a function of relative humidity. All of the films were annealed in the presence of a benzene atmosphere for 3-5 hours to obtain the copolymer orientation. At a relative humidity of 30%, Figure 4.2A, the microdomain orientation is purely parallel, however, annealing at a relative humidity of 55% a mixture of parallel and perpendicular is observed, Figure 4.2B. Further increasing the relative humidity to 80%, Figure 4.2C, fully orients the copolymer microdomains normal to the surface. Finally, at saturation, or a relative humidity of 100%, large variations of the microdomain size is observed, similar to what was observed in solvent casting of the copolymer films in the presence of water, however, here the distribution of microdomains size is non-uniform.

To determine the cause of the difference in the ordering behavior, the samples were fully characterized. The samples are similar in molecular weight and composition, both samples containing some homopolymer, however in similar proportion. More

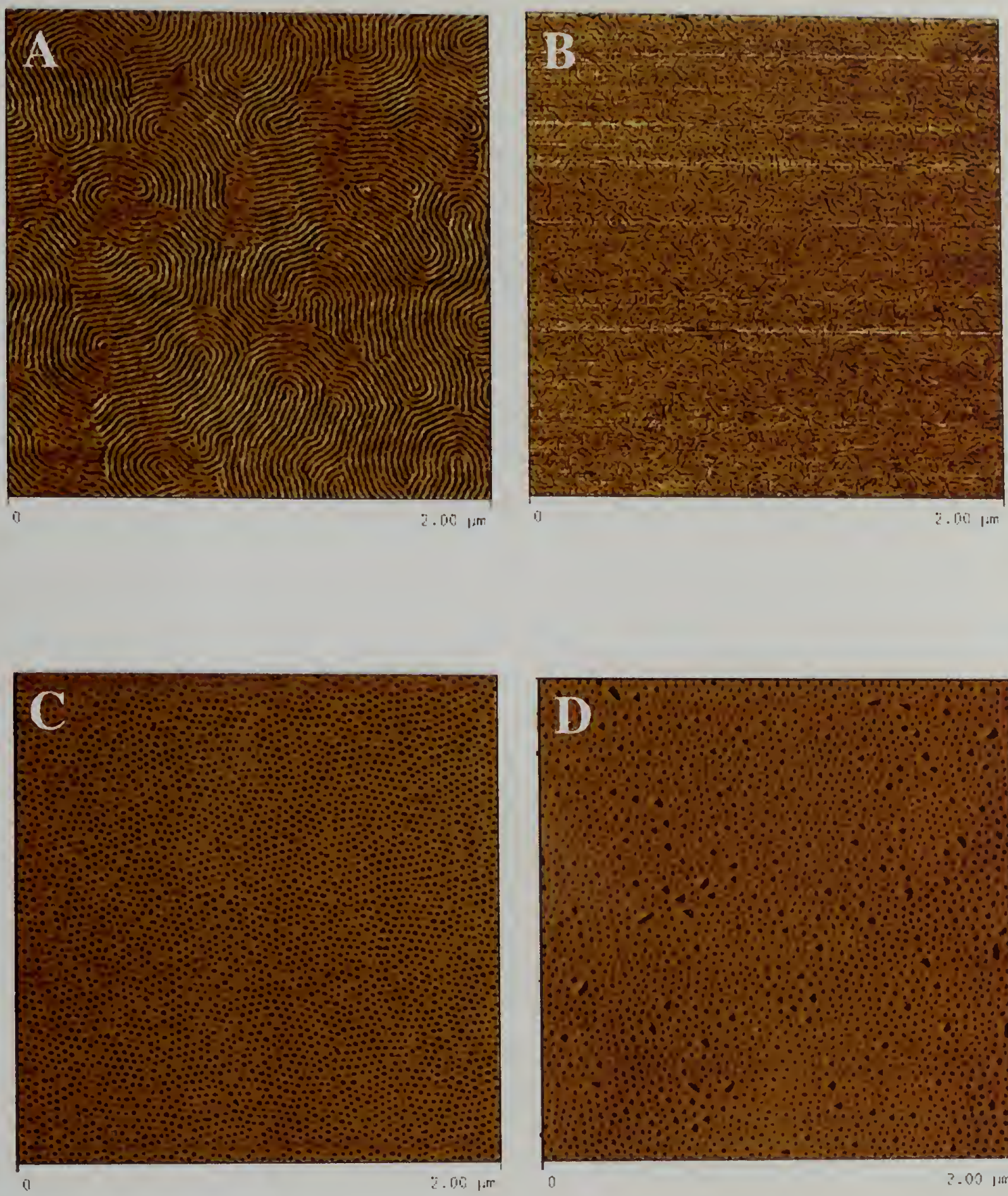

Figure 4.2 SFM images of solvent annealed films of PS-b-PEO in benzene at a relative humidity of A) 30%, B) 55%, C) 80%, and D) 100%.

importantly, the two copolymer samples contained different concentrations of potassium residual from the initiator used in the synthesis of the copolymer.

To investigate the effect of salt concentration on the ordering behavior in block copolymer thin films, controlled amounts of salt were added to PS-*b*-PEO prior to solution casting. Due to the limited solubility of the salts in apolar solvents, the salt and block copolymer were first dissolved in methanol and tetrahydrofuran, respectively, and then mixed together. Subsequently, the block copolymer/salt complexes were precipitated in hexane, re-dissolved in benzene and then spin-coated onto silicon wafers. Figure 4.3a and Figure- 4.3b show the SFM images of thin films of the block copolymer complexed with KI, with a molar ratio of the oxygen in PEO to the cation of the salt of 64 ([O]/[K]), before and after solvent annealing, respectively. The results for films of the block copolymer without salt are shown in Figure 4.3c and Figure 4.3d, respectively. It is clear that the addition of salt gives rise to a change in the orientation of PEO cylinders, from parallel to perpendicular, in the solvent annealed films. The as-spun films exhibit a similar change in the orientation of the cylindrical microdomains from a mixed orientation to an orientation normal to the surface, with and without salt, respectively. Being that the PEO is water soluble and the salts used are fairly hydroscopic, humidity can affect the behavior of block copolymer ordering. Subsequently, the experiments presented here were performed in a controlled humidity environment between 40% and 60%. The complexation of KI with the PEO block is further demonstrated by infrared (IR) spectroscopy. Here the positions of the C-O-C (1) stretching and CH_2 (2) rocking modes in PEO were shifted in comparison to the salt-free polymer film. Figure 4.3e, illustrates that the positions are slightly shifted from 1113 cm^{-1} to 1111 cm^{-1} to 1109 cm^{-1}

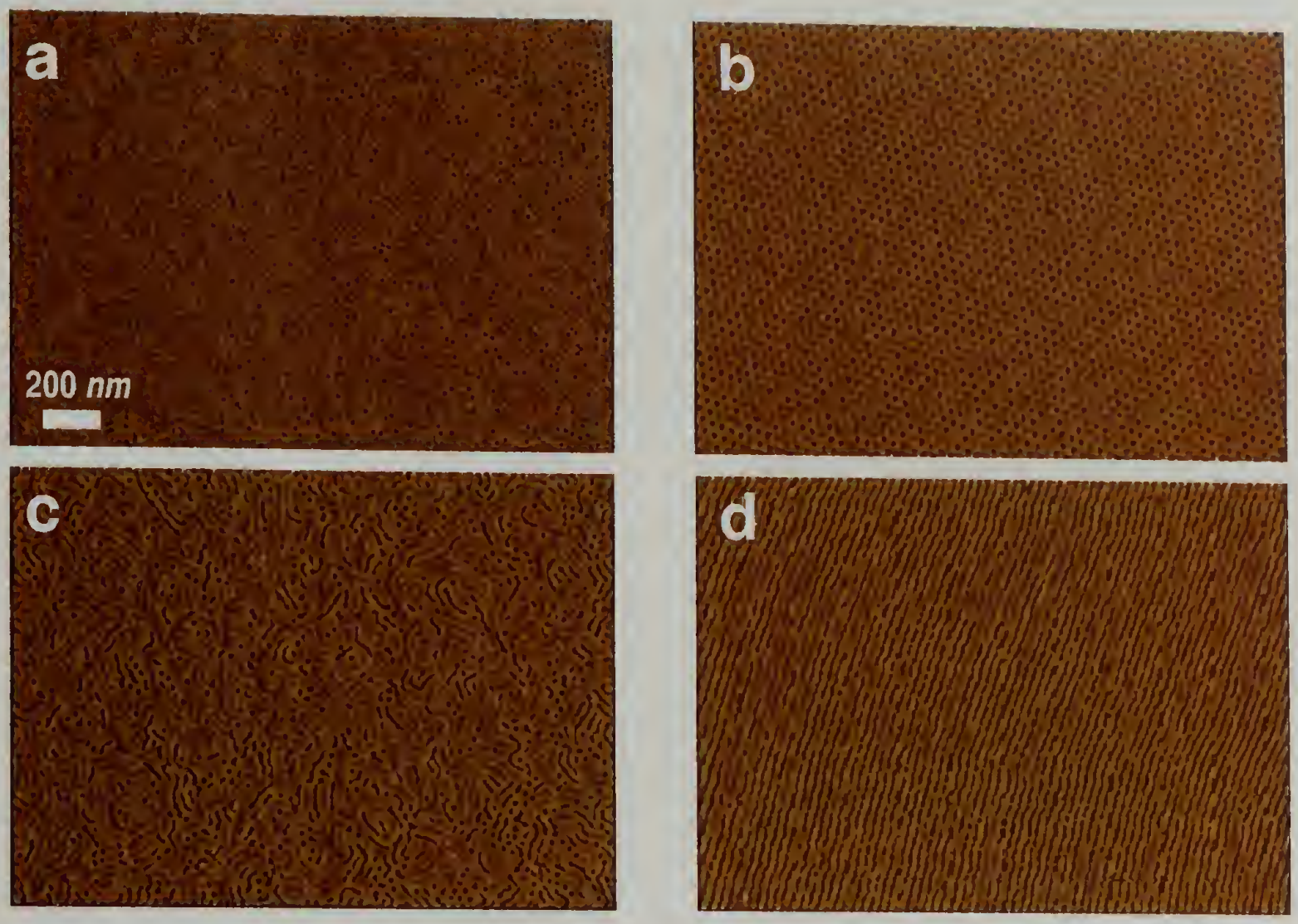

Figure 4.3 a) An SFM image of a block copolymer film containing KI as spun, and b) after solvent annealing; c) copolymer films without added KI as spun, and d) after solvent annealing demonstrate a large effect on the ordering of the copolymer during solvent casting and annealing. Shifts in the IR spectroscopy of the copolymer with varying monomer to salt ratios ([O][K]) indicate complexation of the salt with the PEO.

and 947 cm^{-1} to 949 cm^{-1} to 953 cm^{-1}, as the concentration was increased from [O/K] = ∞ to 64 to 16, respectively.

Large differences in the evolution of structure upon solvent annealing were observed by *in situ* grazing incidence small angle x-ray scattering (GISAXS) for films with different salt concentrations. By exposing the film to a solvent environment the copolymer film is rapidly swollen and, as the solvent atmosphere is depleted, the solvent evaporates from the copolymer film. For the block copolymer with small to medium amounts of added salts, the copolymer film disorders upon swelling and produces a highly ordered array of hexagonally-packed cylindrical microdomains oriented normal to the surface of the film when the solvent is removed. Figure 4.4 shows two GISAXS patterns, where the angle of incidence was above the critical angle of the polymer and full penetration of the x-ray beam into the film occurred. In Figure 4.4a, the copolymer film contained a small amount of salt ([O]/[K]=64) and was swollen to ~250% of the original film thickness. Only diffuse surface scattering was observed, indicating that the copolymer was disordered. It is clear from the scattering from a highly swollen copolymer film without salt, Figure 4.4b, that some order is still present inside the film. This result underscores the significance of preferential interactions of the PEO block of the copolymer with the silicon oxide substrate. Only diffuse scattering was observed below the critical angle, where the penetration of the x-ray beam extends only a few nanometers into the film, indicating that the copolymer was disordered at the free surface. Without the addition of salt to the block copolymer, as the solvent evaporates, the cylindrical microdomains form a hexagonally-packed array of cylinders oriented parallel to the films surface. Together these results indicate that the salt, either by complexation

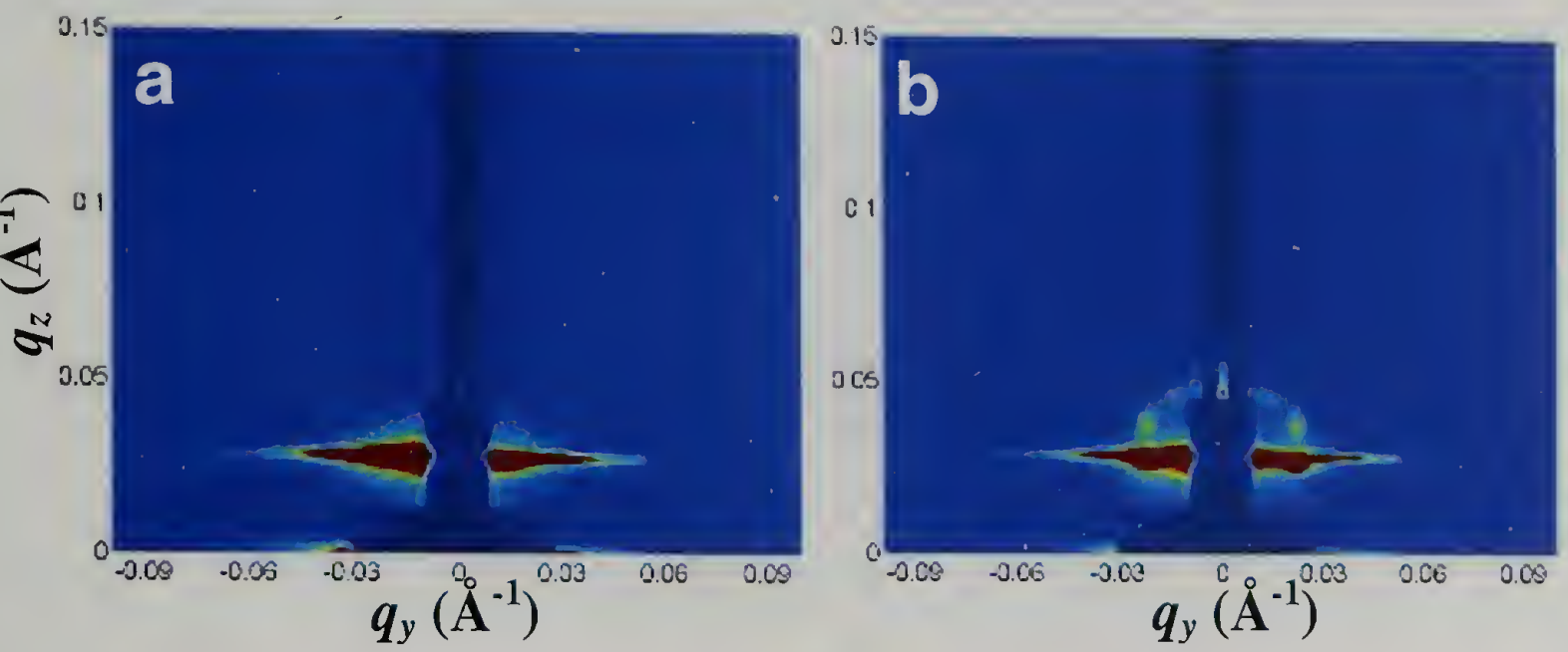

Figure 4.4 GISAXS patterns of swollen copolymer films a) with and b) without a small amount of salt added, where the salts can screen favorable interactions with the substrate, where otherwise the film is completely disordered.

with the PEO or by interactions with the substrate, overcomes preferential interactions between the PEO and the substrate, enabling the propagation of a front of ordered cylindrical microdomains through the film oriented normal to the film surface.

The SFM images shown in Figure 4.5 show the dependence of the orientation and the lateral order of the block copolymer microdomains in thin films on the salt concentration. At a low concentration of salt ([O]/[K]=94), the amount of added salt is insufficient to overcome interfacial interactions and the microdomains orient parallel to the surface. With increasing the salt concentrations ([O]/[K]=64 and 32), highly ordered arrays of cylindrical microdomains oriented normal to the surface are observed. Increasing the salt concentration further ([O]/[K]=12) maintains the orientation of the microdomains normal to the surface, however, the lateral ordering of the cylindrical microdomains is reduced.

To explore the details of the solvent annealing process, *in situ* GISAXS measurements were performed in real-time.[39, 40] Simultaneously, the film thickness was measured by multi-wavelength optical interferometry to assess the concentration of solvent in the film. GISAXS patterns of a swollen and subsequently dried film are shown in Figure 4.6a and 4.6b, respectively, for [O]/[K]=64. Similarly, GISAXS patterns are shown for [O]/[K]=16 in Figure 4.6c and 4.6d for swollen and dried films, respectively. The time from the addition of solvent (t=0) and film thickness at that time are specified in each figure. The Bragg rods (vertical streaks) in the GISAXS patterns correspond to the first order reflection from a 2D hexagonal lattice of cylinders of finite length oriented normal to the surface. At the lower salt concentration ([O]/[K]=64), the copolymer rapidly disordered and underwent microphase separation near the end of solvent

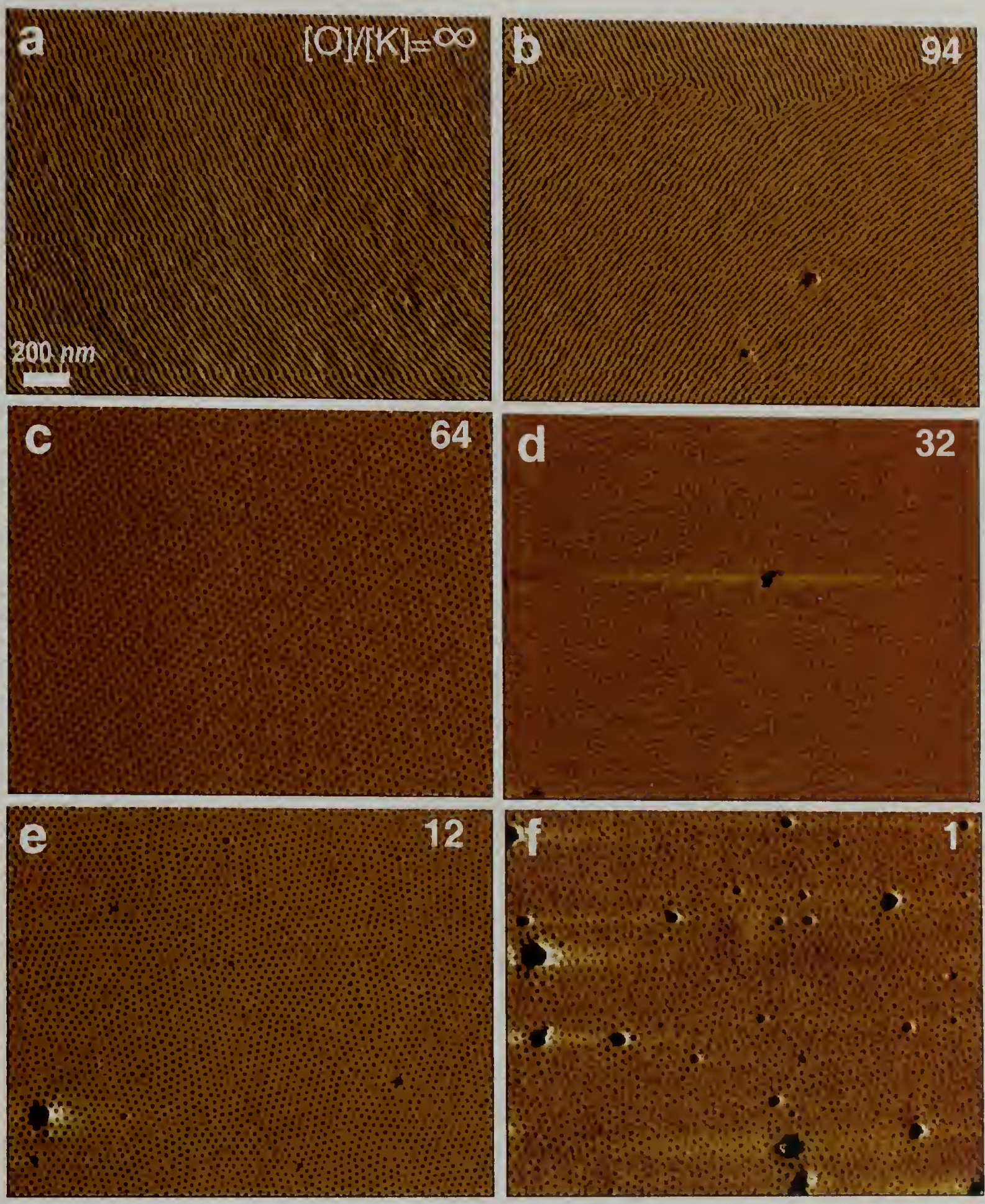

Figure 4.5 SFM images of copolymer films containing different amounts of added salt from no added salt to a ratio of oxygen in the PEO to the number ions of unity. Increasing the salt concentration can induce a change of microdomain orientation in the copolymer film.

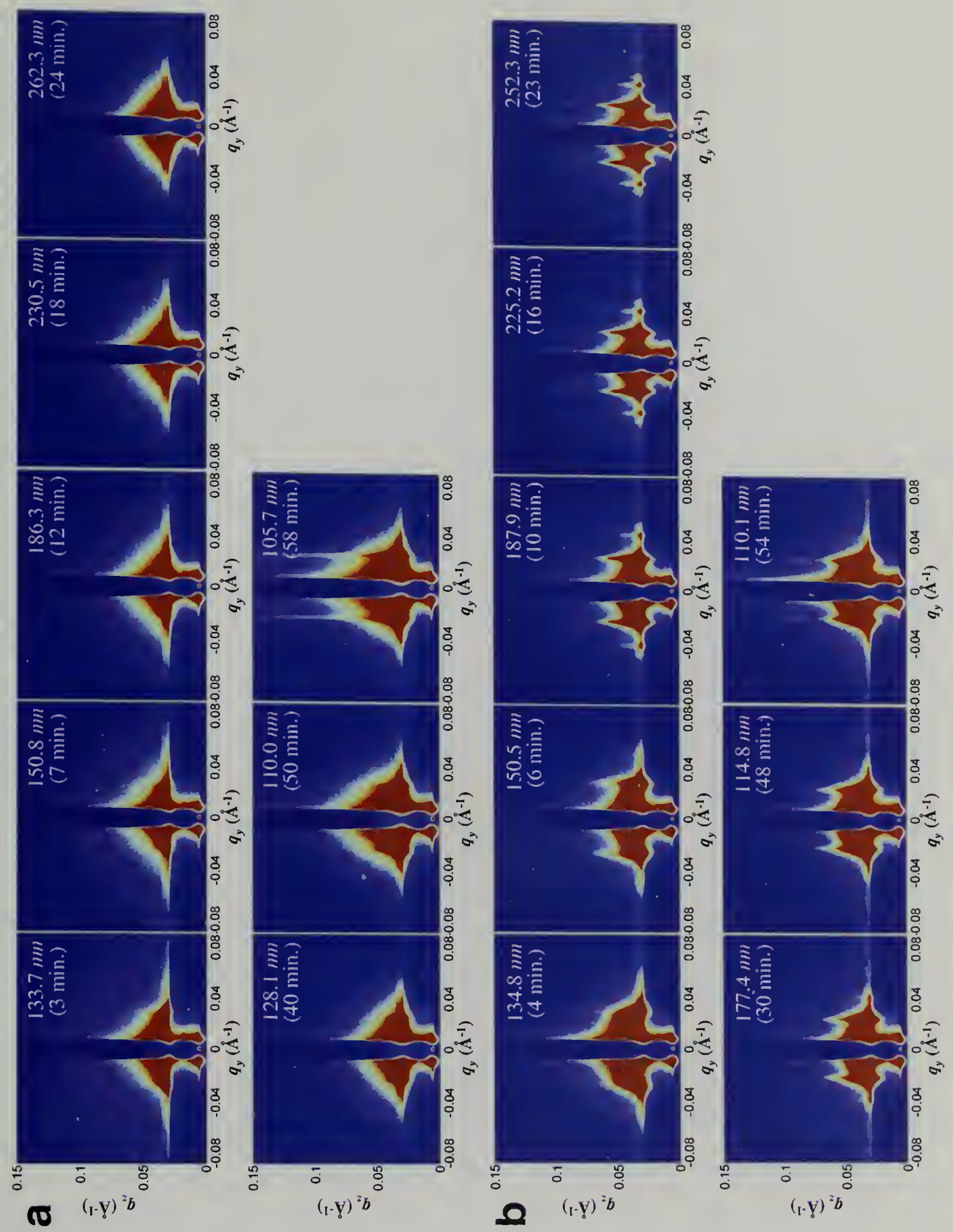

Figure 4.6 Series of *in situ* GISAXS patterns at a) 64 ([O]/[K]) and b) 16 ([O]/[K]), where the top row of each series is while the copolymer film is swelling and the bottom row of each series is while solvent is evaporation from the copolymer film. The copolymer film with a low salt concentration quickly disorders on swelling and then reorders during evaporation of the solvent, while the film with a high salt concentration never disorders and demonstrates an extremely correlated structure in the swollen state. This correlation is lost upon evaporation of the solvent.

evaporation, as discussed before. However, for the sample with the higher salt concentration ([O]/[K]=16), the copolymer remained microphase separated throughout the swelling and, in fact, the lateral ordering and in-plane correlations markedly improved. Many higher-order reflections were observed at scattering vectors characteristic of hexagonally close-packed cylindrical microdomains oriented normal to the film surface. Upon removal of the solvent the higher order reflections in the GISAXS are lost, even though the films show exceptional lateral ordering by SFM over areas tens of square microns in size. That the film remains ordered and the spacing between the microdomains increases during swelling indicates that complexation of the PEO with the salt has increased the effective segmental interactions between the PS and PEO. The increased non-favorable interactions, coupled with the enhanced mobility of the polymer chains in the highly swollen film, give rise to the exceptional degree of lateral ordering in the film seen in the GISAXS experiment. Unfortunately, as the solvent evaporates, the volume change in the film coupled with the lateral confinement to the substrate, results in a loss of lateral order within the film (not observable by SFM). Experiments are in progress to develop systems where the block copolymer can be cross-linked in the swollen state, thereby locking in the highly ordered, oriented cylindrical microdomain morphology.

Figure 4.7a and 8.7b show static GISAXS patterns of copolymer films after solvent annealing with salt concentrations of [O]/[K]=64 and [O]/[K]=16, respectively. Strong vertical streaks in both films indicate the presence of cylindrical microdomains oriented normal to the surface. However with the higher salt concentration there are additional reflections in the GISAXS pattern at an in-plane wave-vector at about half that of the

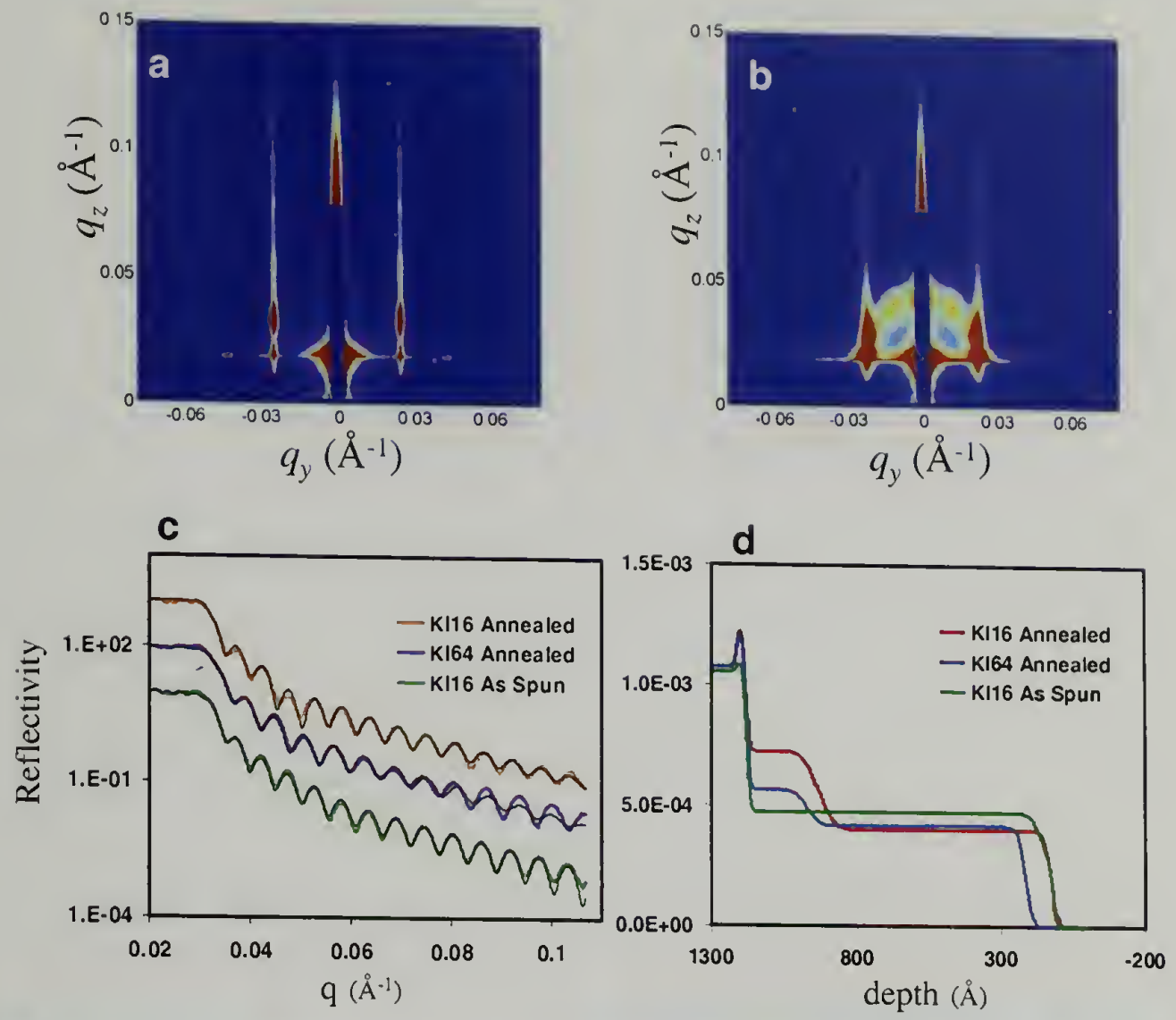

Figure 4.7 Static GISAXS patterns with salt concentrations of a) 64 ([O]/[K]) and b) 16 ([O]/[K]). Additional reflections are observed in the film with higher salt concentration that are not observed in the film with lower salt concentration. X-ray reflectivity profiles, c, and the fitted electron density profiles, d, indicate that the salt is distributed near the substrate. e) 2 × 2 µm SFM height and phase images of a film that has been removed from the substrate and flipped back onto itself such that the top and bottom of the film are exposed. The structure at the bottom of the film is similar to, but different from the top of the film.

first-order reflection from the hexagonal array. The origin of these reflections is not fully understood, though they may arise from either a deformation of the cylindrical microdomains during drying or from an inhomogeneous distribution of salt within the microdomains. Fits to the x-ray reflectivity profiles shown in Figure 4.7c yield the electron density profile shown in Figure 4.7d, which indicate that there is an electron dense or a salt-rich region at the interface between the substrate and the copolymer film after drying. In contrast, fits to the reflectivity profiles for the as-cast film show no excess in electron dénsity at the substrate. Consequently, during solvent evaporation, it appears that an excess salt layer forms at the substrate due, more than likely, to an exclusion of excess salt from the ordering front propagating into the film. This can be likened to the exclusion of excess impurities at the ordering front in a zone refinement processes. However, as will be shown later, some added salt still remains within the cylindrical microdomains of PEO. The SFM image in Figure 4.7e is from a copolymer film with salt ([O]/[K]=16) that was deposited on silicon substrate having a thick oxide layer. Using a buffered HF solution, the film was removed from the substrate and transferred to a water bath. Subsequently, the film was retrieve on a glass substrate and part of the film was flipped over onto the transferred film so that both the top and the bottom of the film could be imaged by SFM. While the bottom of the film does not show a change the orientation of the microdomains, the structure at the bottom of the film is different than at the top surface. At the bottom, the microdomains are larger and ill defined, however this is consistent with the destruction of the microdomains and the accumulation of salt during solvent evaporation in copolymer films that contain high

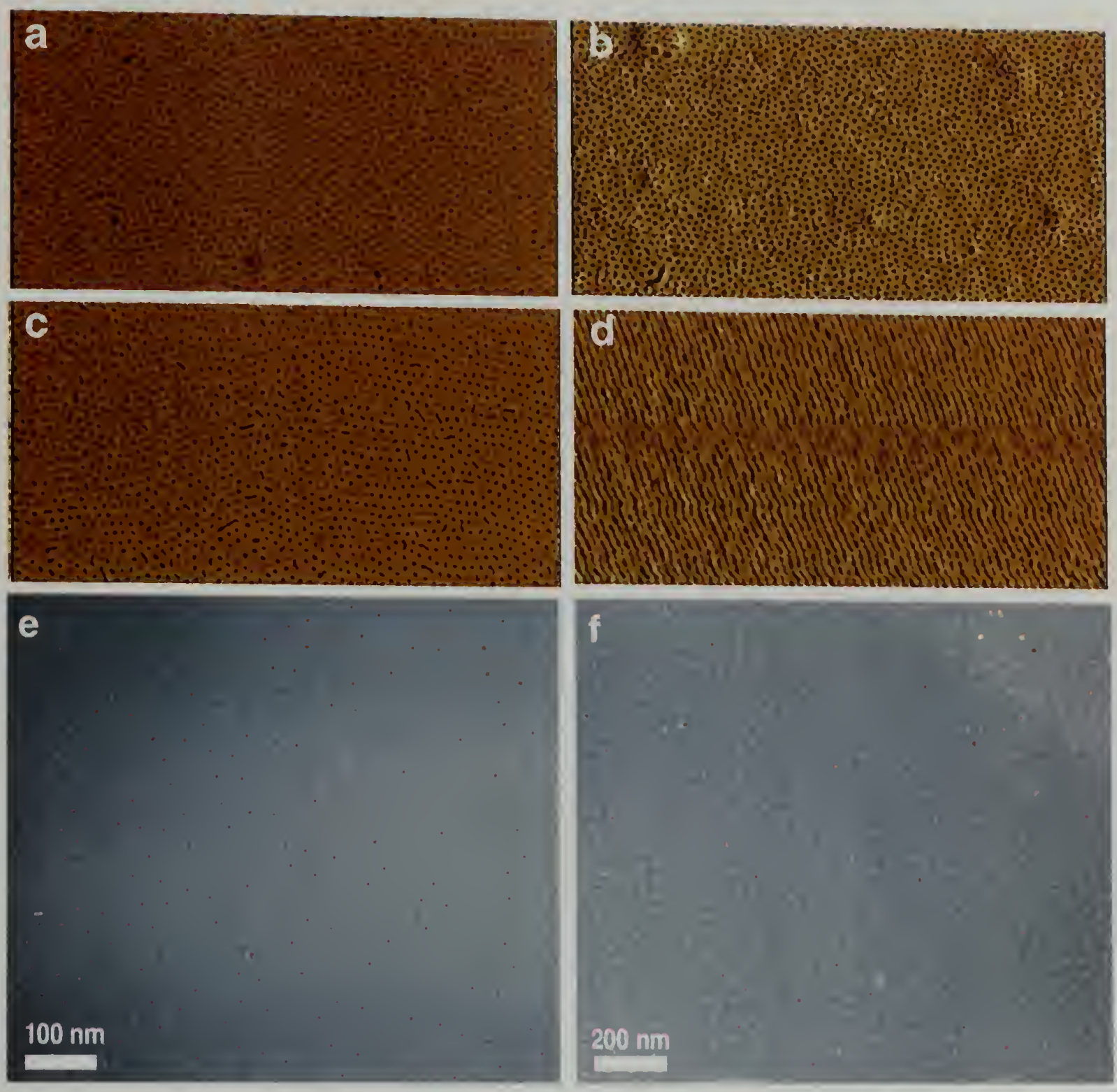

Figure 4.8 Salts that can complex with PEO all show similar results, including a) LiI, b) RbI, and c) LiCl, however d) KCl does not complex and does not induce microdomain reorientation, as seen in the 2 (1 μm SFM images. Through the complexation of e) gold and f) cobalt salts nanoparticles can be generated inside the copolymer microdomains.

amounts of salt. Figure 4.8 shows SFM images of different salts that can complex with PEO.

Cation/anion pairs, other than KI, can be used to complex the PEO block. LiI ([O]/[Li]=16), RbI ([O]/[Rb]=16) and LiCl ([O]/[Li]=16) shown in Figure 4.8 a, b and c, respectively, are known to complex PEO while KCl ([O]/[K]=16), shown in Figure 5d, does not.[42] In cases where the salts complex with the PEO, the cylindrical microdomains orient normal to the surface, while with KCl, the cylindrical microdomains orient parallel to the substrate. Consequently, the specific nature of the salt and its ability to complex with the PEO can be used to effectively tune the orientation of the PEO microdomains. The addition of a salt to the minor component phase has an added benefit in that the metal ions can be reduced to the corresponding metal, forming nanoscopic metal particles within the block copolymer microdomains. Thus, by default, a controlled placement of metallic nanoparticles in a thin film can readily be achieved. As an example, consider $HAuCl_4$, which is known to complex PEO. Shown in Figure 4.8e is the TEM image of a copolymer film removed from the substrate after solvent annealing. During the course of the TEM studies, the $HAuCl_4$, was exposed to the electron beam that reduced it to Au, forming Au nanoparticles. It can be seen that the gold nanoparticles (~4 nm in size) formed and were confined within the PEO microdomains. It should be noted that the size of the Au nanoparticles can be controlled by the concentration of gold ions loaded into the films. Similar results were found with Co ions, as shown in Figure 4.8f, where the cobalt particles are, again, found to be located within the PEO domains. Consequently, the added salt serves a dual role. The first is to orient

and order the copolymer microdomains while the second is to serve as a precursor to the fabrication of metal nanoparticles.

4.4 Conclusions

We have shown that polymer-salt complexation combined with the solvent annealing, affords a simple, yet robust, route to control the orientation and lateral ordering of microdomains in thin films of block copolymer. In addition, the salt can be used as a metal nanoparticle precursor. This strategy is general and can be extended to any block copolymer where one of the components can form a complex with a heavy metal ion salt. Results for PS-*b*-P2VP block copolymers, where the P2VP block can be complexed, shows very similar behavior to that of PS-*b*-PEO. Therefore, this general strategy allows one to generate functional, self-orienting, self-assembling systems that hold promise in the fabrication of nanostructured materials where the spatial placement of each element can be controlled and, as such, opens a pathway to addressable media.

4.5 References

1. Hawker, C. J.; Russell, T. P. *MRS Bulletin* **2005**, *30*, 952.

2. Segalman, R. A. *Materials Science & Engineering R-Reports* **2005**, *48*, 191.

3. Hamley, I. W. *Nanotechnology* **2003**, *14*, R39.

4. Lazzari, M.; Lopez-Quintela, M. A. *Advanced Materials* **2003**, *15*, 1583.

5. Park, M.; Harrison, C.; Chaikin, P. M.; Register, R. A.; Adamson, D. H. *Science* **1997**, *276*, 1401.

6. Thurn-Albrecht, T.; Schotter, J.; Kastle, C. A.; Emley, N.; Shibauchi, T.; Krusin-Elbaum, L.; Guarini, K.; Black, C. T.; Tuominen, M. T.; Russell, T. P. *Science* **2000**, *290*, 2126.

7. Li, R. R.; Dapkus, P. D.; Thompson, M. E.; Jeong, W. G.; Harrison, C.; Chaikin, P. M.; Register, R. A.; Adamson, D. H. *Applied Physics Letters* **2000**, *76*, 1689.

8. Lopes, W. A.; Jaeger, H. M. *Nature* **2001**, *414*, 735.

9. Black, C. T.; Guarini, K. W.; Milkove, K. R.; Baker, S. M.; Russell, T. P.; Tuominen, M. T. *Applied Physics Letters* **2001**, *79*, 409.

10. Cheng, J. Y.; Ross, C. A.; Chan, V. Z. H.; Thomas, E. L.; Lammertink, R. G. H.; Vancso, G. J. *Advanced Materials* **2001**, *13*, 1174.

11. Doshi, D. A.; Gibaud, A.; Goletto, V.; Lu, M. C.; Gerung, H.; Ocko, B.; Han, S. M.; Brinker, C. J. *Journal of the American Chemical Society* **2003**, *125*, 11646.

12. Ludwigs, S.; Boker, A.; Voronov, A.; Rehse, N.; Magerle, R.; Krausch, G. *Nature Materials* **2003**, *2*, 744.

13. Kim, D. H.; Kim, S. H.; Lavery, K.; Russell, T. P. *Nano Letters* **2004**, *4*, 1841.

14. Kim, D. H.; Lau, K. H. A.; Robertson, J. W. F.; Lee, O. J.; Jeong, U.; Lee, J. I.; Hawker, C. J.; Russell, T. P.; Kim, J. K.; Knoll, W. *Advanced Materials* **2005**, *17*, 2442.

15. Lin, Y.; Boker, A.; He, J. B.; Sill, K.; Xiang, H. Q.; Abetz, C.; Li, X. F.; Wang, J.; Emrick, T.; Long, S.; Wang, Q.; Balazs, A.; Russell, T. P. *Nature* **2005**, *434*, 55.

16. Stoykovich, M. P.; Muller, M.; Kim, S. O.; Solak, H. H.; Edwards, E. W.; de Pablo, J. J.; Nealey, P. F. *Science* **2005**, *308*, 1442.

17. De Rosa, C.; Park, C.; Thomas, E. L.; Lotz, B. *Nature* **2000**, *405*, 433.

18. Segalman, R. A.; Yokoyama, H.; Kramer, E. J. *Advanced Materials* **2001**, *13*, 1152.

19. Segalman, R. A.; Hexemer, A.; Hayward, R. C.; Kramer, E. J. *Macromolecules* **2003**, *36*, 3272.

20. Harrison, C.; Angelescu, D. E.; Trawick, M.; Cheng, Z. D.; Huse, D. A.; Chaikin, P. M.; Vega, D. A.; Sebastian, J. M.; Register, R. A.; Adamson, D. H. *Europhysics Letters* **2004**, *67*, 800.

21. Vega, D. A.; Harrison, C. K.; Angelescu, D. E.; Trawick, M. L.; Huse, D. A.; Chaikin, P. M.; Register, R. A. *Physical Review E* **2005**, 71.

22. Mansky, P.; Liu, Y.; Huang, E.; Russell, T. P.; Hawker, C. *Science* **1997**, *275*, 1458.

23. Ryu, D. Y.; Shin, K.; Drockenmuller, E.; Hawker, C. J.; Russell, T. P. *Science* **2005**, *308*, 236.

24. Thurn-Albrecht, T.; DeRouchey, J.; Russell, T. P.; Jaeger, H. M.; *Macromolecules* **2000**, *33*, 3250.

25. DeRouchey, J.; Thurn-Albrecht, T.; Russell, T. P.; Kolb, R. *Macromolecules* **2004**, *37*, 2538.

26. Kim, G.; Libera, M. **Macromolecules 1998**, *31*, 2569.

27. Kim, S. H.; Misner, M. J.; Xu, T.; Kimura, M.; Russell, T. P. *Advanced Materials* **2004**, *16*, 226.

28. Bruce, P. G. *Chemical Communications* **1997**, 1817.

29. MacGlashan, G. S.; Andreev, Y. G.; Bruce, P. G. *Nature* **1999**, *398*, 792.

30. Andreev, Y. G.; Bruce, P. G. *Electrochimica Acta* **2000**, *45*, 1417.

31. Gadjourova, Z.; Andreev, Y. G.; Tunstall, D. P.; Bruce, P. G. *Nature* **2001**, *412*, 520.

32. Tarascon, J. M.; Armand, M. *Nature* **2001**, *414*, 359.

33. Pereira, R. P.; Rocco, A. M.; Bielschowsky, C. E. *Journal of Physical Chemistry B* **2004**, *108*, 12677.

34. Christie, A. M.; Lilley, S. J.; Staunton, E.; Andreev, Y. G.; Bruce, P. G. *Nature* **2005**, *433*, 50.

35. Ruzette, A. V.; Soo, P. P.; Sadoway, D. R.; Mayes, A. M. *Journal of the Electrochemical Society* **2001**, *148(6)*, A537-A543.

36. Spatz, J. P.; Herzog, T.; Mossmer, S.; Ziemann, P.; Moller, M. *Advanced Materials* **1999**, *11*, 149.

37. Breulmann, M.; Forster, S.; Antonietti, M. *Macromolecular Chemistry and Physics* **2000**, *201*, 204.

38. Sohn, B. H.; Yoo, S. I.; Seo, B. W.; Yun, S. H.; Park, S. M. *Journal of the American Chemical Society* **2001**, *123*, 12734.

39. Glass, R.; Moller, M.; Spatz, J. P. *Nanotechnology* **2003**, *14*, 1153.

40. Renaud, G.; Lazzari, R.; Revenant, C.; Barbier, A.; Noblet, M.; Ulrich, O.; Leroy, F.; Jupille, J.; Borensztein, Y.; Henry, C. R.; Deville, J. P.; Scheurer, F.; Mane-Mane, J.; Fruchart, O. *Science* **2003**, *300*, 1416.

41. Dourdain, S.; Rezaire, A.; Mehdi, A.; Ocko, B. M.; Gibaud, A. *Physica B-Condensed Matter* **2005**, *357*, 180.

42. Ratner, M. A.; Shriver, D. F. *Chemical Reviews* **1988**, *88*, 109-24.

CHAPTER 5

TOPOGRAPHICALLY AND CHEMICALLY PATTERNED SUBSTRATES

5.1 Introduction

In recent years diblock copolymers have been studied as a means to template surfaces for use in devices that require structure on the nanometer length scale.[1-14] A set of these devices require aligned structures with a high degree of lateral order. Magnetic storage media is one such application that not only requires long range order and a well-defined grain orientation relative to a macroscopic reference to achieve addressable media. Several routes have been used to address these issues, such as electric fields, shear, solvent evaporation, and thermal gradients.[15-20] Kramer and coworkers have demonstrated the effect of lateral confinement on the lateral order in spherical block copolymers on topographically patterned surfaces.[21] They found that by placing these materials onto stepped surfaces, confinement reduced the number of defects near the step boundary.[22] Subsequently, this work has been applied to cylindrical block copolymers on stepped surfaces with microdomain orientations both parallel and normal to the surface.[23-26] However, in both of these cases, the film thickness was limited to approximately the lattice spacing of the copolymer microdomains for templating purposes.

Previously, we have shown that controlled solvent evaporation in block copolymer thin films can provide a very simple but robust route to generate near defect-free microstructures over large areas in block copolymer films.[27, 28] It was also found that by using this technique, the aspect ratio of the nanostructures generated by the

copolymer was not limited by film thickness. Strong repulsion between the copolymer blocks combined with a highly directional field established during of solvent evaporation, where copolymer ordering is initiated at the surface of the film and propagates through the entire film, leads to high aspect ratio microdomains with a high degree of long-range lateral order.

Here, we will focus on the use of solvent annealing of block copolymer films on patterned surfaces. By combining the flexibility in film thickness along with the speed and quality of lateral order achieved by solvent annealing with the confinement imparted by pattern surfaces, demonstrate a route to generate highly ordered, sectorized surfaces having potential use in storage applications. In addition, surfaces into flat surfaces that are patterned chemically will be used to direct and confine the block copolymers.

5.2 Experimental

Topographically patterned surfaces were prepared by either UV or electron beam lithography. The surfaces were cleaned by placing the wafers into sulfuric acid with an oxidizer (Nochromix) for 12 hours and subsequently rinsed in RO water to remove any residual surface contaminants residual from the lithographic processes. The chemically patterned surfaces were prepared by anchoring octadecyltrichlorosilane (OTS) onto a silicon wafer homogenously. Subsequently, the films were pattered by electro-oxidation of the OTS surface using a SFM probe at Brookhaven National Laboratory. The surfaces were then stored in RO water to prevent contamination until use.

Polystyrene-*block*-poly(ethylene oxide) copolymer, PS-*b*-PEO, with a molecular weight of 25.3 kg/mol and a dispersity of 1.04 was purchased from Polymer Source, Inc.

The weight fraction of PS was 0.75 and, in the bulk, the copolymer self-assembles into hexagonally packed arrays of 20.7 nm diameter cylindrical PEO microdomains in a PS matrix with a lattice period of 31.9 nm. Thin PS-*b*-PEO films were prepared by spin-coating either copolymer solutions in benzene onto topographically patterned silicon wafers or copolymer solutions in a benzene/hexane mixture onto chemically patterned OTS surfaces. The ratio of benzene to hexane was set to where the copolymer remained soluble, but still wet the OTS (~1.7:1). Subsequently the films were solvent annealed in a benzene vapor atmosphere. SFM images were obtained in both the height and phase-contrast mode using a Digital Instruments Dimension 3000 scanning force microscope in the tapping mode.

5.3 Topographically Patterned Substrates

A 150nm thick film of polystyrene-b-poly(ethylene oxide) diblock copolymer (19k:6.3k), which exhibits cylindrical morphology in the bulk, was deposited by spin coated onto a patterned silicon wafer. The wafer was patterned with silicon oxide using standard lithographic techniques. Figure 5.1A shows a SFM height scan across a patterned silicon wafer, where the depth of the trough is 325 nm and the width of the trough is 600 nm with 200 nm spacing between each trough. Subsequently, the film was placed into benzene vapor for 48 hours. In the swollen state the mobility is such that the film heterogeneously dewets from any surface impurity. In particular, the copolymer dewets from the edges of the patterned oxide. However, the block copolymer

Figure 5.1 SFM cross sections of topographically patterned surface with troughs 600 nm wide and 200nm between each trough A) before and B) after the deposition and solvent annealed a spin-coated PS-*b*-PEO thin film. C) An SFM image of the film on the patterned surface after solvent annealing. The inset is an FFT of the entire image, indicating that the grain orientation is uniform across the whole surface.

is trapped within the troughs. Figure 5.1B shows the SFM height scan of the nearly filled trough. In the swollen state, the copolymer has sufficient mobility to remove defects quickly. As more solvent evaporates, the block copolymer at the surface templates an ordering front that goes from the surface to the substrate, generating ordered, oriented microdomains that span the entire film thickness, leaving structures with an aspect ratio of ~10:1. An SFM image of the copolymer confined on the patterned surface is shown in Figure 5.1C. The dark hexagonally packed domains are the PEO within the brighter PS matrix inside of an oxide trough. The copolymer film is nearly defect free across the width of each trough and along the length of the image, 6 μm, and extends further. Additionally, the grain orientation from one trough to the next is identical, as the walls of the patterned oxide dictate the orientation. Included in the figure is a Fast Fourier Transform (FFT) of the entire SFM image. The six spots indicate that the grain orientation of the copolymer in is the same in every trough. It is clear that this process can be used to sectorize a surface and macroscopically align the grain orientation of the block copolymer microdomains to macroscopic reference.

To further examine the effect of lateral confinement on the block copolymer microdomains, substrates with a series of trough widths, w, with a step height of ~50 nm were made, as shown schematically in Figure 5.2A. SFM images with block copolymer films deposited into the troughs that were solvent annealed on the substrates are shown in Figure 5.2, where the widths of the troughs are B) 167 C) 177 D) 234 E) 270 F) 305 G) 387 H) 445 and I) 550. For each SFM image shown is the corresponding FFT. In each image the confinement of the copolymer allows for control over the gain orientation, as

A

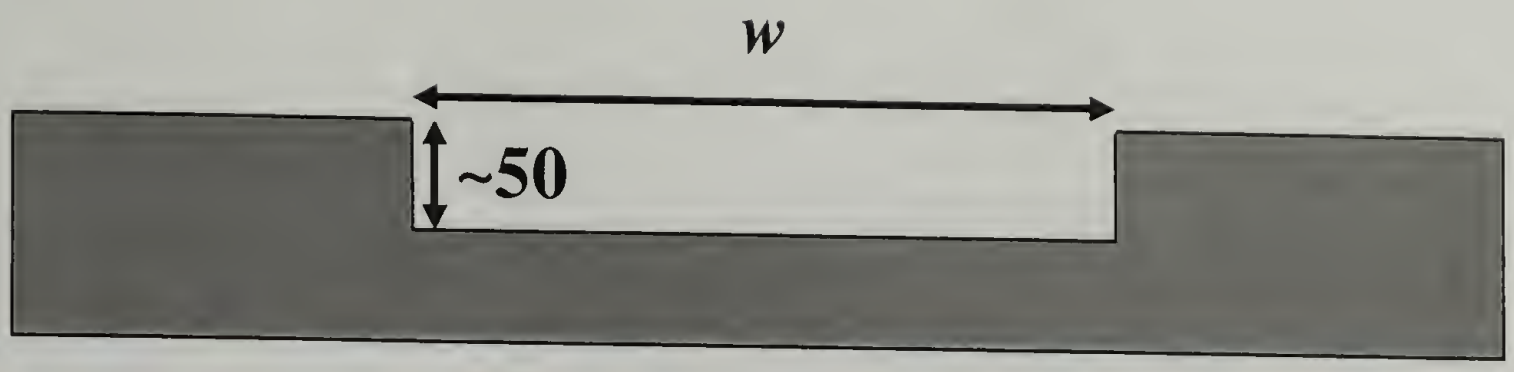

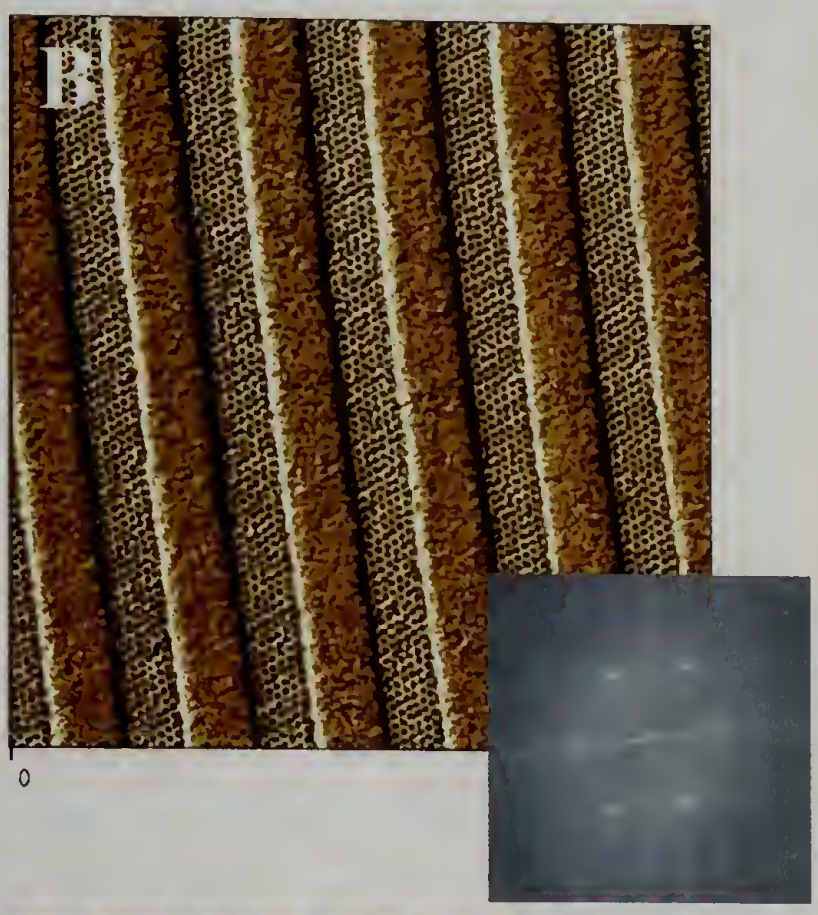

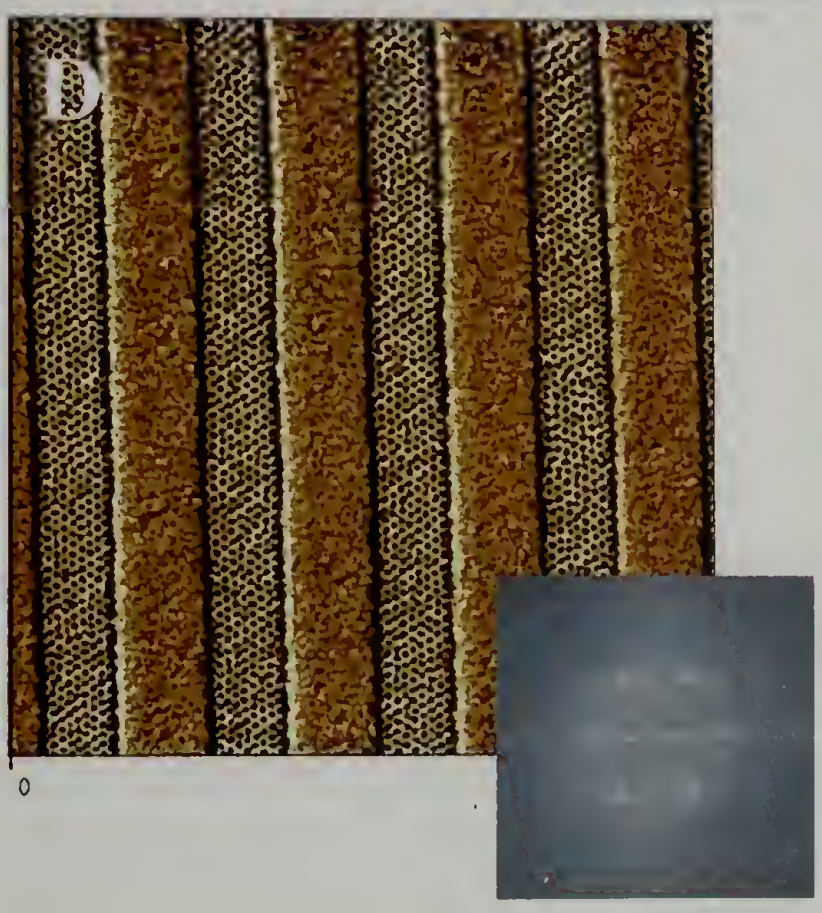

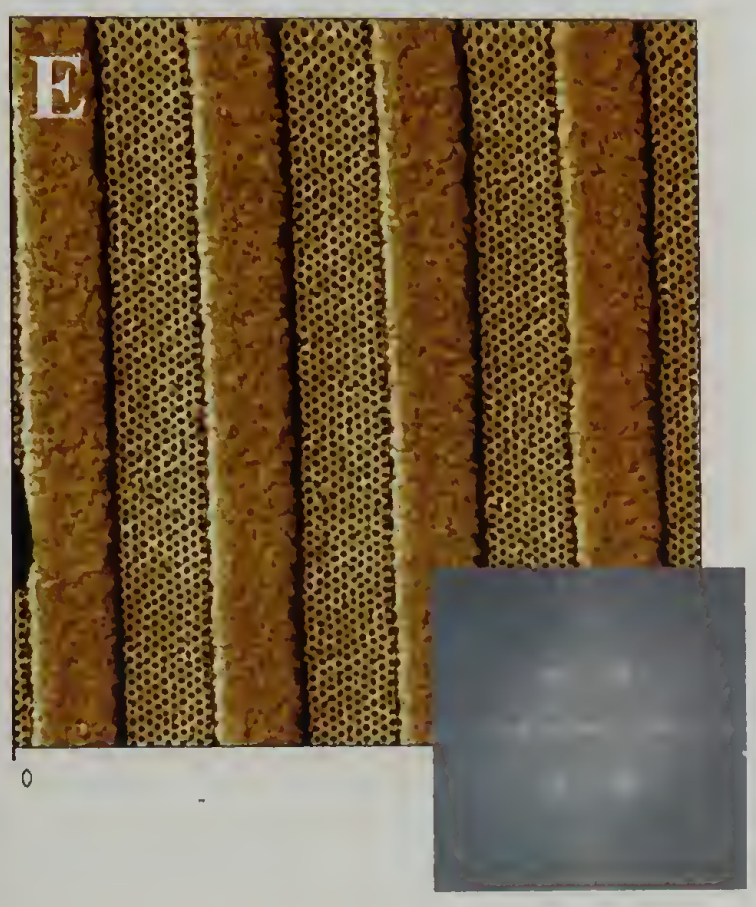

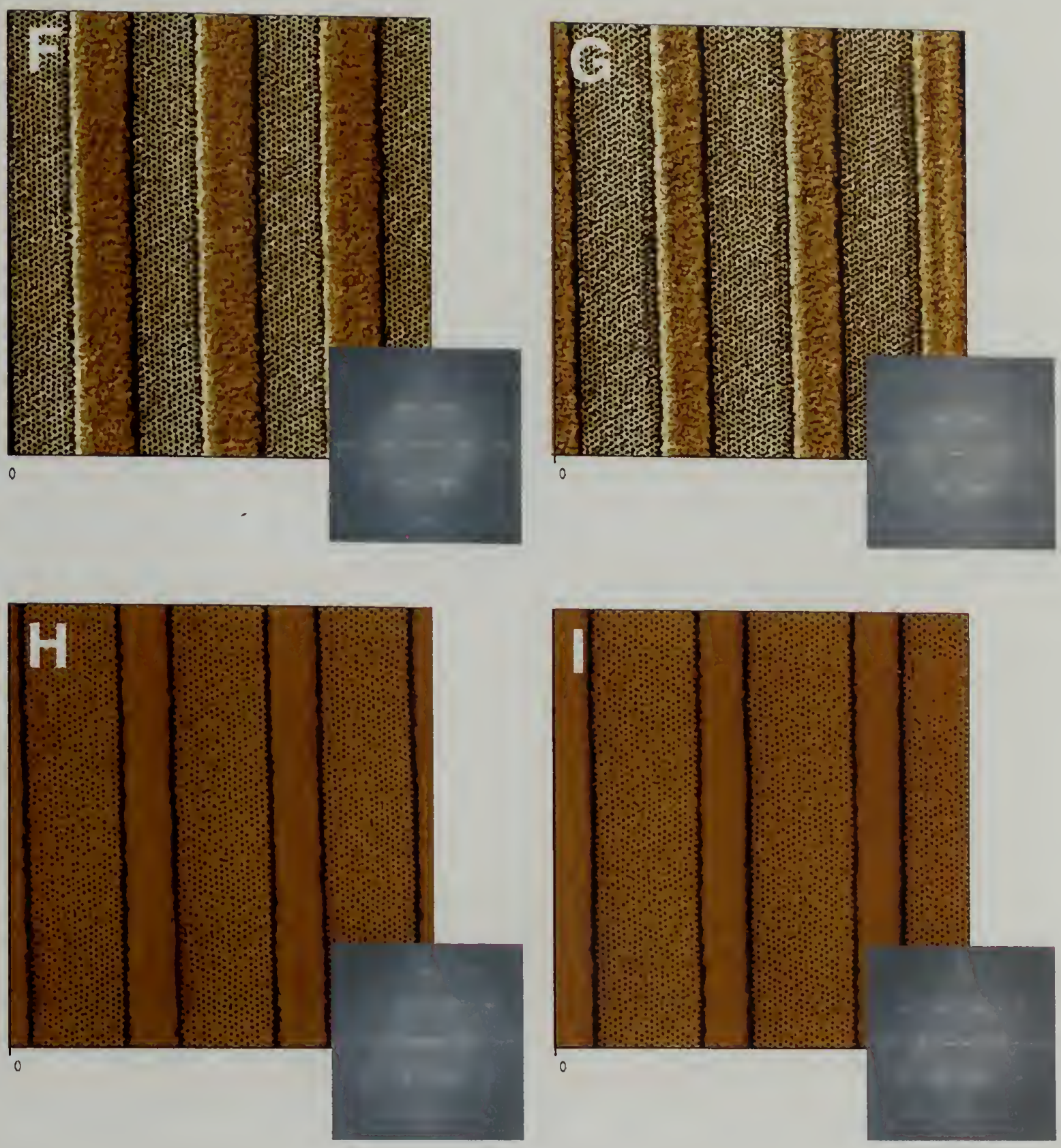

Figure 5.2 A) A schematic of a topographically patterned substrate with a step height of ~50 nm and a trough width of w. SFM images of solvent annealed PS-*b*-PEO spin-coated films onto a substrate patterned with a series of troughs of widths of B) 167 C) 177 D) 234 E) 270 F) 305 G) 387 H) 445 and I) 550. An FFT is included with each image.

each FFT shows six first order spots, and, in fact, in all images very few defects can be seen. Figure 5.3A is a plot of the azimuthally integrated FFTs from the SFM images. As can be seen the copolymer spacing is not constant as the width of the trough is increased. Because the trough widths are not integer multiples of the bulk lattice spacing, some rows of cylinders may be stretched or compressed. Figure 5.3B shows the copolymer spacing from the data in Figure 5.3A. Here, the change in the trough spacing is too large to observe the transition for each newly inserted row of cylinders. However it is worth noting that the changes in the spacing are isotropic within each trough.

The confinement provided by the troughs is in one dimension only. It may be fortuitous to apply confinement in multiple dimensions to sectorize the surface, which may have advantages in device applications. Therefore, several patterns were made photolithographically, including polygons, circles, annuli, and lines. However, this route proved to be challenging in getting the pattern fidelity necessary to effectively confine and direct the copolymer microdomains. In Figure 5.4 an SFM phase image is of PS-*b*-PEO confined within a hexagonal area. In the inset the topographic image of an unfilled patterned surface is shown at a lower magnification. While the topographic image looks as if an acceptable pattern was generated, it is clear in the higher magnified image that the sharpness at the intersection of the walls was much too poor. Because of these poorly defined intersections, locally the polygon is incompatible with the hexagonal lattice of the PS-*b*-PEO, which prohibited a true confinement of the PS-b-PEO or imparting a visible orientation of the lattice. Obviously, a higher resolution patterning technique is needed to further explore confinement in more than one dimension.

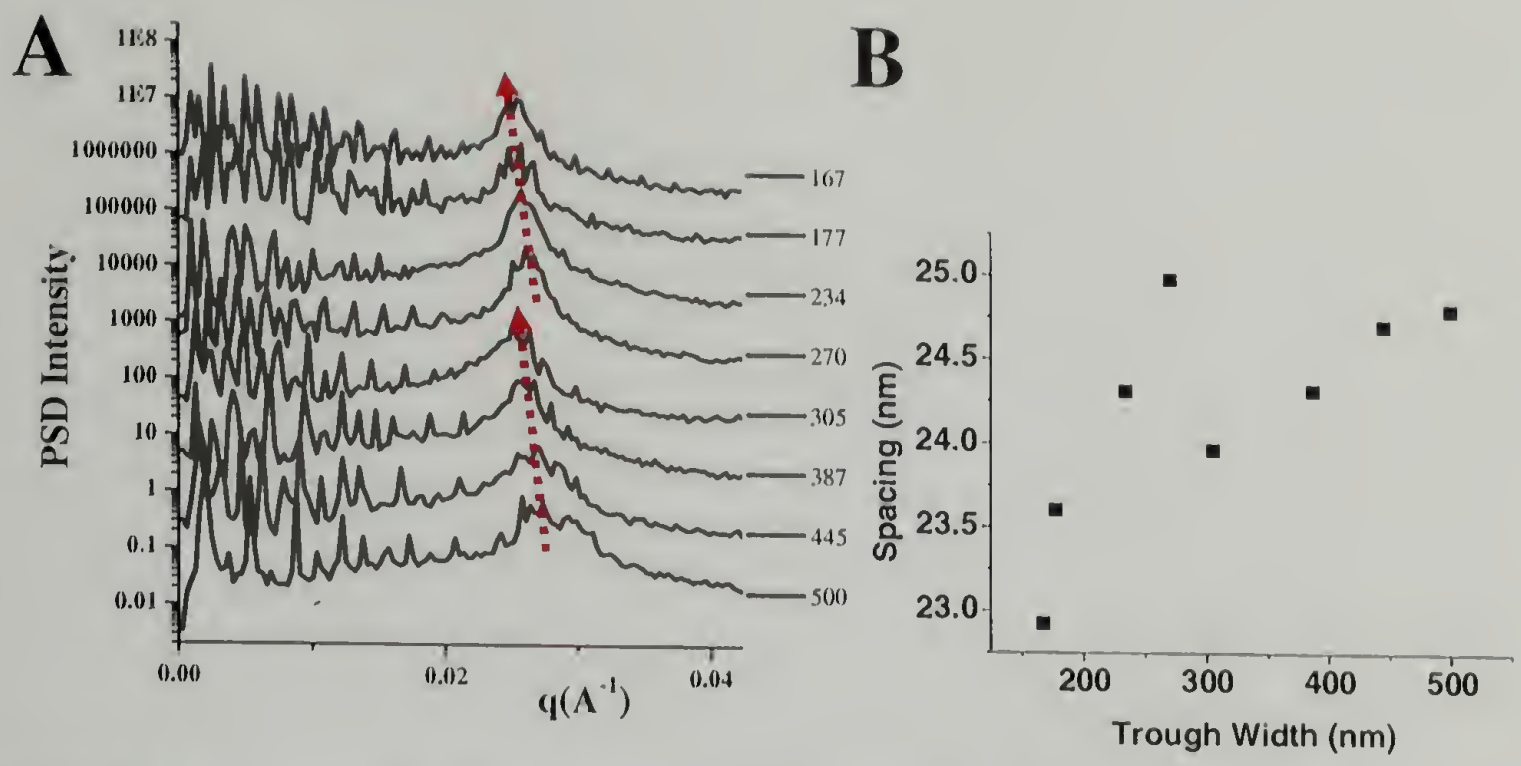

Figure 5.3 A) Plots of the FFTs in Figure 5.2 azimuthally integrated. Here the copolymer spacing is varies in order accommodate changes in the trough spacing that are not integers of the bulk lattice spacing. B) Copolymer spacing fit from the FFT's in A.

Figure 5.4 An SFM image of solvent annealed PS-*b*-PEO spin-coated films onto a substrate patterned with an array of hexagons. The fidelity of the pattern here is insufficient to direct the ordering of the copolymer microdomains.

5.4 Chemically Patterned Surfaces

Electro-pen lithography is a technique where by a conductive SPM tip is moved across a surface covered with a monolayer of alkanes chemically attached to the substrate. Where the tip moves across the surface the alkane is oxidized.[29-32] Figure 5.5A illustrates the electro-pen lithography process. A substrate is coated with a monolayer of hydrophobic silane, here octadecyltrichlorosilane, or OTS. As the tip comes into contact with the surface, water collects from ambient humidity between the tip and the substrate by capillary force. A voltage is then applied across the tip/substrate gap and the substrate and the surface is oxidized by oxygen radicals through the electrolysis of the water at the tip. This reaction replaces the CH_3 end-group at the end of the OTS with COOH, converting the surface from a hydrophobic to hydrophilic surface in the path of the tip. To generate filled shapes such as polygons, several concentric polygons are drawn such that the lines are written close enough to allow for overlap in the oxidation zones such that uniform oxidation inside of the polygons is obtained. Substrates were patterned with shapes including lines and polygons several of these are shown in Figure 5.5B.

Dilute solutions (~1%) of polystyrene-*b*-polyethylene oxide in a blend of hexane and benzene, such that the solution could wet the substrate and still dissolve the polymer, were deposited onto the substrates and spin-coated to obtain uniform films. The films were then placed in a benzene atmosphere for 24 hours to allow the films to swell and selectively dewet the OTS regions of the surface. The SFM phase contrast and hight images in Figure 5.6A and B, respectively, demonstrate a pattern after film deposition and exposure to the benzene atmosphere. Here, a triangle was chosen due to the

A

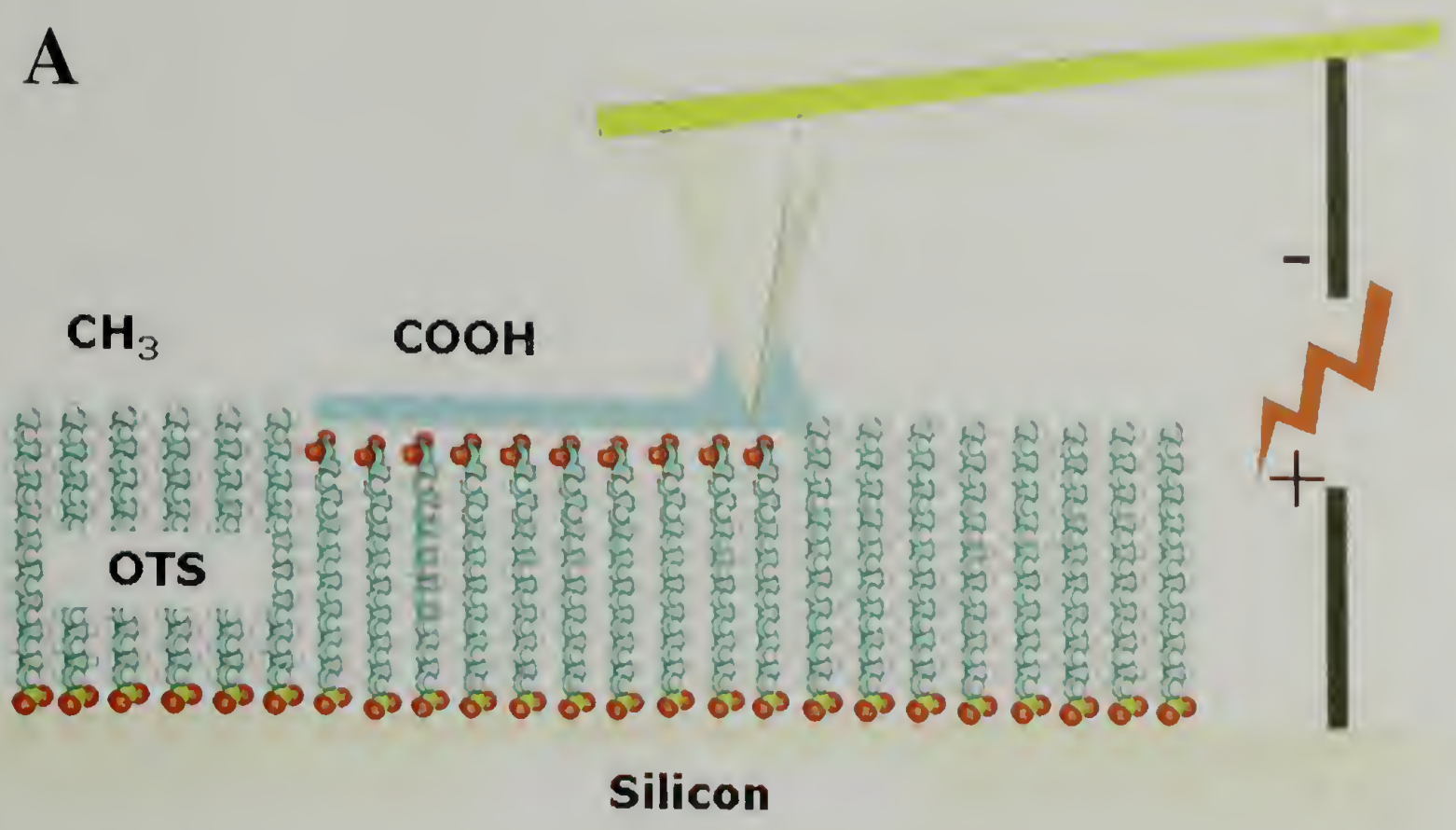

B

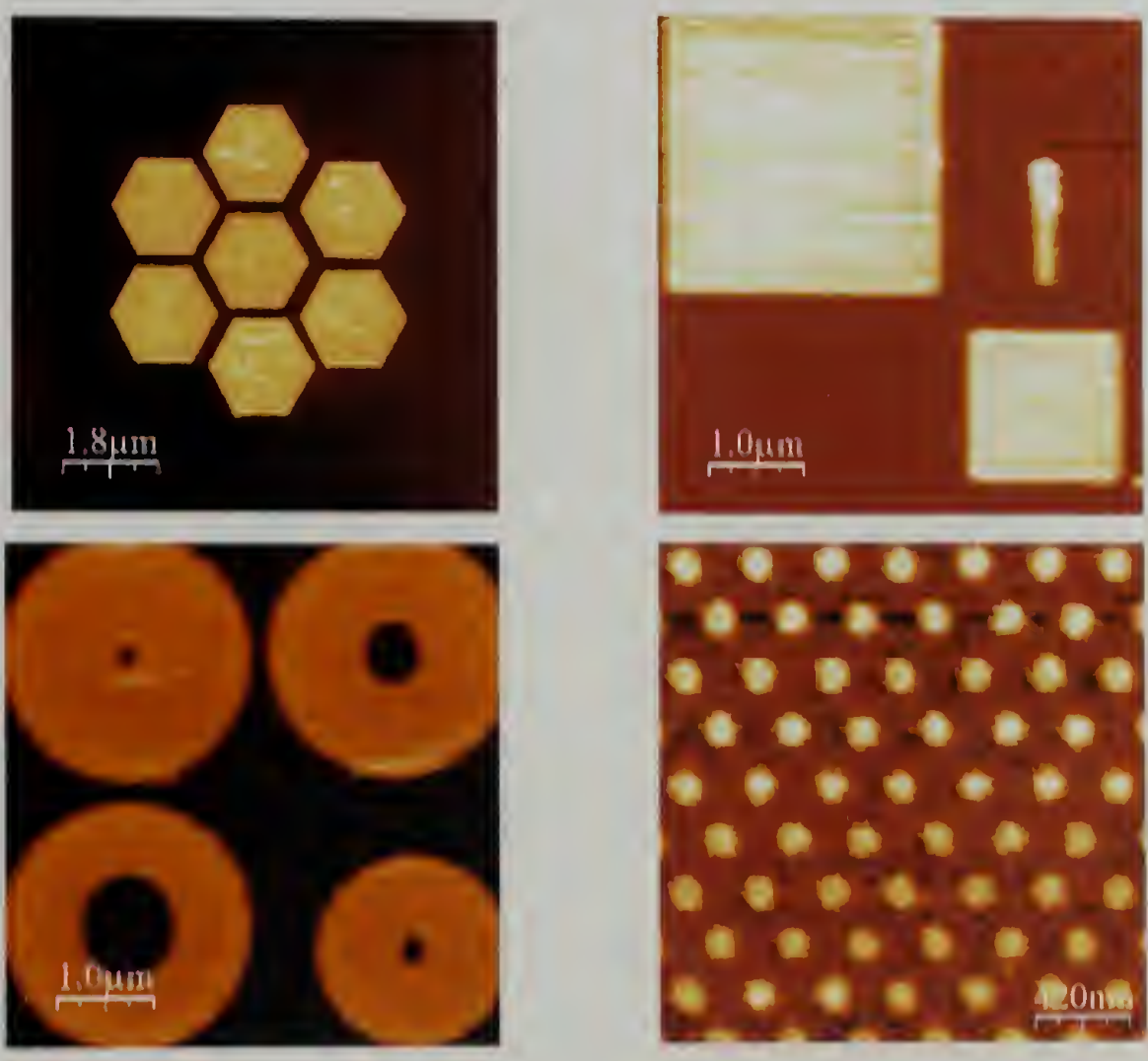

Figure 5.5 A) A schematic of the electro-oxidative patterning by and SFM probe on an OTS surface. B) Several patterns generated by chemically modifying the surface.

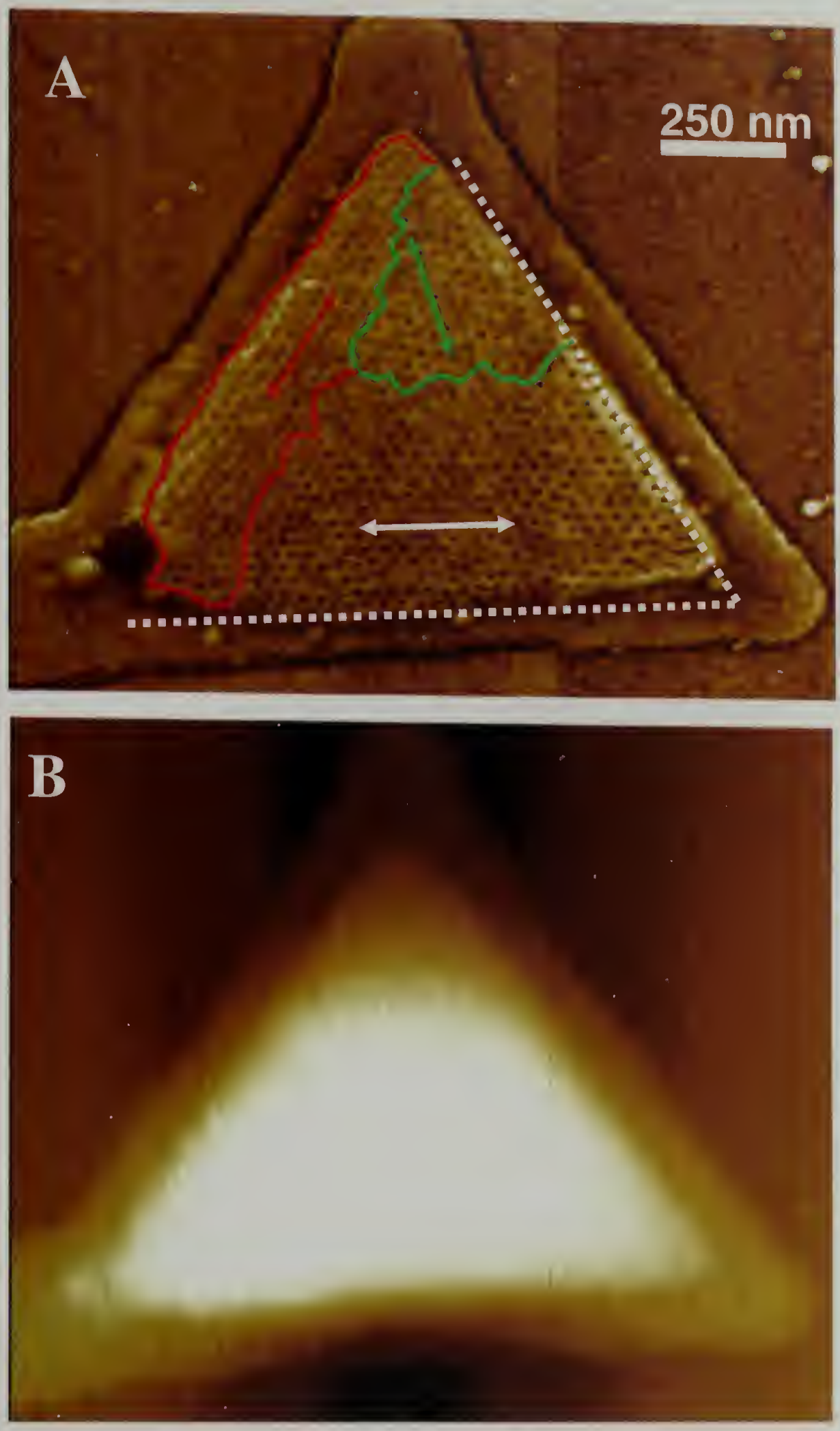

Figure 5.6 SFM A) phase and B) height images of a solvent annealed PS-b-PEO thin film deposited on to a triangularly chemically patterned surface. The pattern directs the dewetting and ordering of the block copolymer.

compatibility with the hexagonal lattice of the copolymer. It can be seen in the phase contrast image that the PEO microdomains are oriented normal to the surface Here, the copolymer microdomains orient with respect to each edge of the triangle. However, since the shape of the droplet is not an ideal equilateral triangle, several grains are apparent, each directed by an edge. It is interesting to note, however, that the shape of the droplet is more ideal than that of the original surface pattern and that the shape of the droplet is dictated by the shape of the pattern and the contact line at the corners of the triangle. Also, the interaction of the oxidized surface with the copolymer produces a half-layer of the copolymer at the edge of the confined area.

Figure 5.7A is a surface pattern that is not compatible with the block copolymer microdomain lattice, namely, a square. Similar to the triangle, the deoposition of the copolymer is directed into the patterned area and, for much of the surface, the ordering of the copolymer is directed by the edges of the pattern. Complete filling of the pattern is not observed. In particular the droplet generally does not fill to the corners, but, rather form a line that is consistent with the copolymer microdomain lattice. Because of this, the overall order and grain orientation remains fairly uniform across the surface, as seen in the FFT of the entire image (the center image in Figure 5.7B). Several FFTs were taken of each quadrant of the SFM image in Figure 5.7A, with the location of where the FFT was placed correspondingly in Figure 5.7B. All but the top left corner shows a single grain orientation, similar to the overall image. In the top left corner, the there are two competing grain orientations, one directed from the top edge and the other directed from the side edge. Here, the withdrawal of the drop of copolymer from the edge is not

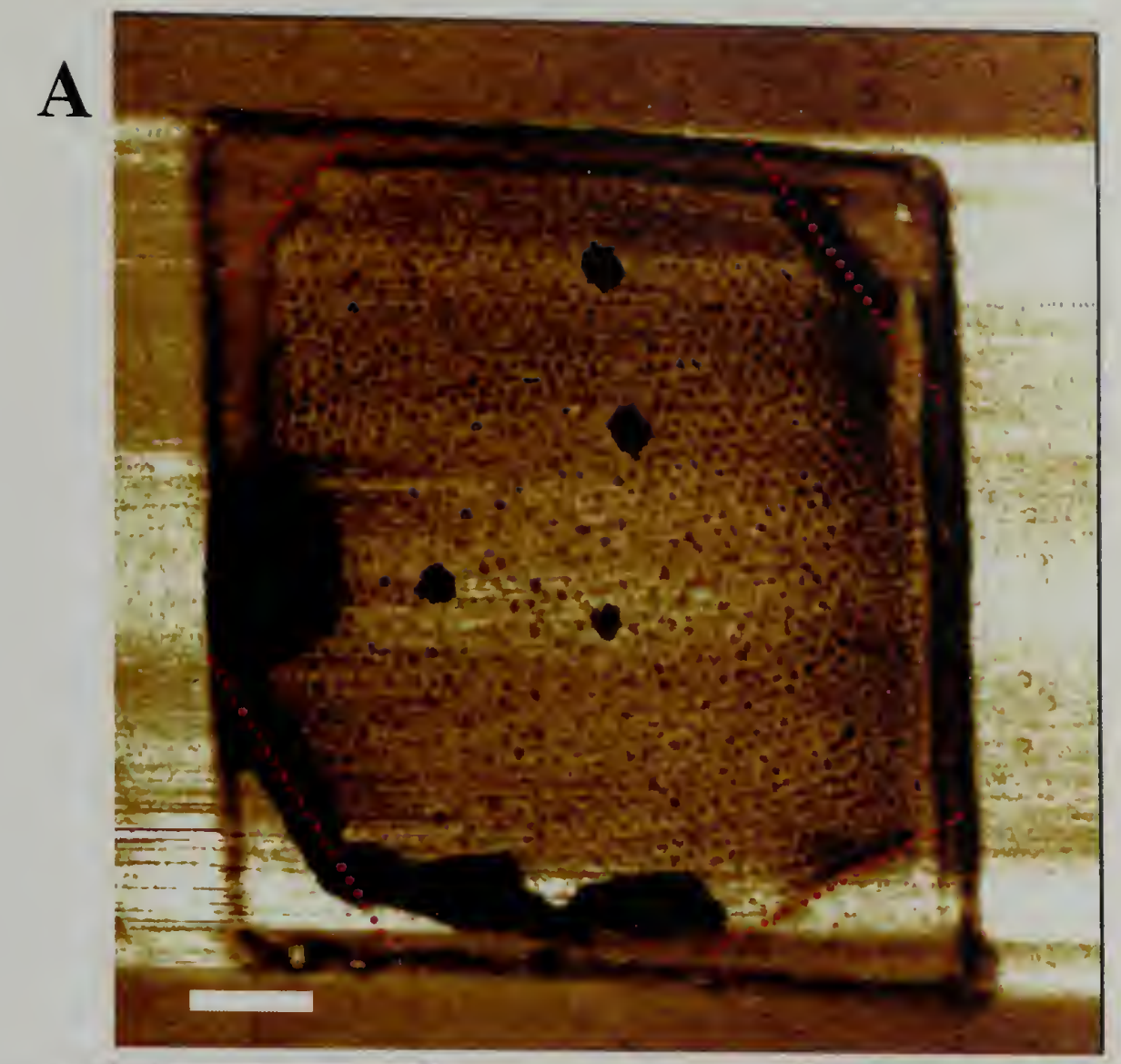

Figure 5.7 A) An SFM phase image of a solvent annealed PS-b-PEO thin film deposited on a chemically patterned surface in the shape of a square. The dotted like are to highlight the irregular filling of the corners. B) FFT images of the image in A. The center FFT is of the whole film, while the other FFTs correspond to the quadrent of the film the FFT was obtained.

as significant as the other corners due to stabilization by the wetting defect on the left edge.

Finally, in Figure 5.8, is an SFM phase image of the block copolymer deposited on to a chemical pattern in the shape of a hexagon. As in the triangle, a hexagon is compatible with the hexagonal lattice of the block copolymer microdomains; however, here the angles are all obtuse angles. Filling of sharp angles or corners, as in the square, are energetically unfavorable, creating extra surface without significant gain in the overall droplet volume. The hexagon in the SFM image is completely filled and, again, the copolymer is directed from each edge of the hexagon. While the translational order is not exceptional here, the grain orientation is well defined and is a promising result that should promote further development.

5.5 Conclusions

The simple process of solvent evaporation has been shown to produce highly order arrays of cylindrical microdomains in block copolymers with long-range lateral order. Solvent evaporation in thin films is unidirectional, which produces a self-assembly directed normal to the film surface, akin to a zone refinement. Topographically and chemically patterned surfaces offer a route to sectoring a surface, which promotes defect removal and control of the lattice orientation of copolymer films with high aspect ratio cylindrical domains. Topographically patterned surfaces, in particular, allow well-defined boundaries to confine the copolymer microdomains on a surface and effectively direct the ordering and grain orientation of the copolymer microdomains. Chemically patterned surfaces provide a route to direct the block copolymer ordering on completely flat surfaces, which may have advantages in applications where adding additional

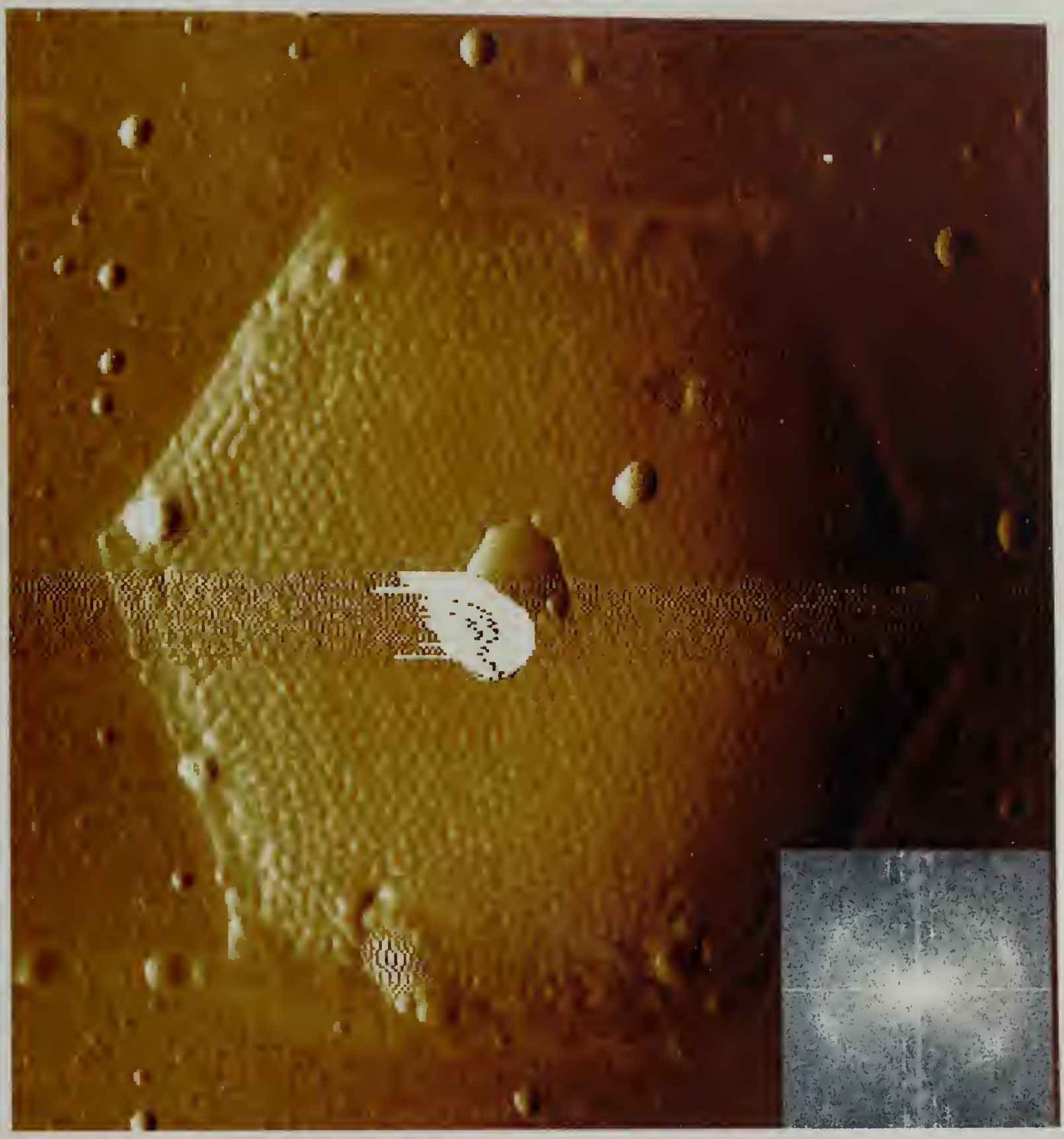

Figure 5.8 An SFM phase image of a solvent annealed PS-b-PEO thin film deposited on to a chemically patterned hexagon on a OTS surface. The copolymer fills the hexagon completely and effectively directs the grain orientation of the copolymer microdomains. The inset is the FFT of the entire image.

topography may be undesirable. Further, chemical patterning by electro-oxidative SFM is a high-resolution, flexible technique that can be used to effectively to direct the dewetting and ordering of block copolymers. These results have significant importance in achieving addressable media from diblock copolymer self-assembly.

5.6 References

1. G. H. Fredrickson & F. S. Bates, *Ann. Rev. Mat Sci*, **1990**, 1-70.

2. F. S. Bates, *Science* **1991**, *251*, 898.

3. Park, M.; Harrison, C.; Chaikin, P. M.; Register, R. A.; Adamson, D. H. *Science* **1997**, *276*, 1401-1404.

4. Li, R. R.; Dapkus, P. D.; Thompson, M. E.; Jeong, W. G.; Harrison, C.; Chaikin, P. M.; Register, R. A.; Adamson, D. H. *Appl. Phys. Lett.* **2000**, *76*, 1689-1691.

5. Templin, M.; Franck, A.; Du Chesne, A.; Leist, H.; Zhang, Y.; Ulrich, R.; Schadler, V.; Wiesner, U. *Science* **1997**, *278*, 1795-1798.

6. Spatz, J. P.; Herzog, T.; Moessmer, S.; Ziemann, P.; Moeller, M. *Adv. Mater.* **1999**, *11*, 149-153.

7. Lopes, W. A.; Jaeger, H. M. *Nature* **2001**, *414*, 735-738.

8. Cheng, J. Y.; Ross, C. A.; Chan, V. Z. H.; Thomas, E. L.; Lammertink, R. G. H.; Vancso, G. J. *Adv. Mater.* **2001**, *13*, 1174-1178.

9. Cheng, J. Y.; Ross, C. A.; Thomas, E. L.; Smith, H. I.; Vancso, G. J. *Appl. Phys. Lett.* **2002**, *81*, 3657-3659.

10. Thurn-Albrecht, T.; Schotter, J.; Kastle, G. A.; Emley, N.; Shibauchi, T.; Krusin-Elbaum, L.; Guarini, K.; Black, C. T.; Tuominen, M. T.; Russell, T. P. *Science* **2000**, *290*, 2126-2129.

11. Kim, H.-C.; Jia, X.; Stafford, C. M.; Kim, D. H.; McCarthy, T. J.; Tuominen, M.; Hawker, C. J.; Russell, T. P. *Adv. Mater.* **2001**, *13*, 795-797.

12. Black, C. T.; Guarini, K. W.; Milkove, K. R.; Baker, S. M.; Russell, T. P.; Tuominen, M. T. *Appl. Phys. Lett.* **2001**, *79*, 409-411.

13. Bal, M.; Ursache, A.; Tuominen, M. T.; Goldbach, J. T.; Russell, T. P. *Appl. Phys. Lett.* **2002**, *81*, 3479-3481.

14. Misner, M. J.; Skaff, H.; Emrick, T.; Russell, T. P. *Adv. Mater.* **2003**, *15*, 221-224.

15. Kim, G.; Libera, M.;, *Macromolecules* **31**, 2670 (1998).

16. Lin, Z.; Kim, D. H.; Wu, X.; Boosahda, L.; Stone, D.; LaRose, L.; Russell, T. P. *Adv. Mater.* **2002**, *14*, 1373.

17. Reiter, G.; Castelein, G.; Hoerner, P.; Riess, G.; Blumen, A.; Sommer, J. U. *Phys. Rev. Lett.* **1999**, *83*, 3844.

18. Hahn, J.; Sibener, S. J. *Langmuir*, **16**, 47766-4769 (2000).

19. Villar, M. A.; Rueda, D. R.; Ania, F.; Thomas, E. L. *Polymer* **2002**, *43*, 5139.

20. Bodycomb, J.; Funaki, Y.; Kimishima, K.; Hashimoto, T. *Macromolecules* **1999**, *32*, 2075.

21. Segalman, R. A.; Yokoyama, H.; Kramer, E. J. *Adv. Mater.* **2001**, *15*, 1152.

22. Segalman, R. A.; Hexemer, A.; Kramer, E. J. *Macromolecules* **2003**, *36(18)*, 6831-6839.

23. Cheng, J. Y.; Ross, C. A.; Thomas, E. L.; Smith, H. I.; Vancso, G. J. *Appl. Phys. Lett.* **2002**, *81*, 3657.

24. Xiao, S.; Yang, X. M.; Edwards, E. W.; La, Y. H.; Nealey, P. F. *Nanotechnology* **2005**, *16(7)*, 324-329.

25. Hammond, M. R.; Cochran, E.; Fredrickson, G. H.; Kramer, E. J. *Macromolecules* **2005**, *38(15)*, 6575-6585.

26. Sundrani, D.; Darling, S. B.; Sibener, S. J. *Langmuir* **2004**, *20(12)*, 5091-5099.

27. Kimura, M.; Misner, M. J.; Xu, T.; Kim, S. H.; Russell, T. P. *Langmuir* **2003**, *19(23)*, 9910-9913.

28. Kim, S. H.; Misner, M. J.; Xu, T.; Kimura, M.; Russell, T. P. *Adv. Mat.*, **2004**, *16(3)*, 226-231.

29. Maoz, R.; Cohen, S.; Sagiv, J. *Adv. Mater.* J., *11*, 55.

30. Cai, Y.; Ocko, B. M. *JACS* **2005**, *127(46)*, 16287-16291.

31. Checco, A.; Gang, O.; Ocko, B. M. *Phys. Rev. Lett.* **2006**, *96(5)*, 056104/1-056104/4.

32. Checco, A.; Cai, Y.; Gang, O.; Ocko, B. M. *Ultramicroscopy* **2006**, *106(8-9)*, 703-708.

CHAPTER 6

SOLVENT-INDUCED ORDERING IN THIN FILM DIBLOCK COPOLYMER/HOMOPOLYMER MIXTURES

6.1 Introduction

The self-assembly of materials is emerging as a key process in the fabrication of functional nanostructured materials, since it provides a powerful "bottom-up" route to well-organized strúctures on the nanoscopic scale. The last few years have seen considerable progress in the development of concepts and methods to generate a variety of the nano and microstructured materials by using such a strategy.[1] Block copolymers, one class of self-assembling materials, offer an attractive route to fabricate nanometer-scale structure, since they spontaneously form a range of well-defined, well-ordered morphologies including spheres, cylinders, and lamellae, depending on the volume fractions of the components. In addition, the molecular weight of the copolymer provides control over the size and separation distance of the microdomains, and specific functionality can be incorporated into the structure by varying the chemical nature of the copolymer. This versatility makes block copolymers ideal candidates for use as templates and scaffolds for nanotechnological applications ranging from magnetic storage to displays and sensors. Tremendous progress and innumerable examples have been reported in the last decade.[2-15] Control of well-organized structures over large scales is still challenging and, in the case of block copolymers, the lack of long-range order can limit their utilization. For applications requiring addressability, long-range lateral order and orientation of elements are key and, therefore, self-assembly is no longer

sufficient. Rather a directed self-assembly or a biased, directed self-assembly is required wherein the precise location of each nanoscopic element is defined by external forces, such as electric fields,[10,16] shear,[17,18] temperature gradient,[19] graphoepitaxy,[9,20,21] crystallization,[22,23] chemically patterned substrate,[24-27] or controlled interfacial interactions.[28-29] Very recently, we showed that the solvent evaporation at a controlled rate can provide a very simple but robust route to generate near defect-free microstructures over large areas in block copolymer films.[30,31] Solvent evaporation is a strong, highly directional field. Strong non-favorable interactions between the copolymer blocks combined with the directionality of solvent evaporation leads to a high degree of long-range lateral order with few defects.[31, 31] Moreover, the use of a cosolvent enables one to control the characteristic length scales in the block copolymer structures even further.

Here, the same strategy is applied to a mixture of a block copolymer with a small amount of homopolymer, which provides another way to control the characteristic dimensions of the morphologies. The addition of homopolymers makes the phase diagram of the system more complicated due to the coexistence of micro- and macrophase separation.[35-41] However, at low homopolymer concentrations or when the homopolymer molecular weight is below or comparable to that of the solubilizing block, the added homopolymer is completely solubilized in the copolymer microdomains. At higher concentrations, the copolymer domains become saturated with the homopolymer and the homopolymers macroscopically phase separates from the block copolymer. This behavior has been observed in the block copolymers with lamellar microdomains and cylindrical microdomains oriented normal to the surface.[40] Here, we demonstrate that

controlled solvent annealing and casting produce the long-range lateral order over large areas for copolymer/homopolymers blends. The size of microdomains increases due to the incorporation of homopolymer and depends on the concentration and molecular weight of added homopolymers. The confinement of the added homopolymer to the core of the cylindrical microdomain also enhances the propagation of the orientation of the microdomains normal to the surface over large distances.[37] Finally, by the selective removal of the homopolymer from the film, well-organized, nearly defect-free arrays of nanoscopic holes are produced in the block copolymer film.

6.2 Experimental

Commercially available polymers were used. Polystyrene-block-poly(ethylene oxide) copolymer, PS-*b*-PEO, with a molecular weight of 25.3 kg/mol and two PMMA homopolymers with molecular weight of 3.8 kg/mol and 21.2 kg/mol, were purchased from Polymer Source, Inc., and two PEO homopolymers with 4.6 kg/mol and 10.0 kg/mol were purchased from Aldrich. It should be noted that narrow molecular weight distribution homopolymers were not critical for these studies. PS-*b*-PEO, with a PS weight fraction of 0.75 and self-assembled into hexagonally packed arrays of 20.7 nm cylindrical microdomains with a lattice period of 31.9 nm. Solutions of the mixtures of block copolymer with small amount of homopolymers were spin-coated or solution-cast on silicon substrate. The compositions of the mixtures were reported as the weight fraction of homopolymer with respect to the total weight of the mixture. Spin-coated films were placed in a benzene-saturated chamber at room temperature, and the solution-casting was done in the same chamber. The film thickness was controlled by spinning

rate and/or solution concentration. To remove the PMMA homopolymer from the mixture, the film was exposed to UV irradiation and the rinsed in acetic acid.

SFM images were obtained in both the height and phase contrast mode using a Digital Instruments Dimension 3000 scanning force microscope in the tapping mode. Transmission electron microscopy (TEM) studies were performed on a JEOL 100CX electron microscope operated at 100 kV. For TEM, the samples were prepared on silicon substrates with a thick layer of silicon oxide. The film was floated onto the surface of 5 wt% HF solution, transferred to a water bath, then picked up on a Cu grid for measurement. GASAXS (grazing angle small angle X-ray scattering) measurements were performed at the Advanced Photon Source (APS) at Argonne National Laboratory.

6.3 Results and Discussion

Asymmetric, cylinder-forming polystyrene-*block*-poly(ethylene oxide) copolymer, PS-*b*-PEO, with a molecular weight of 25.3 kg/mol was used, where the weight fraction of PS was 0.75. PEO and poly(methyl methacrylate) (PMMA) were chosen as the homopolymers to be added to the block copolymer. Both homopolymers are expected to preferentially segregate to the PEO block phase in the mixture. Figure 6.1A shows the scanning force microscopy (SFM) phase image of an as-spun film of PS-*b*-PEO/PEO mixture (5 wt% PEO homopolymer) spin coated from benzene. The molecular weight of the homopolymer used here is 4.6 kg/mol (4.6k-PEO), slightly lower than that of the corresponding block chain (6.3 kg/mol). The darker (lower) phase regions corresponds to the minor component, PEO microdomains, and the lighter (higher phase) the matrix, are the major

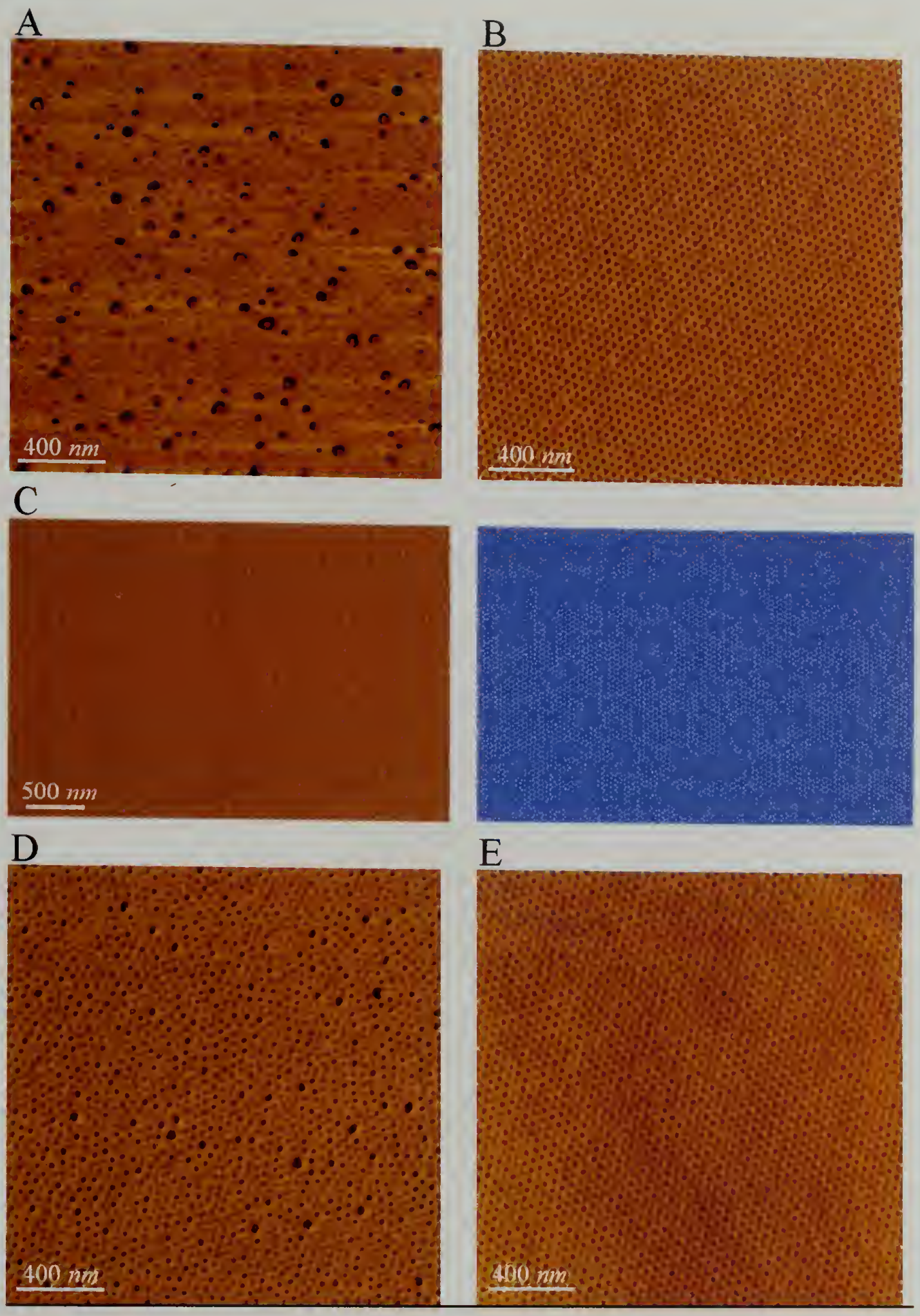

Figure 6.1 (A) SFM phase image of thin film of PS-*b*-PEO/4.6k-PEO blend with 5 wt% content of PEO homopolymer obtained by spin-coating, (B) SFM phase image after annealing the film in (A) for 48 hrs in a benzene vapor, (C) SFM phase image over large area for the film in (B) and its triangular image, and (D) and (E) SFM phase images of PS-*b*-PEO/10.0k-PEO blend film with 5 wt% homopolymer and PS-*b*-PEO/4.6k-PEO blend film with 15 wt% of homopolymer after annealing for 48 hrs in a benzene vapor, respectively.

component, PS. The surface of the as-spun film is found to show two different length scales of phase-separated domains. Considering the size of each domain and volume fraction of copolymer, it suggests that the nanoscopic arrays of small domains result from the microphase separated block copolymers and isolated, larger domains of homopolymer that has phase separated from the block copolymer, despite the low concentration of homopolymer. However, this morphology is kinetically trapped during spin-coating. Shown in Figure 6.1B is the SFM image for the same film annealed in benzene vapor for two days, where benzene was used as a solvent. Upon exposure to benzene at room temperature, the film swells and saturates within one hour as indicated by *in situ* interferometery measurement of the film thickness. Upon removal from the benzene atmosphere, the remaining solvent within the film evaporates and the film exhibits a well-organized structure where the average center-to-center distance is 42.8nm. As seen, the macrophase-separated domains of PEO homopolymer disappear, indicating that all the homopolymer chains are sequestered within the PEO microdomains of the block copolymer. Moreover, the ordering of the PEO domains in the film improves considerably, showing one grain of defect-free, hexagonal packed cylinders over the $2 \times 2\ \mu m^2$ SFM image. The bottom surface of the film shows the same structure as the top, which implies that the cylindrical domains containing the homopolymers span the entire film thickness. The perfection of the array is easily seen in the triangulation map (Figure 6.1C), where domain with six-nearest neighbors is colored blue, and defects with five- or seven-nearest neighbors are colored red and yellow, respectively. Every domain is shown to have six-nearest neighbors, indicating the perfect hexagonal packing of the cylindrical domains. This high degree of lateral order was found to extend over a length

scale of more than $15 \times 15\ \mu m^2$. Shown in Figure 6.1D is the result for the mixture having PEO homopolymer with higher molecular weight (10.0 kg/mol) than the copolymer PEO block (6.3 kg/mol). After solvent annealing, mixtures also show a long-range ordering of the cylindrical domains without macrophase separation with up to 5 wt% homopolymer. Compared to the case with lower molecular weight PEO (Figure 6.1B), the average center-to-center distance of cylindrical domains increases from 42.8 *nm* to 45.2 *nm*. According to previous experiments,[35-39] when the molecular weight of homopolymer is much lower than that of corresponding block, the added homopolymer chains are uniformly distributed in the copolymer domains. When the polymer chain length is comparable to or longer than the block length, the homopolymer is confined to the center of copolymer domains (as long as macrophase separation dose not occur). This leads to the increase in the domain size and center-to-center distance compared to the shorter chain length of the homopolymer. However, when the content of homopolymer chains in the blend exceeds ~12-15 wt.%, even after solvent-annealing, large PEO homopolymer domains remain, indicating that further incorporation of the homopolymer into the block copolymer is limited. For higher molecular weight PEO homopolymers (10.0k-PEO), this boundary occurs at lower homopolymer concentrations at 6 wt.%. Determination of a more complete phase diagram is currently under study.

Similar phase behavior and long-range ordering of phase-separated domains can be found in a blend of PS-*b*-PEO and PMMA. Figures 6.2A and 6.2B show the SFM phase images of thin film of PS-*b*-PEO/PMMA blends having 5 wt% PMMA, where the molecular weights of the PMMA homopolymers are 3.8 kg/mol and 21.2 kg/mol, respectively. Both films were annealed in the benzene vapor for 48 hours. It is evident

A

B

Figure 6.2 SFM phase images of PS-*b*-PEO/PMMA blends with 5 wt% of PMMA homopolymer in which the molecular weight of homopolymers are 3.8 kg/mol (A) and 21.2 kg/mol (B), respectively, after annealing for 48 hrs in a benzene vapor.

that no macrophase separation occurs in either film even though the molecular weight of the PMMA used in Figure 6.2B is much higher than that of the PEO block. As observed in PS-*b*-PEO/PEO blends, a near perfect lateral ordering of cylindrical domains is seen over the entire image. Such perfect lateral ordering persists over $10 \times 10\ \mu m^2$, comparable to those shown in PS-*b*-PEO and PS-*b*-PEO/PEO blend systems. As expected, as the molecular weight of homopolymer in the blend increases from 3.8 kg/mol to 21.2 kg/mol, the average center-to-center distance increases from 43.0 *nm* to 44.7 *nm*. In both systems, the macrophase separation occurs at higher concentrations of homopolymer when the copolymer is saturated and cannot solubilize the added homopolymer.

Removal of homopolymer from these arrays provides a simple route to generate a nanoporous arrays with long-range lateral order. Such results are shown in Figure 6.3A, which shows TEM image for a PS-*b*-PEO/3.8k-PMMA blend after the PMMA homopolymer has been extracted from the mixture using acetic acid. For the films of the mixtures the contrast between the three polymers is minimal and it is difficult to view the structure by TEM. However, the formation of pores in the film increases the contrast and thus the film structure is easily seen in TEM, as shown in Figure 6.3A. As expected, highly oriented, nearly defect-free arrays of nanopores are produced. These pores span the entire thickness of film. The formation and ordering of cylindrical pores was also studied by grazing angle small x-ray scattering (GASAXS), where a highly collimated, monochromatic x-ray beam impinges on the surface the film near the critical angle of the substrate, so that the film is fully penetrated by x-rays. X-rays scattered out of the plane of incidence can be used to characterize the lateral ordering and internal structure in the

A

B

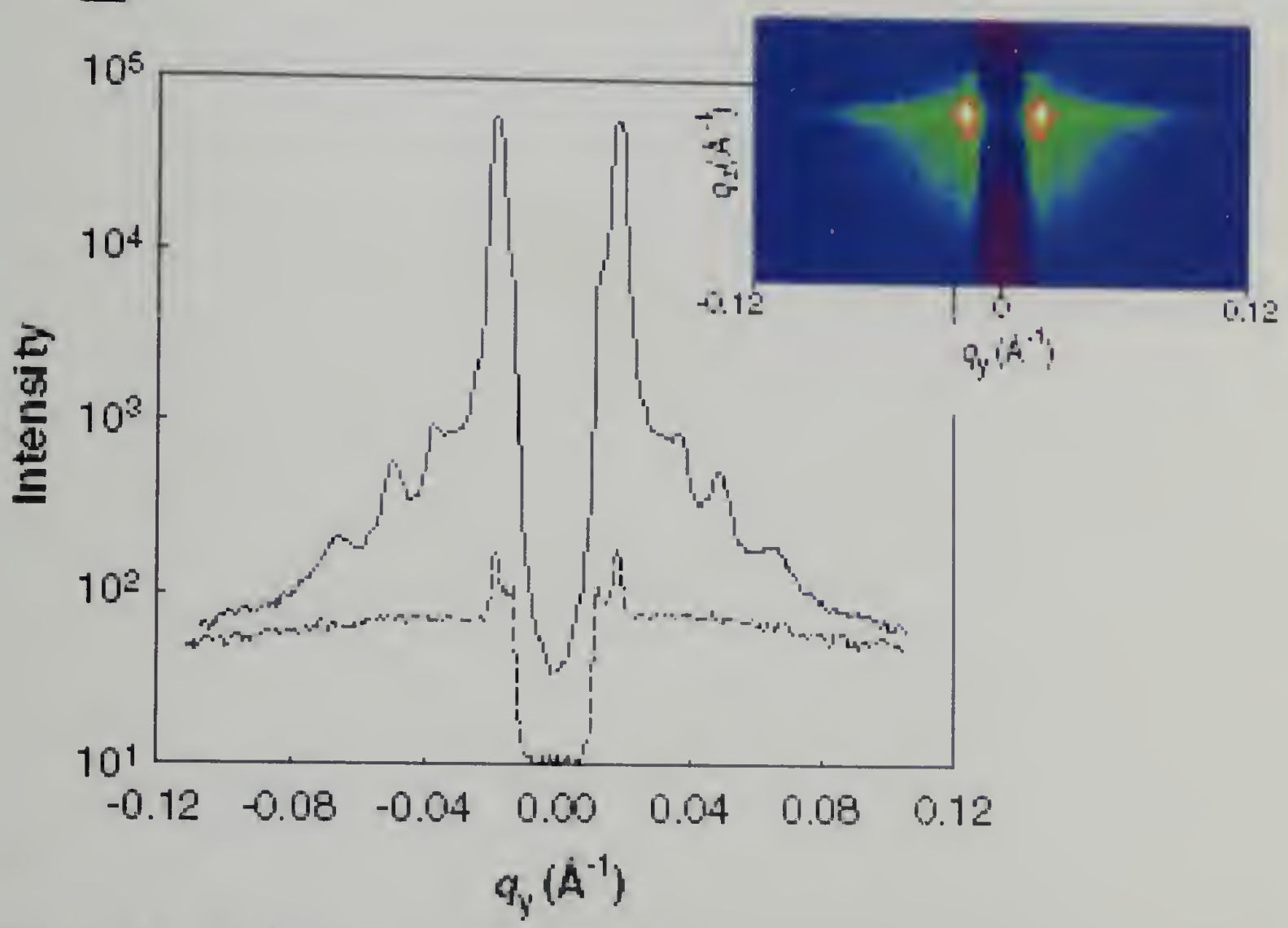

Figure 6.3 (A) TEM image of PS-*b*-PEO/3.8k-PMMA blend film (5 wt% homopolymer content) after the removal of PMMA homopolymers and (B) the intensity profiles of GASAXS patterns of PS-*b*-PEO/3.8k-PMMA blend (5 wt% homopolymer content) before (dashed line) and after (solid line) removal of homopolymer. The inset in (B) corresponds to the GASAXS patterns for PS-*b*-PEO/PMMA blend after removal of homopolymer from which the intensity profile (solid line) in (B) is obtained.

film.[31] Shown in the inset of Figure 6.3B is the typical 2-D scattering profile from PS-*b*-PEO/3.8k-PMMA blend film with 5 wt% of homopolymer after the pore formation. Compared to the case of block copolymer where the only two spots parallel to the film surface are seen,[31] higher order peaks are observed in the case of mixture after removal of the PMMA. The intensity profiles parallel to the surface of the film (q_y direction) of the GASAXS pattern shown in the inset are plotted in Figure 6.3B. For comparison, the intensity profile of the blend before removal of PMMA homopolymer is included. It is evident that the intensity increases significantly and higher order peaks are evident removal of homopolymer and the formation of pores. The positions of the higher-order reflections are consistent with a hexagonally packed array of cylindrical microdomains oriented normal to the surface. Further, it can be seen that the position of the first-order peaks in the two profiles before and after the pore formation are identical, indicating that the pore formation does not induce any change in the film structure.

Previously it was shown by using the difference in the solubility of the PS and PEO blocks with a cosolvent, such as water, that further control over the size and separation distance of nanoscopic domains could be achieved. When the same strategy is applied to the mixture systems, similar results are found, as shown in Figure 6.4. Films of the copolymer/homopolymer mixture were solution-cast from the benzene in a chamber containing an atmosphere of benzene and water. Water is a highly selective solvent for PEO. Due to the retention of water by the PEO during casting, the size and center-to-center distance of the cylindrical domains has increased for both blend systems, as shown in Figures 4A and 4B, in comparison to the structure produced for the mixtures

A

B

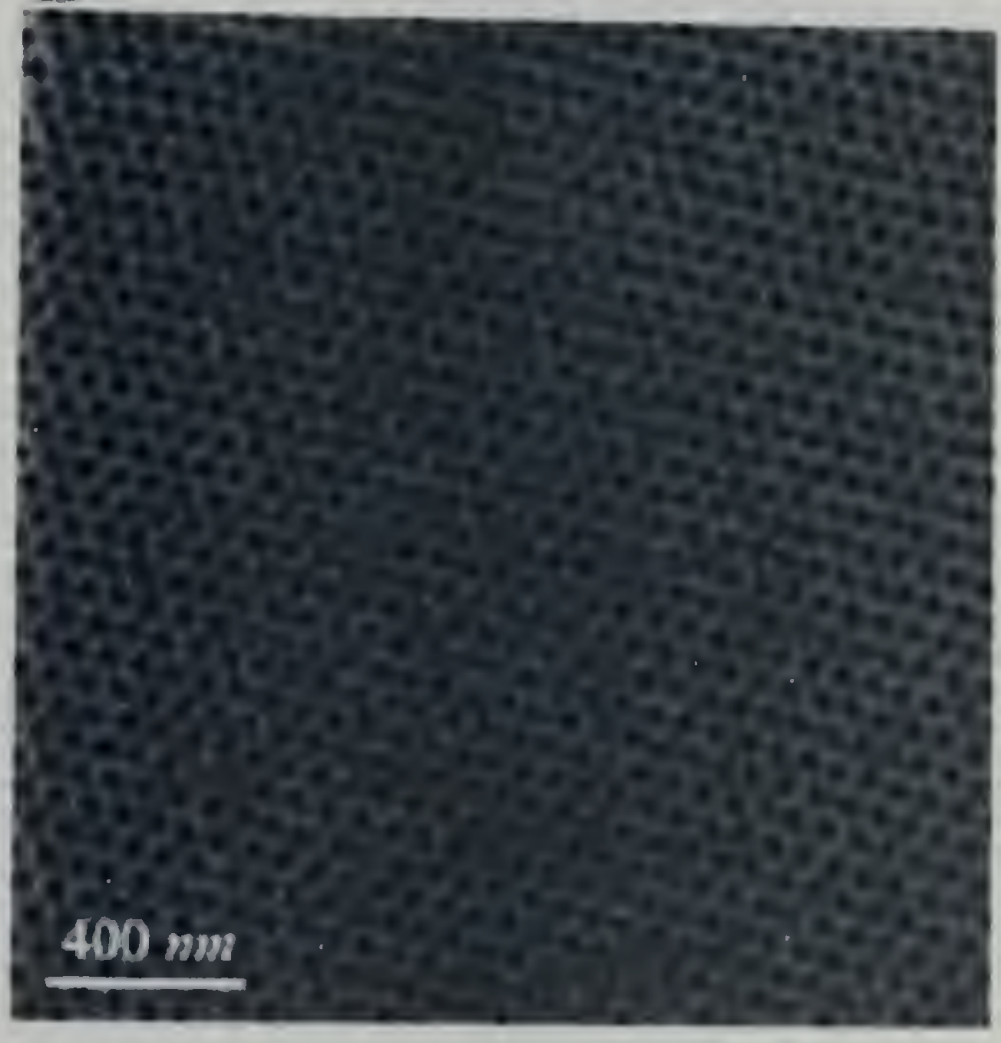

Figure 6.4 SFM phase images of PS-*b*-PEO/4.6k-PEO (A) and PS-*b*-PEO/3.8k-PMMA (B) blend films with 5 wt% homopolymer, solution cast from the benzene in a benzene/water atmosphere for 48 hrs.

of PS-b-PEO with homopolymers with the same molecular weight and the same concentration PEO. Due to the retention of water by the PEO during casting, the size and center-to-center distance of the cylindrical domains has increased for both blend systems, as shown in Figures 4A and 4B, in comparison to the structure produced for the mixtures of PS-b-PEO with homopolymers with the same molecular weight and the same concentration prepared under dry conditions. As compared to films prepared without water present, the center-to-center distance increases from 42.8 *nm* to 67.1 *nm* and from 43.0 *nm* to 68.6 *nm* for PEO homopolymer and PMMA homopolymer, respectively. A high degree of order can still be seen in both films and, upon removal of the homopolymer, well-ordered arrays of pores with increased size are obtained.

6.4 Conclusions

Consequently, as with the block copolymer system, blends of block copolymers with homopolymers can produce highly ordered arrays of cylindrical microdomains with long-range order via a simple solvent evaporation. All experimental results show that the development of order in the blend system follows the same mechanism shown in the pure block copolymer. Under a solvent atmosphere, the film is fully swollen and forced to disorder. As the solvent evaporates, the concentration of solvent at the surface is lowest and a gradient in solvent concentration develops normal to the surface. Microphase separation of the block copolymer occurs at the surface, the structure rapidly coarsens, and the ordering propagates through the film as the solvent further evaporates. In addition, the added homopolymers are preferentially segregated to the cylindrical microdomains, which affords several advantages over the pure block copolymer alone.

One can easily control the size and center-to-center distance of microdomains. Selective removal of the homopolymer produces highly ordered arrays of nanopores with high aspect ratio in the film. Moreover, the use of a cosolvent enables further manipulation of the characteristic length scales in the system due to the difference in the solubility of components of the copolymer. Overall, these results show a method to obtain highly ordered nanoporous arrays with lateral ordering that extends over large areas.

6.5 References

1. Whitesides, G. M.; Grzybowski, B. *Science* **2002**, *295*, 2418.

2. Park, M.; Harrison, C.; Chaikin, P. M.; Register, R. A.; Adamson, D. H. *Science* **1997**, *276*, 1401.

3. Li, R. R.; Dapkus, P. D.; Thompson, M. E.; Weon, G. J.; Harrison, C.; Chaikin, P. M.; Register, R. A.; Adamson, D. H. *Appl. Phys. Lett.* **2000**, *76*, 1689.

4. Park, M.; Chaikin, P. M.; Register, R. A.; Adamson, D. A. *Appl. Phys. Lett.* **2001**, *79*, 253.

5. Templin, M.; Franck, A.; Chesne, A. D.; Leist, H.; Zhang, Y.; Ulrich, R.; Schadler, V.; Wiesner, U. *Science* **1997**, *278*, 1795.

6. Spatz, J. P.; Herzog, T.; Mobmer, S.; Ziemann, P.; Moller, M. *Adv. Mater.* **1999**, *11*, 149.

7. Lopes, W. A.; Jaeger, H. M. *Nature* **2001**, *414*, 735.

8. Cheng, J. Y.; Ross, C. A.; Chan, Z. H.; Thomas, E. L.; Lammertink, R. G. H.; Vancso, G. J. *Adv. Mater.* **2001**, *13*, 1174.

9. Cheng, J. Y.; Ross, C. A.; Thomas, E. L.; Smith, H. I.; Vancso, G. J. *Appl. Phys. Lett.* **2002**, *81*, 3657.

10. Thurn-Albrecht, T.; Schotter, J.; Kastle, G. A.; Emley, N.; Shibauchi, T.; Krusin-Elbaum, L.; Guarini, K.; Black, C. T.; Tuominen, M. T.; Russell, T. P. *Science* **2000**, *290*, 2126.

11. Kim, H. C.; Jia, X. Q.; Stafford, C. M.; Kim, D. H.; McCarthy, T. J.; Tuominen, M. T.; Hawker, C. J.; Russell, T. P. *Adv. Mater.* **2001**, *13*, 795.

12. Black, C. T.; Guarini, K. W.; Milkove, K. R.; Baker, S. M.; Russell, T. P.; Tuominen, M. T. *Appl. Phys. Lett.* **2001**, *79*, 409.

13. Bal, M.; Ursache, A.; Tuominen, M. T.; Russell, T. P. *Appl. Phys. Lett.* **2002**, *81*, 3479.

14. Misner, M. J.; Skaff, H.; Emrick, T.; Russell, T. P. *Adv. Mater.* **2003**, *15*, 221.

15. Forster, S.; Plantenberg, T. *Angew, Chem. Int. Ed.* **2002**, *41*, 688.

16. Morkved, T. L.; Lu, M.; Urbas, A. M.; Ehrichs, E. E.; Jaeger, H. M.; Mansky, P.; Russell, T. P. *Science* **1996**, *273*, 931.

17. Albalak, R. J.; Thomas, E. L.; Capel, M. S. *Polymer* **1998**, *38*, 3819.

18. Villar, M. A.; Rueda, D. R.; Ania, F.; Thomas, E. L. *Polymer* **2002**, *43*, 5139.

19. Bodycomb, J.; Funaki, Y.; Kimishima, K.; Hashimoto, T. *Macromolecules* **1999**, *32*, 2075.

20. Segalman, R. A.; Yokoyama, H.; Kramer, E. J. *Adv. Mater.* **2001**, *15*, 1152.

21. Cheng, J. Y.; Ross, C. A.; Thomas, E. L.; Smith, H. I.; Vancso, G. J. *Adv. Mater.* **2003**, *15*, 1599.

22. Reiter, G.; Castelein, G.; Hoerner, P.; Riess, G.; Blumen, A.; Sommer, J. U. *Phys. Rev. Lett.* **1999**, *83*, 3844.

23. De Rosa, C.; Park, C.; Thomas, E. L.; Lotz, B. *Nature* **2000**, *405*, 433.

24. Fasolka, M. J.; Harris, D. J.; Mayes, A. M.; Yoon, M.; Mochrie, S. G. J. *Phys. Rev. Lett.* **1997**, *79*, 3018.

25. Rockford, L.; Liu, Y.; Mansky, P.; Russell, T. P.; Yoon, M.; Mochrie, S. G. J. *Phys. Rev. Lett.* **1999**, *82*, 2602.

26. Rockford, L.; Russell, T. P.; Yoon, M.; Mochrie, S. G. J. *Macromolecules* **2001**, *34*, 1487.

27. Kim, S.O.; Solak, H.H.; Stoykovich, M.P.; Ferrier, N.J.; dePablo, J.J.; Nealey, P.F. *Nature* **2003**, ***424***, 411.

28. Mansky, P.; Liu, Y.; Huang, E.; Russell, T. P.; Hawker, C. *Science* **1997**, 275, 1458.

29. Huang, E.; Rockford, L.; Russell, T. P.; Hawker, C. *Nature* **1998**, *395*, 757.

30. Kimura, M.; Misner, M. J.; Xu, T.; Kim, S. H.; Russell, T. P. *Langmuir* **2003**,19, 9910.

31. Kim, S. H.; Misner, M. J.; Xu, T.; Kimura, M.; Russell, T. P. *Adv. Mater.* **2003**, 16, 226.

32. Fukunaga, K.; Elbs, H.; Magerle, R.; Krausch, G. *Macromolecules*, **2000**, 33, 947.

33. Fukunaga, K.; Hashimoto, T.; Elbs, H.; Krausch, G. *Macromolecules*, **2002**, 35, 4006.

34. Ludwigs, S.; Böker, A., Voronov, A.; Rehse, N. Magerle, R.; Krausch, G. *Nat. Mat.*, **2003**, 2, 744.

35. Mayes, A. M.; Russell, T. P. Satija, S. K.; Majkrzak, C. F. *Macromolecules* **1992**, *25*, 6523.

36. Torikai, N.; Takabayashi, N.; Noda, I.; Koizumi, S.; Morii, Y.; Matsushita, Y. *Macromolecules* **1997**, *30*, 5698.

37. Orso, K. A.; Green, P. F. *Macromolecules* **1999**, *32*, 1087.

38. Smith, M. D.; Green, P. F.; Saunders, R. *Macromolecules* **1999**, *32*, 8392.

39. Jeong, U.; Kim, H. C.; Rodriguez, R. L.; Tsai, I. Y.; Stafford, C. M.; Kim, J. K.; Hawker, C. J.; Russell, T. P. *Adv. Mater.* **2002**, *14*, 274.

40. Jeong, U.; Ryu, D. Y.; Kho, D. H.; Lee, D. H.; Kim, J. K.; Russell, T. P. *Macromolecules*, **2003**, *36*, 3626.

41. Corvazier, L.; Messe, L.; Salon, C. L.; Young, R. N.; Fairclough, J. P.; Ryan, A. J. *J. Mat. Chem,* **2001**, 11, 2864.

CHAPTER 7

NANOPOROUS THIN FILMS FROM CLEAVABLE BLOCK COPOLYMERS

7.1 Introduction

The self-assembly of block copolymers has attracted considerable attention as a simple, versatile route to nanostructured materials and has led to the development of block copolymer lithography as a viable technique for the fabrication of microelectronic devices.[1-15] As a "bottom up" molecular system, block copolymer lithography allows exquisite control over the size and, to a lesser extent, the two-dimensional arrangement of nanoscale features. By simply changing the molecular weight and/or the relative ratio of constituent blocks, the morphology and size scales of the features can be controlled. In terms of thin films, the nanoporous materials derived from block copolymers have also been actively studied as nano-templates, membranes, separation media, high surface area support for catalysts, and sensors.[1,8,12,14,16-28] Several routes to generate nanoporous films via block copolymer self-assembly have been reported since Nakahama and co-workers[29] first demonstrated the formation of nanoporous polymer films from a siloxane-functionalized poly(styrene-*b*isoprene) system. The most common strategy is to remove the minor component selectively after self-assembly and, as a result, generate nanoscopic pores in a matrix of the majority component. A wide variety of diblock copolymers have been used, in some cases incorporating functionality to cross-link the majority component or homopolymers to modify the morphology. In contrast, only a small number of ABC-triblock copolymers have been studied, which is surprising given their richer phase morphologies.[27,28] One of the major shortcomings with all of these

systems is the presence of defects or grain boundaries in the nanoporous array, which limits the range of applications for these nanoscale templates to those that do not require registration or alignment.

To overcome the drawback of lateral order and defects, we have recently demonstrated that the self-assembly of polystyrene-*b*-poly(ethylene oxide) (PS-*b*-PEO) diblock copolymers leads to a highly ordered arrays of cylindrical microdomains of PEO in a PS matrix. By the use of solvent evaporation and annealing, defect-free arrays can be achieved over large lateral areas.[30,31] In comparison to poly-(styrene-*b*-methyl methacrylate) (PS-*b*-PMMA) diblock copolymer system, the long-range order in PS-*b*-PEO arises from the stronger nonfavorable interactions between PS and PEO, combined with the directionality of solvent evaporation. Although a high degree of long-range lateral order of PEO cylindrical microdomains is obtained with few defects, it is extremely difficult to selectively remove the PEO block by simple etching processes. Hillmyer and co-workers recently reported the successful use of iodic acid to achieve this.[28] However, the degradation requires immersion in a 57 wt % aqueous HI solution at 60 °C for 5 days and was only applicable to bulk samples and not thin films. This is in direct contrast to PS-*b*-PMMA discussed above where irradiation with UV light for less than 10 min leads to degradation of the PMMA and generation of porosity.

Two routes to generate nanoporous thin films with long-range lateral order will be shown here. The first combines the facile degradation of PS-*b*-PMMA with the long-range lateral order of PS-*b*-PEO-based systems. By employing an ABC triblock copolymer, the advantages of different diblock copolymer systems can be combined. To achieve these desired characteristics, the triblock copolymers have a general PS-*b*-

PMMA-*b*-PEO structure in which the central PMMA block imparts degradability to the system while the terminal PEO block permits long-range ordering.

Another route to allow for the removal of one component of block copolymer, where chemical, photochemical or thermal degradation is unavailable, is to introduce a cleavable junction point between the two blocks. The synthesis and cleavability of such a copolymer was reported, where it was shown that a tritylether junction point was found to be stable for synthesis and easily cleaved in a toluene solution with trifluoroacetic acid.[32] The volatility of the trifluoroacetic acid should allow for the cleavage of copolymer by exposing films to the acid vapor, rather than in solution. This method should provide a path around the limitations in block copolymers that cannot undergo selective degradation to achieve nanoporous thin films.

7.2 Experimental

The PEO-b-PMMA-b-PS triblock copolymers were synthesized by Reversible Addition Fragmentation Chain Transfer (RAFT) polymerization. Monomethoxy Poly(ethylene oxide) (M_n = 5,000, PDI = 1.05) was obtained commercially. Subsequently, the PMMA and PS blocks were sequentially added to generate the desired triblock copolymer. The polymers were characterized by ^{1}H nuclear magnetic resonance (NMR), using a Bruker 200 MHz spectrometer with the residual solvent signal as an internal reference. Size exclusion chromatography (SEC), using refractive index, photodiode array and light scattering detectors (Waters) was employed to give the overall molecular weight, polydispersity and chain end functionality of the materials.

The PEO-*b*-PMMA-*b*-PS triblock copolymers were spin coated from benzene solutions onto silicon substrates and then annealed in a benzene atmosphere, where the relative humidity was between 70 and 90%. The film thickness was controlled by adjusting the solution concentration and the spinning speed.[30] To cleave the PMMA block, the copolymer films were irradiated by UV for 10 minutes, rinsed in acetic acid and then in water.

To determine the bulk morphologies for triblock copolymers, small angle x-ray scattering (SAXS) was performed using the beam line at the Materials Research Laboratory, University of California, Santa Barbara. CuK_α x-rays (λ = 1.54Å) are generated by a Rigaku rotating anode x-ray generator. A sample-to-detector distance of 1.7 m was used to access the necessary q range. The 2-D SAXS images were azimuthally averaged to produce one-dimensional profiles of intensity, I vs. wavevector, q, using the two-dimensional data reduction program FIT2D.

The synthesis of the PS-*b*-PEO with an acid cleavable junction was described previously.[32] The synthetic route is similar to that of the triblock copolymer as the PEO was prepared first, which was then functionalized with the cleavable tritylether group, which also contained TEMPO for the subsequent polymerization of the PS. To crosslink the PS, some films were exposed to UV irradiation for 35 minutes under vacuum. Cleavage of the copolymer films was done by placing the films into a chamber containing trifluoroacetic acid vapor for 1 hour. Subsequently the films were rinsed in a 50:50 water/ethanol solution to remove the PEO.

SFM images were obtained in both the height and phase-contrast mode using a Digital Instruments Dimension 3000 scanning force microscope in the tapping mode.

Films for transmission electron microscopy (TEM) were prepared on silicon substrates having a thick layer of silicon oxide. These films were floated onto the surface of a 5 wt% HF solution, transferred to a water bath, and then picked up on a Cu grid. A JEOL 100CX electron microscope operated at 100 kV was used to examine the morphology.

7.3 Triblock Copolymer

The synthesis of a library of ABC triblock copolymers, poly(ethylene oxide-*b*-methyl methacrylate-*b*-styrene) (PEO-*b*-PMMA-*b*-PS), with various PMMA block lengths necessitated the use of a living free radical polymerization process and due to its synthetic versatility and ability to polymerize MMA under controlled conditions, reversible addition fragmentation transfer (RAFT) polymerization was the procedure of choice. The sequence of polymerization was therefore ethylene oxide, followed by MMA and styrene with the volume fraction of PEO and PMMA blocks being controlled to allow the formation of cylindrical PEO/PMMA microdomains. Several triblock copolymers were synthesized and shown in Table 7.1. In each of these materials, the overall PS fraction (~70%) would yield matrix of PS with cylindrical mircrodomains in a diblock copolymer.

Table 7.1 Characterization of triblock copolymers.

Sample ID	M_{PS} (kDa)	M_{PMMA} (kDa)	M_{PEO} (kDa)	f_{PS}	f_{PMMA}	f_{PEO}	M_n/M_w	D_{c-c} (nm)[a]
OMS1	13.5	1.5	5.0	0.69	0.07	0.24	1.03	22.9
OMS2	19.4	2.6	5.0	0.74	0.08	0.18	1.03	27.6
OMS5	32.4	6.0	5.0	0.77	0.13	0.11	1.05	36.4

Figure 7.1 SFM phase images for PEO-*b*-PMMA-*b*-PS triblock copolymer thin films of (a) OMS1, (b) OMS2, and (c) OMS5 after spin-coating.

To investigate the morphology of the corresponding thin films, scanning force microscopy, SFM, was used and Figure 7.1 shows the SFM phase images of a selection of three triblock copolymers on silicon substrates, OMS1, OMS2 and OMS5, shortly after spin-coating. The resulting structures are poorly defined and it is difficult to identify any morphology or orientation of the microdomains. However, if the films are annealed in the presence of benzene vapor and a controlled humidity atmosphere (70-90% relative humidity) well-defined structures are observed, where arrays of nanoscopic, cylindrical microdomains of the minor components are seen at the surface of films for all three triblocks (Figure 7.2A-C). As these systems are intended as templates in block copolymer lithography it was also very important to examine the nanostructure present at the substrate surface since it may be significantly different from the surface structure. The wafer-polymer interface was therefore examined by first removing the substrate and floating of the polymeric film using HF followed by flipping of the film and examining the 'bottom' side by SFM. Significantly, the same structure was observed at this interface as compared to the surface which indicates that the cylindrical domains span the entire thickness of films and are oriented normal to the film surface.

Of perhaps greater importance is the observation that these triblock copolymers films develop a defect-free, hexagonal-packed cylindrical array as was observed for the PEO-*b*-PS diblock copolymers.[30,31] It is noteworthy that the incorporation of the third, middle block has little effect on the ordering behavior of PS and PEO which suggests that a wide range of structural and functional units may be incorporated as a middle block without disrupting long range ordering, further enhancing the potential applications of these systems. The perfection of order is dramatically shown in the triangulation map in

Figure 7.2 SFM phase images for PEO-*b*-PMMA-*b*-PS triblock copolymer thin films of (a) OMS1, (b) OMS2, and (c) OMS5 after annealing for 12 hours in a benzene vapor with the controlled humidity. (d), (e), and (f) correspond to triangulation images of SFM images shown in (a), (b), and (c), respectively.

Figures 7.2D-F, where every domain center is connected by a line to the adjacent domain centers. Each 'perfect' domain with six nearest neighbors is colored blue, and defects with five or seven nearest neighbors are colored red and yellow, respectively. As seen in Figure 7.2D, every domain has six nearest neighbors, and this high degree of lateral order was found to extend over large areas for all triblock copolymers. The domain spacing calculated from the SFM images exactly matches that measured by SAXS (see Table 7.1). However, there is not enough phase contrast to identify all three phases in the triblock copolymer film by SFM, and it is impossible to state whether the cylindrical microdomains are composed of a single mixed PEO/PMMA phase or distinct PEO and PMMA phases.

The selective removal of the minor components, crosslinking of the major component, and generation of a nanoporous structure in PEO-*b*-PMMA-*b*-PS triblock copolymers were achieved by deep UV irradiation followed by acetic acid rinsing. This treatment is well known to degrade and remove PMMA but does not induce any cleavge or degradation in PEO-*b*-PS diblock copolymer films. Figure 6 shows TEM images of six triblock copolymer films after UV irradiation and acetic acid rinsing. For OMS1 and OMS2, contrary to expectations, the minor components were only partially removed and in some areas not removed at all (Figures 7.3A and 7.3B). The same results were observed for different film thickness and for even longer UV exposure times. When the PMMA block increases in length (OMS5), essentially all of the microdomains were removed, Figure 7.3C. Significantly, this irradiation and subsequent washing did not induce any change in the film structure and highly-oriented, defect-free, nanoporous films are prepared. It is also evident from all of the TEM images that the nanopores span

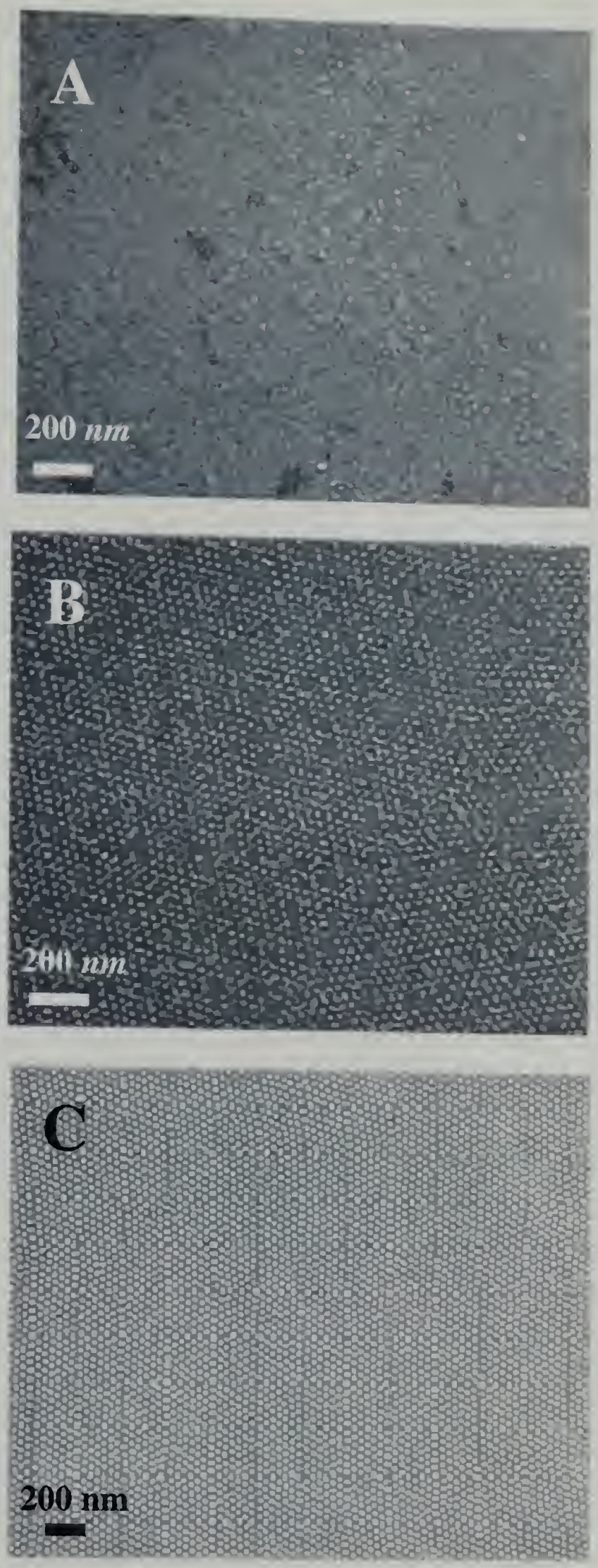

Figure 7.3 TEM images for PEO-*b*-PMMA-*b*-PS triblock copolymer thin films of A) OMS1, B) OMS2, and C) OMS5 after solvent annealing, followed by UV irradiation. The bright circles correspond to nanopores where the cylindrical microdomains are removed after UV irradiation.

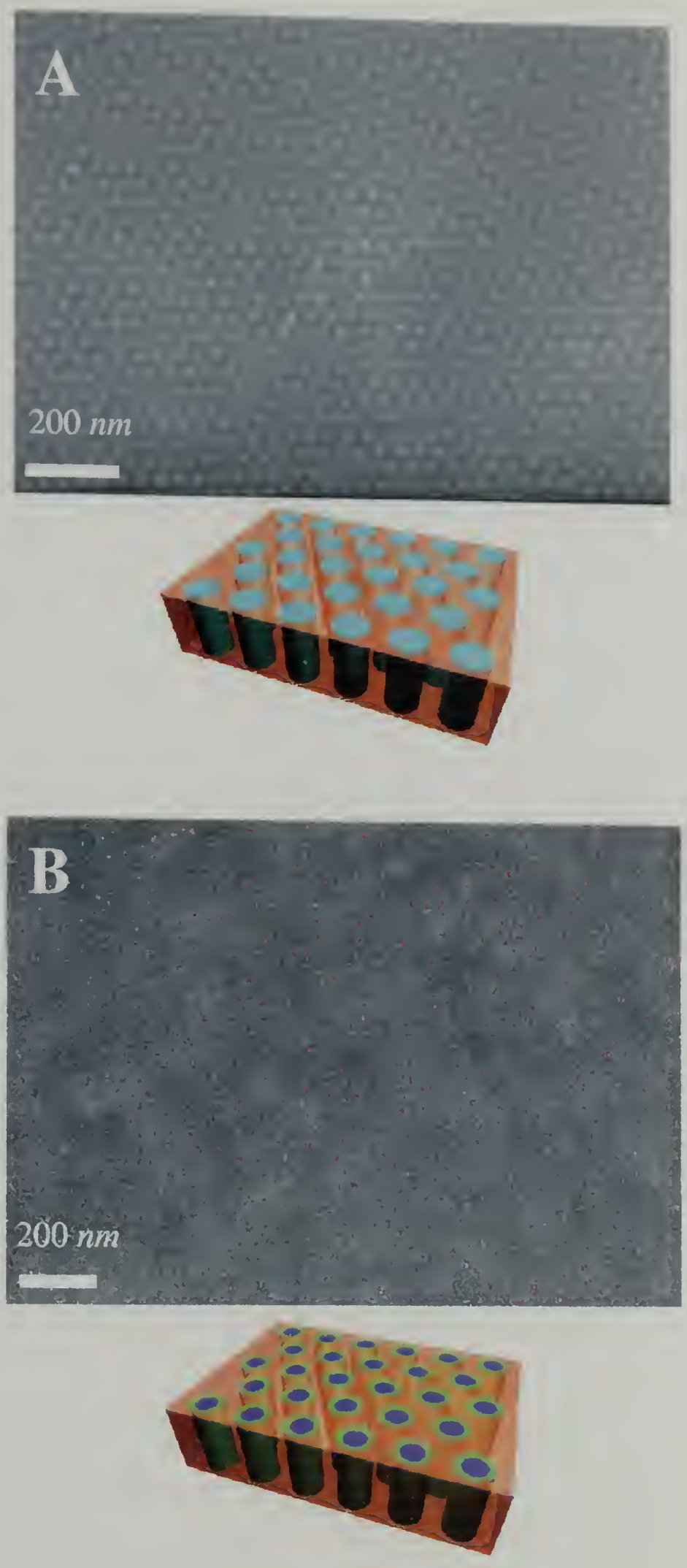

Figure 7.4 TEM images (top view) for PEO-*b*-PMMA-*b*-PS triblock copolymer thin films of (a) OMS2 and (b) OMS5 after solvent annealing. The schematics below illustrate the possible structures of the cylindrical microdomains.

the entire film. However it is apparent from these samples that there is a critical composition for the triblock copolymer systems.

To understand the origin of this lower critical molecular weight (<5,000 g/mol) in greater detail, thin film morphologies of a range of samples before UV exposure were examined. As a representative example, Figures 7.4A and 7.4B show the TEM images of OMS2 (PMMA = 2,600 and PEO = 5,000 g/mol) and OMS5 (PMMA = 6,000 and PEO = 5,000 g/mol) prior to UV irradiation, respectively. Below the TEM images are shown schematic representations of the proposed morphologies and it is immediately apparent that the two triblock copolymers exhibit different morphologies. For the lower molecular weight OMS2 derivative, the cylindrical microdomains are composed of one phase, where the PEO and PMMA minor components are miscible. In contrast, OMS5 produces a core-shell cylindrical morphology where the core is PEO and the shell is PMMA. In this case, the increased molecular weight of the PMMA blocks leads to phase separation between PMMA and PEO which combined with the strong repulsion between PS and PEO domains forces the PMMA block to mediate interactions along the cylinder walls, forming a distinct layer between the PS and PEO.

7.4 Acid Cleavable Junction

A schematic of the acid cleavable PS-b-PEO is shown in Figure 7.5A before and after cleavage by the trifluoroacetic acid (CF_3COOH). After exposure to the acid, the copolymer is reduced into two homopolymer components. This is different than that of typical selective degradation of a block copolymer where one component is broken into smaller, even monomeric, units. The cleavable PS-*b*-PEO ($f_{ps} = 0.7$) was spin-coated

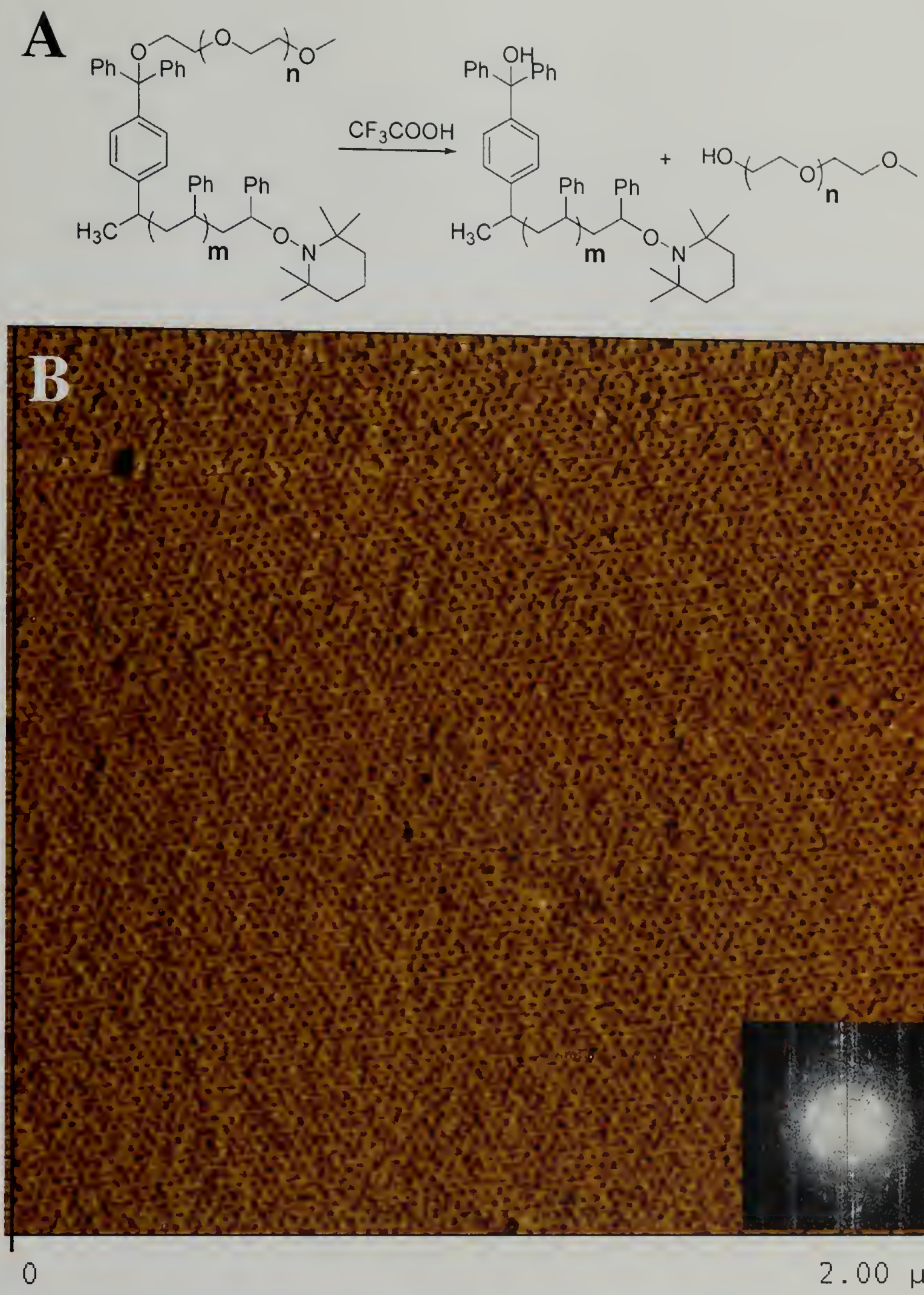

Figure 7.5 A) Schematic of the acid cleavable PS-*b*-PEO before and after cleavage by CF_3COOH. B) A 2 x 2 mm SFM image of a solvent annealed PS-*b*-PEO thin film, the inset is a FFT of the image indicating that the structure is highly ordered.

onto a silicon substrates with a thick layer of thermal oxide with a thickness of ~40 nm. The films were then solvent annealed for 48 hours in a benzene atmosphere. Figure 7.5 is an SFM micrograph of the copolymer film after solvent annealing. As can be seen, the cleavable PS-*b*-PEO microphase separates into highly-ordered, cylindrical microdomains oriented normal to the surface, similar to the standard diblock copolymer. The inset in the Figurer 7.5 shows a Fast Fourier Transform (FFT) of the SFM micrograph, indicating that the high degree of order in the film.

In Figure 7.6A, an SFM phase image of a solvent annealed PS-b-PEO film after exposing the film to trifluoroacetic acid for an hour. In the image, it can be seen that the nanostructured copolymer film remains intact. However, PEO homopolymer has diffused to the surface and has crystallized, which is a clear indication that the trifluoroacetic acid vapor successfully cleaved the copolymer. Subsequently, the film was rinsed in 50 vol% mixture of water and ethanol for 18 hours. The film removed from the substrate by etching the thick oxide layer and floated onto a solution of 5% HF in water. The film was then retrieved by a copper grid. A TEM micrograph of the cleaved copolymer film is shown in Figure 7.6B. It is clear, while not complete, that the PEO has been removed from the microdomains to generate a nanoporous film.

To improve the thermal and chemical stability of the nanoporous thin films, the films can be cross-linked by UV irradiation. An SFM image is shown in Figure 7.7A where a solvent annealed copolymer film was first exposed to UV radiation for 35 minutes, to cross-link the PS, and then exposed to trifluoroacetic acid vapor for one hour. Here, while the film remains nanostructured, crystallization of the PEO is not apparent at the film surface. After rinsing the film in the water/ethanol mixture, the film does not

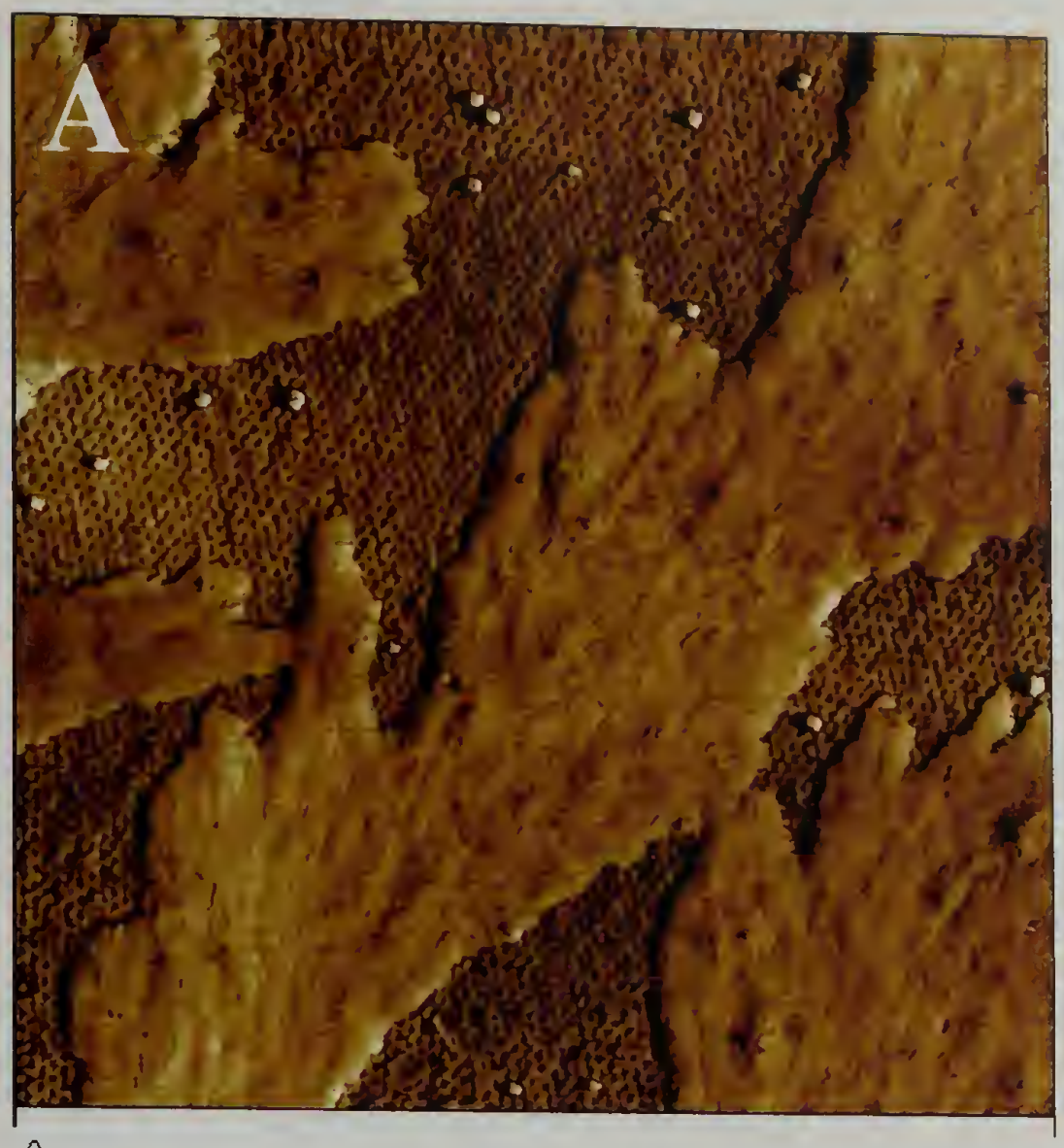

Figure 7.6 A) A SFM micrograph of the cleavable PS-*b*-PEO after exposure to CF_3COOH only. B) The film in A after rinsing in a water/methanol mixture.

appear to nanoporous by TEM, Figure 7.7B. This result is similar to the triblock copolymer system where the PEO and PMMA were miscible and the minor components could not be removed. Rather than the core-shell structure, where the PEO was separated from the PS by the PMMA layer, in both of these cases the PEO is in direct contact with the PS. To examine the interaction of PS and PEO during UV irradiation PS homopolymer was spin-coated onto a silicon wafer. On top of that, a layer of PEO homopolymer was cast to form a bi-layer. Table 7.1 lists receding and advancing contact angle measurements for the bi-layer was then exposed to UV radiation and then rinsed to remove the PEO. As a control for the removal of the PEO after rinsing a bi-layer film without UV exposure is shown. Also, shown is a layer PS only exposed to UV and then rinsed to account for the change in the PS during cross-linking. As can be seen by reduction of the receding contact angle in the bi-layer film where the PS and PEO are exposed to UV and then rinsed, the surface has become more hydrophilic. This result indicates that PS can cross-link to the PEO, making the PEO unable to be removed from the microdomains.

Table 7.1 Contact angle measurements.

Sample	**Advancing**	**Receding**
Bi-layer film UV exposed & rinsed	90°	64°
Bi-layer film not UV exposed & rinsed	91°	77°
PS film UV exposed & rinsed	90°	75°

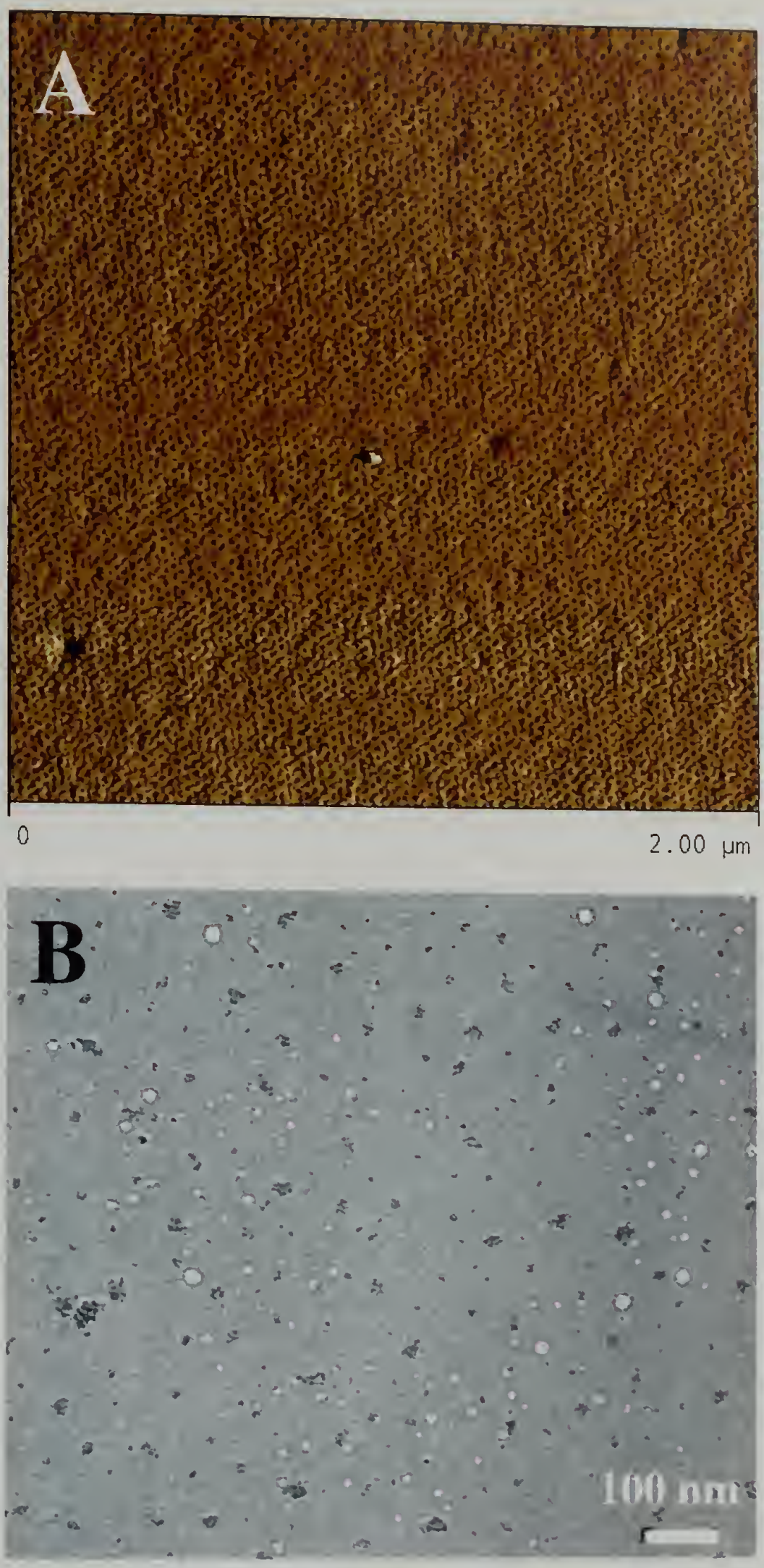

Figure 7.7 A) A SFM micrograph of the cleavable PS-*b*-PEO thin films after exposure to UV and to the CF_3COOH acid vapor. B) The film in A after rinsing in a water/ethanol mixture.

7.5 Conclusions

Exploiting the facile degradability of PS-*b*-PMMA block copolymers combined with the long range ordering of PEO-*b*-PS systems has allowed the development of a versatile methodology for the fabrication of highly ordered arrays of nanopores via the self-assembly of triblock copolymers. The synthesis of PEO-*b*-PMMA-*b*-PS triblock copolymers by RAFT polymerization allows the middle PMMA block to function as a sacrificial block while the terminal PEO block directs phase separation. Significantly, this behavior was found to depend critically on the molecular weight and phase behavior of the central PMMA block and only when the PMMA block formed a distinct microdomain did facile degradation occur. The ability to exploit and combine the best features of multiple block copolymers in a single system offers greater variability and nanostructural control when compared to traditional diblock copolymer systems.

The incorporation of a cleavable junction point allows for a additional route to generate nanoporous thin films in block copolymer otherwise difficult to selectively degrade. Here, the tritylether junction between the two blocks of the PS-b-PEO block copolymer is cleavable by trifluoroacetic acid in solution and by exposure to vapor in thin films. After cleaving the copolymer films and rinsing with a selective solvent to remove the cleaved homopolymer, it is evident that highly-ordered, highly-oriented, nanoporous thin films can be generated.

References

1. Park, M.; Harrison, C.; Chaikin, P. M.; Register, R. A.; Adamson, D. H. Science 1997, 276, 1401-1404.

2. Li, R. R.; Dapkus, P. D.; Thompson, M. E.; Jeong, W. G.; Harrison, C.; Chaikin, P. M.; Register, R. A.; Adamson, D. H. Appl. Phys. Lett. 2000, 76, 1689-1691.

3. Templin, M.; Franck, A.; Du Chesne, A.; Leist, H.; Zhang, Y.; Ulrich, R.; Schadler, V.; Wiesner, U. Science 1997, 278, 1795-1798.

4. Spatz, J. P.; Herzog, T.; Moessmer, S.; Ziemann, P.; Moeller, M. Adv. Mater. 1999, 11, 149-153.

5. Lopes, W. A.; Jaeger, H. M. Nature 2001, 414, 735-738.

6. Cheng, J. Y.; Ross, C. A.; Chan, V. Z. H.; Thomas, E. L.; Lammertink, R. G. H.; Vancso, G. J. Adv. Mater. 2001, 13, 1174-1178.

7. Cheng, J. Y.; Ross, C. A.; Thomas, E. L.; Smith, H. I.; Vancso, G. J. Appl. Phys. Lett. 2002, 81, 3657-3659.

8. Thurn-Albrecht, T.; Schotter, J.; Kastle, G. A.; Emley, N.; Shibauchi, T.; Krusin-Elbaum, L.; Guarini, K.; Black, C. T.; Tuominen, M. T.; Russell, T. P. Science 2000, 290, 2126-2129.

9. Kim, H.-C.; Jia, X.; Stafford, C. M.; Kim, D. H.; McCarthy, T. J.; Tuominen, M.; Hawker, C. J.; Russell, T. P. Adv. Mater. 2001, 13, 795-797.

10. Black, C. T.; Guarini, K. W.; Milkove, K. R.; Baker, S. M.; Russell, T. P.; Tuominen, M. T. Appl. Phys. Lett. 2001, 79, 409-411.

11. Bal, M.; Ursache, A.; Tuominen, M. T.; Goldbach, J. T.; Russell, T. P. Appl. Phys. Lett. 2002, 81, 3479-3481.

12. Misner, M. J.; Skaff, H.; Emrick, T.; Russell, T. P. Adv. Mater. 2003, 15, 221-224.

13. Kim, D. H.; Kim, S. H.; Lavery, K.; Russell, T. P. Nano Letters 2004, 4, 1841-1844.

14. Zhang, Q.; Xu, T.; Butterfield, D.; Misner, M. J.; Ryu, D. Y.; Emrick, T.; Russell, T. P. Nano Letters 2005, 5, 357-361.

15. Lin, Y.; Boeker, A.; He, J.; Sill, K.; Xiang, H.; Abetz, C.; Li, X.; Wang, J.; Emrick, T.; Long, S.; Wang, Q.; Balazs, A.; Russell, T. P. Nature 2005, 434, 55-59.

16. Liu, G.; Ding, J.; Hashimoto, T.; Kimishima, K.; Winnik, F. M.; Nigam, S. Chem. Mat. 1999, 11, 2233-2240.

17. Liu, G.; Ding, J.; Stewart, S. Angew. Chem. -Int. Edit. 1999, 38, 835-838.

18. Stewart, S.; Liu, G. Angew. Chem. -Int. Edit. 2000, 39, 340-344.

19. Liu, X.; Jiang, M.; Yang, S.; Chen, M.; Chen, D.; Yang, C.; Wu, K. Angew. Chem. - Int. Edit. 2002, 41, 2950-2953.

20. Johnson, B. J. S.; Wolf, J. H.; Zalusky, A. S.; Hillmyer, M. A. Chem. Mat. 2004, 16, 2909-2917.

21. Olayo-Valles, R.; Lund, M. S.; Leighton, C.; Hillmyer, M. A. J. Mater. Chem. 2004, 14, 2729-2731.

22. Mao, H.; Arrechea, P. L.; Bailey, T. S.; Johnson, B. J. S.; Hillmyer, M. A. Faraday Discuss. 2005, 128, 149-162.

23. Li, M.; Douki, K.; Goto, K.; Li, X.; Coenjarts, C.; Smilgies, D. M.; Ober, C. K. Chem. Mat. 2004, 16, 3800-3808.

24. Liang, C.; Hong, K.; Guiochon, G. A.; Mays, J. W.; Dai, S. Angew. Chem. -Int. Edit. 2004, 43, 5785-5789.

25. Pai, R. A.; Humayun, R.; Schulberg, M. T.; Sengupta, A.; Sun, J.-N.; Watkins, J. J. Science 2004, 303, 507-511.

26. Xu, Y.; Gu, W.; Gin, D. L. J. Am. Chem. Soc. 2004, 126, 1616-1617.

27. Rzayev, J.; Hillmyer, M. A. Macromolecules 2005, 38, 3-5.

28. Rzayev, J.; Hillmyer, M. A. J. Am. Chem. Soc. 2005, 127, 13373-13379.

29. Lee, J. S.; Hirao, A.; Nakahama, S. Macromolecules 1988, 21, 274-276.

30. Kim, S. H.; Misner, M. J.; Xu, T.; Kimura, M.; Russell, T. P. Adv. Mater. 2004, 16, 226-231.

31. Kim, S. H.; Misner, M. J.; Russell, T. P. Adv. Mater. 2004, 16, 2119-2123.

32. Yurt, S.; Anyanwu, U. K.; Scheintaub, J. R.; Coughlin, E. B.; Venkataraman, D. *Macromolecules,* **2006**, *39(5)*, 1670-1672.

CHAPTER 8

FUTURE DIRECTIONS

Presented in this thesis was a set of work that described the advantages of using solvent to augment the kinetics and interfacial and surface energies during ordering of block copolymer thin films. Solvent casting and annealing in a solvent atmosphere was shown to be highly effective in controlling the microdomain orientation as well as markedly enhancing the degree of lateral order of the microdomains in thin films. It was shown that cosolvents and ionic impurities can play a significant roll in block copolymers ordering. Also, it was shown that solvent techniques are applicable to use on patterned surfaces, where lateral confinement can be used to direct copolymer ordering. Finally, several routes were shown to produce nanoporous thin films for templating applications. However, there are still several areas that merit continued work and will be outlined here. Some of these are direct continuations of topics presented here; others may be considered "next steps" in the more general understanding and characterization of block copolymer thin films ordering in the presence of a solvent.

On of the more interesting, and surprising, results was the degree of order observed in swollen block copolymer films with added salts, as discussed in chapter 4. *In situ* GISAXS measurements showed several orders of reflections in the swollen state, far beyond what we typically see with dried, un-salted, yet highly-ordered, copolymer film. Unfortunately, this order is lost in the evaporation process. Because of the potential this level of ordering has, it is clear that it must be further explored. To now, we have some concepts and evidence of how this order is lost, but it needs to be better characterized so that the system can be tuned to maximize the order in the dried state. The other option is

to explore routes to lock in the copolymer structure while it is the swollen state. This may be done by rapidly removing the solvent and/or thermal quenching to drive one of the blocks of the copolymer into the glassy state. Another route to lock in the structure may be to introduce a cross-linking mechanism in the copolymer.

Second, there are areas to be explored in patterned surfaces. In topographically patterned surfaces, improvements in the lithography can be made to further study the effects of confinement, where the resolution of the trough width is on the order or smaller than that of the copolymer microdomain spacing. Additionally, in this geometry, the effects of the edge roughness should be explored. Improvements in polygonal patters need to be made as well in topographically pattered surfaces to that 2D confinement can be studied with hard walls. Finally, there is significant work to be done on the chemically patterned surfaces, including the roll of pattern defects, the geometry of confinement, the minimum and maximum length scales this is applicable to, and droplet shape. It may also be interesting to explore routes to chemically pattern with higher throughput.

While the use of solvents to control microdomain orientation and improve the lateral order of the copolymer microdomains is a general process, it is not, at this point, easily extended to other systems. Work has been done in this group, as well as others, on a number of systems and arriving at the correct solvent and conditions prove to be daunting. This is because the system becomes fairly complex, where interfacial energies, surface energies, film thickness, and mobility are all influenced by the addition of a solvent, where the quality and selectivity of the solvent, as well as the volatility, are additional important parameters. When a cosolvent is used, such as, but limited to water,

the complexity of the system increases again. Being able to *a priori* narrow the range of solvents for a given copolymer is crucial for this work to be applied generally. Subsequently, a variety of systems and/or theoretical modeling would be a recommended area of further exploration.

Finally, one of the major motivations for this work is for the application of these materials into addressable media for data storage. This application requires a high degree of long-range lateral order in the copolymer films. There has been work to characterize this order by correlation functions and defect analysis, however, these characterizations do not yet define what it means to be addressable. Correlation functions describe the aggregate of a surface; however, do not provide a necessarily accurate description of point defects and local lattice distortions. Conversely, analysis of point defects can locally describe the quality of the lateral order; however do not necessarily describe systematic lattice distortions that, over large distances, can lead to a loss of translational order. Additionally, characterization by purely surface techniques to not account for the three-dimensional nature of anisotropic microdomains and their arrangement in the film, which should be of consideration for templating applications. Being able to fully characterize the order in block copolymer films is critical in determining over what length scales and geometries a surface can be sectorize into addressable regions and, thus, the limits of block copolymers in technology.

BIBLIOGRAPHY

Albalak, R. J.; Thomas, E. L.; Capel, M. S. *Polymer,* **1998**, *38*, 3819.

Alexander, L. E. *X-Ray Diffraction Methods in Polymer Science*, Wiley & Sons, Inc., New York, 1969.

Andreev, Y. G.; Bruce, P. G. *Electrochimica Acta,* **2000**, *45*, 1417.

Angelescu, D. *Ph.D. Thesis*, Princeton University, 2003.

Angelescu, D. Waller, J. H.; Register, R. A.; Chaikin, P. M. *Advanced Materials*, **2005**, *17*, 1878-1881.

Bal, M.; Ursache, A.; Tuominen, M. T.; Goldbach, J. T.; Russell, T. P. *Appl. Phys. Lett,.* **2002**, *81*, 3479-3481.

Banaszak, M.; Whitmore, M. D. *Macromolecules,* **1992**, *25*, 3406.

Bates, F. S. *Science,* **1991**, *251*, 898.

Bates, F. S. *Science,* **1991**, *251*, 898.

Bates, F. S.; and Fredrickson, G. H. *Physics Today,* **1999,** 32.

Black, C. T.; Guarini, K. W.; Milkove, K. R.; Baker, S. M.; Russell, T. P.; Tuominen, M. T. *Applied Physics Letters,* **2001**, *79*, 409.

Bodycomb, J.; Funaki, Y.; Kimishima, K.; Hashimoto, T. *Macromolecules,* **1999**, *32*, 2075.

Breulmann, M.; Forster, S.; Antonietti, M. *Macromolecular Chemistry and Physics,* **2000**, *201*, 204.

Bruce, P. G. *Chemical Communications,* **1997**, 1817.

Cai, Y.; Ocko, B. M. *JACS,* **2005**, *127(46)*, 16287-16291.

Cha, J. N.; Stucky, G. D.; Morse, D. E.; Deming, T. J. *Nature,* **2000**, *403*, 289.

Checco, A.; Cai, Y.; Gang, O.; Ocko, B. M. *Ultramicroscopy,* **2006**, *106(8-9)*, 703-708.

Checco, A.; Gang, O.; Ocko, B. M. *Phys. Rev. Lett.,* **2006**, *96(5)*, 056104/1-056104/4.

Cheng, J. Y.; Ross, C. A.; Chan, V. Z. H.; Thomas, E. L.; Lammertink, R. G. H.; Vancso, G. J. *Adv. Mater.*, **2001**, *13*, 1174-1178.

Cheng, J. Y.; Ross, C. A.; Thomas, E. L.; Smith, H. I.; Vancso, G. J. *Adv. Mater.*, **2003**, *15*, 1599.

Cheng, J. Y.; Ross, C. A.; Thomas, E. L.; Smith, H. I.; Vancso, G. J. *Appl. Phys. Lett.*, **2002**, *81*, 3657-3659.

Chow, T. S. *Macromolecules,* **1980**, *13*, 362-364.

Christie, A. M.; Lilley, S. J.; Staunton, E.; Andreev, Y. G.; Bruce, P. G. *Nature,* **2005**, *433*, 50.

Connell, S. D.; Collins, S.; Fundin, J.; Yang, Z.; Hamley, I. W. *Langmuir,* **2003**, *19(24)*, 10449-10453.

Corvazier, L.; Messe, L.; Salon, C. L.; Young, R. N.; Fairclough, J. P.; Ryan, A. J. *J. Mat. Chem,* **2001**, 11, 2864.

Coulon, G.; Daillant, J.; Collin, B.; Benattar, J. J.; Gallot, Y. *Macromolecules,* **1993**, *26*, 1582-1589.

De Rosa, C.; Park, C.; Thomas, E. L.; Lotz, B. *Nature,* **2000**, *405*, 433.

Deegan, R. D.; Bakajin, O.; Dupont, T. F.; Huber, G.; Nagel, S. R.; Witten, T. A. *Nature,* **1997**, *389*, 827-829.

Deegan, R. D.; Bakajin, O.; Dupont, T. F.; Huber, G.; Nagel, S. R.; Witten, T. A. *Phys. Rev E,* **2000**, *62*, 756-765.

DeRouchey, J.; Thurn-Albrecht, T.; Russell, T. P.; Kolb, R. *Macromolecules,* **2004**, *37*, 2538.

Dimarzio, E. A., Gibbs, J. H. *J. of Poly. Sci. Part A,* **1963**, *1*, 1417-1428.

Dimension 3000 Instruction Manual, Digital Instruments, Inc. Santa Barbara, CA, 1996.

Doshi, D. A.; Gibaud, A.; Goletto, V.; Lu, M. C.; Gerung, H.; Ocko, B.; Han, S. M.; Brinker, C. J. *J. Am. Chem. Soc.,* **2003**, *125*, 11646.

Dourdain, S.; Rezaire, A.; Mehdi, A.; Ocko, B. M.; Gibaud, A. *Physica B-Condensed Matter,* **2005**, *357*, 180.

F. S. Bates, *Science,* **1991**, *251*, 898.

Fasolka, M. J.; Harris, D. J.; Mayes, A. M.; Yoon, M.; Mochrie, S. G. J. *Phys. Rev. Lett.*, **1997**, *79*, 3018.

Flory, P. J. *Principles of Polymer Chemistry,* Cornell University Press, Ithaca, NY, 1953.

Forster, S.; Plantenberg, T. *Angew, Chem. Int. Ed.*, **2002**, *41*, 688.

Fredrickson, G. H., Leibler, L. *Macromolecules,* **1989,** 22, 1238-1250.

Fredrickson, G. H.; Bates, F. S. *Ann. Rev. Mat Sci,* **1990** 1-70.

Fredrickson, G. H.; Bates, F. S. *Annu. Rev. Mater. Sci.,* **1996**, *26*, 501.

Fuchs, N. *Evaporations and Droplet Growth in Gaseous Media,* Pergamon, Oxford, 1951.

Fukunaga, K.; Elbs, H.; Magerle, R.; Krausch, G. *Macromolecules,* **2000**, *33*, 947.

Fukunaga, K.; Hashimoto, T.; Elbs, H.; Krausch, G. *Macromolecules,* **2002**, *35*, 4406.

G. H. Fredrickson & F. S. Bates, *Ann. Rev. Mat Sci.*, **1990**, 1-70.

Gadjourova, Z.; Andreev, Y. G.; Tunstall, D. P.; Bruce, P. G. *Nature,* **2001**, *412*, 520.

Glass, R.; Moller, M.; Spatz, J. P. *Nanotechnology,* **2003**, *14*, 1153.

Hahn, J.; Sibener, S. J. *Langmuir,* **2000**, *16*, 4766-4769.

Hamley, I. W. *Nanotechnology*, **2003**, *14*, R39.

Hammond, M. R.; Cochran, E.; Fredrickson, G. H.; Kramer, E. J. *Macromolecules,* **2005**, *38(15)*, 6575-6585.

Hanley, K. J.; Lodge, T. P.; Huang, C. I. *Macromolecules,* **2000**, *33(16)*, 5918-5931.

Harrison, C.; Angelescu, D. E.; Trawick, M.; Cheng, Zhengdong, Huse, D. A.; Chaikin, P. M.; Vega, D. A.; Sebastian, J. M.; Register, R. A.; Adamson, D. H. *Europhysics Letters,* **2004**, *67*, 800-806.

Hawker, C. J.; Russell, T. P. *MRS Bulletin,* **2005**, *30*, 952.

Heier, J. Genzer, J.; Kramer, E. J.; Bates, F. S.; Walheim, S.; Krausch, G. *J. Chem. Phys.*, **1999**, *111*, 11101-11110.

Huang, E.; Rockford, L.; Russell, T. P.; Hawker, C. *Nature,* **1998**, *395*, 757.

Jeong, U.; Kim, H. C.; Rodriguez, R. L.; Tsai, I. Y.; Stafford, C. M.; Kim, J. K.; Hawker, C. J.; Russell, T. P. *Adv. Mater.*, **2002**, *14*, 274.

Jeong, U.; Ryu, D. Y.; Kho, D. H.; Lee, D. H.; Kim, J. K.; Russell, T. P. *Macromolecules*, **2003**, *36*, 3626.

Johnson, B. J. S.; Wolf, J. H.; Zalusky, A. S.; Hillmyer, M. A. *Chem. Mat.*, **2004**, *16*, 2909-2917.

Kim, D. H.; Kim, S. H.; Lavery, K.; Russell, T. P. *Nano Letters,* **2004**, *4*, 1841.

Kim, D. H.; Lau, K. H. A.; Robertson, J. W. F.; Lee, O. J.; Jeong, U.; Lee, J. I.; Hawker, C. J.; Russell, T. P.; Kim, J. K.; Knoll, W. *Adv. Mat.,* **2005**, *17*, 2442.

Kim, G.; Libera, M. *Macromolecules,* **1998**, *31*, 2569-2577.

Kim, G.; Libera, M. *Macromolecules,* **1998**, *31*, 2670.

Kim, H.-C.; Jia, X.; Stafford, C. M.; Kim, D. H.; McCarthy, T. J.; Tuominen, M.; Hawker, C. J.; Russell, T. P. *Adv. Mater.,* **2001**, *13*, 795-797.

Kim, S. H.; Misner, M. J.; Russell, T. P. *Adv. Mater.,* **2004**, *16*, 2119-2123.

Kim, S. H.; Misner, M. J.; Xu, T.; Kimura, M.; Russell, T. P. *Adv. Mat.*, **2004**, *16(3)*, 226-231.

Kim, S.O.; Solak, H.H.; Stoykovich, M.P.; Ferrier, N.J.; dePablo, J.J.; Nealey, P.F. *Nature,* **2003**, ***424***, 411.

Kimura, M.; Misner, M. J.; Xu, T.; Kim, S. H.; Russell, T. P. *Langmuir,* **2003**, *19(23)*, 9910-9913.

Knoll, A.; Horvat, A.; Lyakhova, K. S.; Krausch, G.; Sevink, G. J. A.; Zvelindovsky, A. V.; Magerle, R. *Phys. Rev. Lett.,* **2002**, *89*, 035501-1-4.

Lambooy, P.; Russell, T. P.; Kellogg, G. J.; Mayers, A. M.; Gallagher, P. D.; Satija, S. K. *Phy. Rev. Lett.,* **1995**, *72*, 2899-2902.

Lazzari, M.; Lopez-Quintela, M. A. *Adv. Mat.,* **2003**, *15*, 1583.

Lazzari, R. *J. Appl. Cryst.*, **2002**, *35,* 406-421.

Lee, B.; Park, I.; Yoon, J.; Park, S.; Kim, J.; Kim, K. W.; Chang, T.; Ree, M. *Macromolecules,* **2005**, *38(10)*, 4311-4323.

Lee, B.; Yoon, J.; Oh, W.; Hwang, Y.; Heo, K.; Jin, K. S.; Kim, J.; Kim, K W.; Ree, M. *Macromolecules,* **2005**, *38(8)*, 3395-3405.

Lee, J. S.; Hirao, A.; Nakahama, S. *Macromolecules,* **1988**, *21*, 274-276.

Leibler, L. *Macromolecules*, **1980,** *13,* 1602-1617.

Li, R. R.; Dapkus, P. D.; Thompson, M. E.; Jeong, W. G.; Harrison, C.; Chaikin, P. M.; Register, R. A.; Adamson, D. H. *Applied Physics Letters,* **2000**, *76*, 1689.

Liang, C.; Hong, K.; Guiochon, G. A.; Mays, J. W.; Dai, S. *Angew. Chem. Int. Edit.,* **2004**, *43*, 5785-5789.

Lin, Y.; Boker, A.; He, J. B.; Sill, K.; Xiang, H. Q.; Abetz, C.; Li, X. F.; Wang, J.; Emrick, T.; Long, S.; Wang, Q.; Balazs, A.; Russell, T. P. *Nature,* **2005**, *434*, 55.

Lin, Z.; Kim, D. H.; Wu, X.; Boosahda, L.; Stone, D.; LaRose, L.; Russell, T. P. *Adv. Mater.,* **2002**, *14*, 1373-1376.

Liu, G.; Ding, J.; Hashimoto, T.; Kimishima, K.; Winnik, F. M.; Nigam, S. *Chem. Mat,.* **1999**, *11*, 2233-2240.

Liu, G.; Ding, J.; Stewart, S. *Angew. Chem. Int. Edit.,* **1999**, *38*, 835-838.

Liu, X.; Jiang, M.; Yang, S.; Chen, M.; Chen, D.; Yang, C.; Wu, K. *Angew. Chem. Int. Edit.,* **2002**, 41, 2950-2953.

Lodge, T. P., Pan, C., Jin, X., Liu, Z., Zhao, J., Maurer, W. W., Bates, F. S. *J. of Poly. Sci. Part B,* **1995**, *33*, 2289-2293.

Lopes, W. A.; Jaeger, H. M. *Nature,* **2001**, *414*, 735-738.

Ludwigs, S.; Boker, A.; Voronov, A.; Rehse, N.; Magerle, R.; Krausch, G. *Nature Materials,* **2003**, *2*, 744.

M. S. Turner, *Phys Rev. Lett.,* **1992**, *69*, 1788-1791.

MacGlashan, G. S.; Andreev, Y. G.; Bruce, P. G. *Nature*, **1999**, *398*, 792.

Mansky, P.; Harrison, C. K.; Chaikin, P. M.; Register, R. A.; Yao, N. *Appl. Phys. Lett.,* **1996**, *68*, 2586-2588.

Mansky, P.; Liu, Y.; Huang, E.; Russell, T. P.; Hawker, C. *Science,* **1997**, *275*, 1458-1460.

Mao, H.; Arrechea, P. L.; Bailey, T. S.; Johnson, B. J. S.; Hillmyer, M. A. *Faraday Discuss.*, **2005**, *128*, 149-162.

Maoz, R.; Cohen, S.; Sagiv, J. *Adv. Mater.* J., *11*, 55.

Mayes, A. M.; Russell, T. P. Satija, S. K.; Majkrzak, C. F. *Macromolecules,* **1992**, *25*, 6523.

Meiners, J. C.; Quintel-Ritzi, A.; Mlynek, J.; Elbs, H.; Krausch, G. *Macromolecules,* **1997**, *30*, 4945-4951.

Misner, M. J.; Skaff, H.; Emrick, T.; Russell, T. P. *Adv. Mater.,* **2003**, *15*, 221-224.

Morkved, T. L.; Lü, M.; Urbas, A. M.; Ehrichs, E. E.; Jaeger, H. M.; Mansky, P.; Russell, T. P. *Science,* **1996**, *273*, 931-933.

Muller-Buschbaum, P.; Cubitt, R.; Petry, W. *Langmuir*, **2003**, *19*, 7778.

Muthukumar, M.; Ober, C. K.; Thomas, E. L. *Science,* **1997**, *277*, 1225.

Olayo-Valles, R.; Lund, M. S.; Leighton, C.; Hillmyer, M. A. *J. Mater. Chem.,* **2004**, *14*, 2729-2731.

Orso, K. A.; Green, P. F. *Macromolecules,* **1999**, *32*, 1087.

Pai, R. A.; Humayun, R.; Schulberg, M. T.; Sengupta, A.; Sun, J.-N.; Watkins, J. J. *Science,* **2004**, *303*, 507-511.

Park, C.; De Rosa, C.; Thomas, E L. *Macromolecules,* **2001**, 34, 2602-2606.

Park, M.; Chaikin, P. M.; Register, R. A.; Adamson, D. A. *Appl. Phys. Lett.*, **2001**, *79*, 253.

Park, M.; Harrison, C.; Chaikin, P. M.; Register, R. A.; Adamson, D. H. *Science,* **1997**, *276*, 1401-1404.

Pereira, R. P.; Rocco, A. M.; Bielschowsky, C. E. *Journal of Physical Chemistry B,* **2004**, *108*, 12677.

Ratner, M. A.; Shriver, D. F. *Chemical Reviews,* **1988**, *88*, 109-24.

Reiter, G.; Castelein, G.; Hoerner, P.; Riess, G.; Blumen, A.; Sommer, J. U. *Phys. Rev. Lett.*, **1999**, *83*, 3844-3847.

Renaud, G.; Lazzari, R.; Revenant, C.; Barbier, A.; Noblet, M.; Ulrich, O.; Leroy, F.; Jupille, J.; Borensztein, Y.; Henry, C. R.; Deville, J. P.; Scheurer, F.; Mane-Mane, J.; Fruchart, O. *Science,* **2003**, *300*, 1416.

Rockford, L.; Liu, Y.; Mansky, P.; Russell, T. P.; Yoon, M.; Mochrie, S.G. *J. Phys. Rev. Lett.,* **1999**, *82*, 2602-2605.

Rockford, L.; Russell, T. P.; Yoon, M.; Mochrie, S. G. J. *Macromolecules,* **2001**, *34*, 1487.

Rosa, C. D.; Park, C.; Thomas, E. L.; Lotz, B. *Nature,* **2000**, *405*, 433-437.

Ruokolainen, J.; Makinen, R.; Torkkeli, M.; Makela, T.; Serimaa, R.; Ten Brinke, G.; Ikkala, O. *Sciencé,* **1998**, *280*, 557.

Russell, T. P. *Physica B*, **1996**, *221*, 267-283.

Ruzette, A. V.; Soo, P. P.; Sadoway, D. R.; Mayes, A. M. *Journal of the Electrochemical Society,* **2001**, *148(6)*, A537-A543.

Ryu, D. Y.; Shin, K.; Drockenmuller, E.; Hawker, C. J.; Russell, T. P. *Science,* **2005**, *308*, 236.

Rzayev, J.; Hillmyer, M. A. *J. Am. Chem. Soc.*, **2005**, *127*, 13373-13379.

Rzayev, J.; Hillmyer, M. A. *Macromolecules,* **2005**, *38*, 3-5.

Segalman, R. A. *Materials Science & Engineering R-Reports,* **2005**, *48*, 191.

Segalman, R. A.; Hexemer, A.; Hayward, R. C.; Kramer, E. J. *Macromolecules,* **2003**, *36*, 3272-3288.

Segalman, R. A.; Hexemer, A.; Kramer, E. J. *Macromolecules,* **2003**, *36(18)*, 6831-6839.

Segalman, R. A.; Yokoyama, H.; Kramer, E. J. *Advanced Materials,* **2001**, *13*, 1152-1155.

Segalman, R. A.; Yokoyama, H.; Kramer, E. J. *Adv. Mater.,* **2001**, *13*, 1152-1155.

Seul, M.; Andelman, D. *Science,* **1995**, *267*, 476.

Shibayama, M.; Hashimoto, T.; Hasegawa, H.; Kawai, H. *Macromolecules,* **1983**, *16(9)*, 1427-33.

Shin, K.; Leach, K. A.; Goldbach, J. T.; Kim, D. H.; Jho, J. Y.; Tuominen, M.; Hawker, C. J.; Russell, T. P. *Nano Letters,* **2002**, *2*, 933-936.

Smith, M. D.; Green, P. F.; Saunders, R. *Macromolecules,* **1999**, *32*, 8392.

Sohn, B. H.; Yoo, S. I.; Seo, B. W.; Yun, S. H.; Park, S. M. *J. Am. Chem. Soc.*, **2001**, *123*, 12734.

Spatz, J. P.; Herzog, T.; Moessmer, S.; Ziemann, P.; Moeller, M. *Adv. Mater.*, **1999**, *11*, 149-153.

Stewart, S.; Liu, G. *Angew. Chem. Int. Edit.*, **2000**, *39*, 340-344.

Stoykovich, M. P.; Muller, M.; Kim, S. O.; Solak, H. H.; Edwards, E. W.; de Pablo, J. J.; Nealey, P. F. *Science,* **2005**, *308*, 1442.

Stupp, S. I.; LeBonheur, V.; Walker, K.; Li, L. S.; Huggins, K. E.; Keser, M.; Amstutz, A. *Science*, **1997**, *276*, 384.

Sundrani, D. Sibener, S. J. *Macromolecules,* **2002**, *35*, 8531-8539.

Sundrani, D.; Darling, S. B.; Sibener, S. J. *Langmuir,* **2004**, *20(12)*, 5091-5099.

Taking the Mystery Out of Thin-Film Measurement, Filmetrics, Inc. San Diego, CA.

Tarascon, J. M.; Armand, M. *Nature,* **2001**, *414*, 359.

Templin, M.; Franck, A.; Du Chesne, A.; Leist, H.; Zhang, Y.; Ulrich, R.; Schadler, V.; Wiesner, U. *Science,* **1997**, *278*, 1795-1798.

Thurn-Albrecht, T.; DeRouchey, J.; Russell, T. P.; Jaeger, H. M.; *Macromolecules,* **2000**, *33*, 3250.

Thurn-Albrecht, T.; Schotter, J.; Kastle, G. A.; Emley, N.; Shibauchi, T.; Krusin-Elbaum, L.; Guarini, K.; Black, C. T.; Tuominen, M. T.; Russell, T. P. *Science,* **2000**, *290*, 2126-2129.

Thurn-Albrecht, T.; Steiner, R.; DeRouchey, J.; Stafford, C. M.; Huang, E.; Bal, M.; Tuominen, M.; Hawker, C. J.; Russell, T. P. *Advanced Materials,* **2000**, *12*, 787-790.

Tompkins, H. G. *A Users Guide to Ellipsometry*, Academic Press, Inc. San Diego, CA, 1993.

Torikai, N.; Takabayashi, N.; Noda, I.; Koizumi, S.; Morii, Y.; Matsushita, Y. *Macromolecules,* **1997**, *30*, 5698.

Vega, D. A.; Harrison, C. K.; Angelescu, D. E.; Trawick, M. L.; Huse, D. A.; Chaikin, P. M.; Register, R. A. *Physical Review E,* **2005**, 71.

Villar, M. A.; Rueda, D. R.; Ania, F.; Thomas, E. L. *Polymer,* **2002**, *43*, 5139.

Wang, Y.; Song, R.; Li, Y.; Shen, J. *Surface Science,* **2003**, *530(3)*, 136-148.

Whitesides, G. M.; Grzybowski, B. *Science,* **2002**, *295*, 2418.

Xiao, S.; Yang, X. M.; Edwards, E. W.; La, Y. H.; Nealey, P. F. *Nanotechnology,* **2005**, *16(7)*, 324-329.

Xu, T.; Goldbach, J. T.; Misner, M. J.; Kim, S. H..; Gibaud, A.; Gang, O.; Ocko, B.; Guarini, K. W.; Black, C. T.; Hawker, C. J.; Russell, T. P. *Macromolecules,* **2004**, *37(8)*, 2972-2977.

Xu, Y.; Gu, W.; Gin, D. L. *J. Am. Chem. Soc.*, **2004**, *126*, 1616-1617.

Yang, X. M.; Peters, R. D.; Nealey, P. F.; Solak, H. H.; Cerrina, F. *Macromolecules,* **2000**, *33*, 9575-9582.

Yurt, S.; Anyanwu, U. K.; Scheintaub, J. R.; Coughlin, E. B.; Venkataraman, D. *Macromolecules,* **2006**, *39(5)*, 1670-1672.

Zhang, Q.; Tsui, O. K. C.; Du, B.; Zhang, F.; Tang, T.; He, T. *Macromolecules,* **2000**, *33*, 9561-9567.

Zhang, Q.; Xu, T.; Butterfield, D.; Misner, M. J.; Ryu, D. Y.; Emrick, T.; Russell, T. P. *Nano Letters*, **2005**, 5, 357-361.